Coastal ocean response to near-resonant sea breeze/land breeze near the critical latitude in the Georgia Bight

by
Catherine Richardson Edwards

A dissertation submitted to the faculty of the University of North Carolina at Chapel Hill in partial fulfillment of the requirements for the degree of Doctor of Philosophy in the Department of Marine Sciences.

Chapel Hill
2008

Approved by:

Advisor:Harvey E. Seim

Reader: John M. Bane, Jr.

Reader: Francisco E. Werner

Reader: Thomas J. Shay

Reader: Alberto D. Scotti

Reader: Brian O. Blanton

ABSTRACT

CATHERINE RICHARDSON EDWARDS: Coastal ocean response to near-resonant sea breeze/land breeze near the critical latitude in the Georgia Bight

(Under the advisement of Harvey E. Seim)

On the mid- to outer shelf of the Georgia Bight, surface-intensified non-tidal diurnal currents can exceed 25 cm/s more than 120 km offshore, with currents in a lower layer 180°out of phase upper layer currents. Persistent from April through October, these diurnal motions appear to be inertial oscillations and near-inertial internal waves, forced by sea breeze/land breeze (SBLB) and other diurnal winds, resonant with the inertial frequency at 30°N or S.

Observational wind and current data from 1999-2007 are analyzed from a moored array in the Georgia Bight, between 29-32°N, where linear theory predicts maximum SBLB magnitude and offshore extent. Complex empirical orthogonal function analysis is used to separate non-tidal diurnal/inertial currents from the tidal currents at frequencies that cannot be simultaneously resolved at relevant time scales. The spatial structure, variability, and phase of diurnal/inertial currents are described and compared to those of SBLB as both the atmospheric forcing and ocean response pass through the critical latitude for diurnal/inertial resonance. Diurnal variance of observed and modeled winds indicate SBLB winds on the order of 1-2 m/s at least 250 km offshore, nearly an order of magnitude greater than the anticipated offshore scale.

The magnitude of coastal ocean response is strongly controlled by the interaction of bottom friction and stratification, and increases with distance offshore, producing diurnal/inertial divergence/convergence over the inner to mid-shelf. Examination of shear and stratification on the mid- to outer shelf reveals that the pycnocline partially decouples the water column. The level of maximum shear bounds rather than coincides with the pycnocline, which contains a sub-surface jet that rotates anticyclonically but is 180°out of phase with the directly-forced surface currents. The vertical structure of the currents is not-well represented by models that describe the vertical structure observed elsewhere, and more closely resembles a three-layer structure: a wind-forced surface layer overlying a stratified inertial jet layer and a well-mixed quiescent bottom layer. The vertical structure and its variability has significant implica-

tions for mixing, as the shelf of the Georgia Bight appears to trap near-inertial energy input from the wind, enhanced near the critical latitude for diurnal/inertial resonance.

ACKNOWLEDGMENTS

I would like to thank my committee members, John M. Bane, Jr., Brian O. Blanton, Alberto D. Scotti, Harvey E. Seim, Thomas J. Shay, and Francisco E. Werner, for their encouragement, support, and suggestions. I thank you for being great teachers and friends. I owe particular gratitude to Harvey for his advisement, providing support (funding and personal), over the last five years.

Many thanks to my friends and collaborators at the Naval Research Laboratory and at Skidaway Institute of Oceanography: Cheryl Ann Blain, Ruth Preller, Gregg Jacobs, Dana Savidge, Julie Amft, Trent Moore, and Jim Nelson. I've been quite lucky to work with Captain Raymond Sweatte and crew of the R/V Savannah, without whom the shelf of the Georgia Bight would certainly be littered with lost and broken oceanographic instruments.

I am extraordinarily grateful to Mrs. Caroline H. Royster and the late Dr. Thomas S. Royster, Jr., whose support through the Royster Society of Fellows made this work possible. The analysis was also supported as part of SEACOOS, sponsored by the Office of Naval Research under Award N00014-02-1-0972.

Finally, to my friends and family, you know who you are, and I hope you know how much your love and friendship mean to me.

A dissertation haiku

Wind blows, water moves,
ellipse and circle, their paths,
noose-like, strangle me.

TABLE OF CONTENTS

LIST OF TABLES

LIST OF FIGURES

CHAPTER 1. Introduction

The shallow shelf of the South Atlantic Bight (SAB), with water depths of less than 50 m, is narrowest at the SAB's southern- and northern-most extremes, with a shelf-width maximum along the Georgia-South Carolina coasts in the Georgia Bight, the embayment bounded by Cape Romain, SC to the north and Cape Canaveral to the south. Over this wide shallow shelf, the dynamics are predominantly tidal in origin, particularly on the inner to mid-shelf, where the influence of the Gulf Stream is minimal (*Pietrafesa et al.*, 1985); it is estimated that 80-90% of cross-shelf and 20-40% of alongshelf current variance can be attributed to the barotropic tide (*Tebeau and Lee*, 1979; *Lee and Brooks*, 1979). The M_2 tide, significantly amplified over the shelf (*Redfield*, 1958) and with current ellipses oriented cross-shore, accounts for much of this variance, with current magnitudes on the order of 30-40 cm/s (*Blanton et al.*, 2004).

While barotropic M_2 tidal currents typically dominate the current variance, diurnal variability has recently been observed to approach that of semidiurnal barotropic tide on synoptic and seasonal time scales on the shelf of the Georgia Bight. Seasonal variability of tidal currents are often attributed to the presence of internal tidal energy derived from the barotropic tide under seasonal stratification (*Foreman et al.*, 1995; *Ray and Mitchum*, 1997; *Holloway*, 2001). *Blanton et al.* (2004) report statistically significant seasonal variability in M_2 tidal amplitude and phase, computed from National Ocean Service (NOS) water level records at Fort Pulaski, Georgia, and suggest that temporal variability of tidal elevation and barotropic currents may be significant on the shelf. However, as shown in the following chapters, the strong seasonal signal in the diurnal currents does not appear to be tidal, but rather, arises from sea breeze/land breeze wind forcing of the coastal ocean.

Near the critical latitude of 30°N or S, the local inertial and diurnal frequencies coincide, and diurnal/inertial motions come into resonance with diurnal forcing. Inertial energy in the atmosphere is large relative to other frequencies at all latitudes, but is significantly enhanced at the critical latitude (*Stockwell et al.*, 2004), which suggests that diurnal winds may be a significant pathway for energy transfer

from the atmosphere into the ocean near 30°N or S. In fact, diurnal/inertial energy in the ocean is found to be enhanced near 30°N (*Skyllingstad et al.*, 2000; *van Haren*, 2005), which may reflect an increased efficiency of momentum and energy transfer into the ocean's surface boundary layer near the critical latitude (*Skyllingstad et al.*, 2000). Ocean observations and modeling studies in the northwestern Gulf of Mexico (*Daddio et al.*, 1978; *Chen et al.*, 1996; *Chen and Xie*, 1997; *DiMarco et al.*, 2000; *Lewis*, 2001), the DeSoto Canyon in the northern Gulf of Mexico (*Jarosz et al.*, 2007), and off the coast of Namibia (*Simpson et al.*, 2002) report increased inertial/diurnal energy in the surface ocean in response to wind forcing at resonant and non-resonant frequencies, similar to that observed in the Georgia Bight.

The dynamical setting of the Georgia Bight makes it a unique laboratory for investigating the processes that control the fate of wind energy input near the resonant frequency. SBLB, enhanced over the broad shallow shelf of the Georgia Bight, could be a significant source of shelf-wide forcing of the coastal ocean near the resonant frequency. Unlike other observational studies, moorings instrumented to measure winds and currents form cross- and alongshelf transects, and the availability of data from 1999-2007 provides the ability to describe synoptic, seasonal, and interannual variability of the diurnal/inertial variability in the ocean and atmosphere. The relatively shallow water depths and energetic tides of the Georgia Bight may alter the dynamical balance observed in the Gulf of Mexico and on the Namibian slope. While dynamically dominated by tidal processes on the inner to mid-shelf, the Georgia Bight is bounded by the Gulf Stream, which may contribute diurnal/inertial energy to the ocean and atmosphere, and affect how the input wind energy is redistributed on the shelf. While the available observations are not sufficient to describe the ultimate fate of the enhanced diurnal/inertial energy at the critical latitude, potential pathways of energy transfer can be described based on analysis of multiple years of observational data now available.

In the following chapters, the sea breeze forcing mechanism and the near-resonant response of the coastal ocean of the Georgia Bight will be explored using data from regional coastal ocean observing systems and their partner institutions. New methods to isolate vertical structure of internal motions in energetic shallow water environments have been developed and tested, and allow for the separation of the wind-forced diurnal/inertial motions from the barotropic tide. Available data on the shelf from multiple sources are then analyzed and compiled into composite climatologies of the atmospheric forcing and coastal ocean response. This descriptive approach is a necessary step before addressing further scientific questions, as neither the strong diurnal motions nor the offshore structure of the SBLB system in the Georgia Bight is discussed in the literature. Finally, the role of stratification in determining the redistribution of input wind energy in space and time is considered on seasonal, synoptic, and tidal/inertial

time scales.

As of this writing (November 4, 2008), the CEOF methods paper (Chap. 2) is in print (*Edwards and Seim*, 2008a). The SBLB met paper (Chap. 3) is near final form, and will be submitted to JGR-Oceans as *Edwards and Seim* (2008b). Chapters 4 and 5 are companion papers, focusing on the horizontal and vertical structure of the coastal ocean's response to near-resonant forcing. These chapters are referred to herein as *Edwards and Seim* (2008d) and *Edwards and Seim* (2008c), respectively, in preparation for submission of these manuscripts to JPO.

CHAPTER 2. Complex EOF Analysis as a Method to Separate Barotropic and Baroclinic Velocity Structure in Shallow Water

2.1 Introduction

Internal tides have been widely studied over the coastal ocean and can be important pathways of energy transfer from the barotropic tide to dissipation and mixing in shallow water (e.g., *Huthnance*, 1989; *MacKinnon and Gregg*, 2003a; *Rippeth and Inall*, 2002; *Holloway et al.*, 2001). However, separating the baroclinic tidal motion from the barotropic currents in measured data can be a challenge due to both barotropic and baroclinic motions operating at the same frequency, but with different vertical and temporal modes of variability. The traditional approach has been to assume that baroclinic motions are responsible for observed vertical shear at tidal frequencies and assign the barotropic currents to be the depth-average of measured data. However, in shallow water, development of boundary layers near the surface or bottom can add significant shear to the barotropic tidal current profile. A standard time series analysis technique is investigated to determine if it can isolate internal modes of motion in shallow regions where bottom boundary layers can occupy a significant fraction of the water column.

Complex empirical orthogonal function (CEOF) analysis is proposed as a better alternative to depth-averaging methods to estimate barotropic tidal currents from measured data, allowing an improved representation of internal tidal motions. Away from the surface and bottom boundary layers, depth-averaging measured velocity can give an excellent estimate of barotropic tidal flow, and is a widely used method for separating barotropic and baroclinic tidal currents in the coastal ocean. Depth-averaging can provide reasonable estimates of a relatively weak barotropic tidal current in moderately shallow water (e.g., *MacKinnon and Gregg*, 2003b), of a stronger barotropic tide in deeper water (e.g., *Holloway et al.*, 2001; *Rippeth and Inall*, 2002), or of relatively weak tides over a range of depths (e.g., *Lerczak*

et al., 2003).

Where the bottom boundary layer occupies a significant fraction of the water column, depth-averaging a current profile $u(z,t)$ and subtracting the depth average $\bar{u}_z(t)$ from every point in the profile to remove the barotropic current can leave a boundary layer signature in the difference. Figure 1 depicts a cartoon snapshot of an idealized 1-dimensional barotropic tidal current profile in shallow water, $u(z)$, its depth average, $\bar{u}$, and $\tilde{u}(z) \equiv u(z) - \bar{u}$. When $u(z)$ is an oscillating current, the difference $\tilde{u}(z)$ has a 180^o temporal phase difference surface to bottom, and can resemble an internal tide trapped near-bottom, where the bottom boundary layer effects are greatest. *Simionato et al.* (2005) define the baroclinic velocity by subtracting the depth average of measured current profiles in the Rio de Plata Estuary, Brazil and report a slightly bottom-enhanced M_2 internal tide near the mouth of the estuary. Though the Rio de Plata is classified as a microtidal system, the use of depth-averaging in 15 m of water suggests that the bottom boundary layer structure principally associated with the barotropic tidal dynamics may have been mistakenly identified to result from an internal tide.

Complex EOF analysis is investigated herein as a tool that can account for the bottom boundary layer structure of barotropic tidal currents, allowing a better isolation of the current structure of internal tides and waves in the vertical. Several studies have employed similar analyses to describe the vertical structure of shallow water currents. However, the input time series are typically low-pass filtered to examine subtidal dynamics (*Webster*, 1986; *Münchow and Chant*, 2000), harmonically analyzed to remove the tide (*Lentz*, 1994), analyzed as the difference between model solutions with tidal and/or wind forcing (*Hall and Davies*, 2002), or those in which the barotropic tide at that frequency could be neglected altogether (*Lerczak et al.*, 2003). *Apel et al.* (1997) use real-valued EOF analysis to identify vertical structure of currents measured on the outer shelf of the Mid-Atlantic Bight (MAB), but the tidal environment and ADCP configuration were such that the barotropic currents had no appreciable vertical structure. Thus, while the use of EOF and CEOF analyses to examine internal structure is reflected in the literature, the application of the method to unfiltered currents in a highly energetic shallow water environment has not been reported. Successful isolation of internal tidal structure in such an environment is an important test of the method.

Flows on the mid-shelf of the South Atlantic Bight (SAB) are largely controlled by the tides and the wind *Lee et al.* (1991). It is estimated that 80-90% of cross-shelf and 20-40% of alongshelf current variance can be attributed to the tidal band (*Tebeau and Lee*, 1979; *Lee and Brooks*, 1979). The M_2 tide, significantly amplified over the shelf (*Redfield*, 1958) and with current ellipses oriented cross-shore, accounts for much of this variance, with current magnitudes of the order of 30-40 cm/s (*Blanton et al.*,

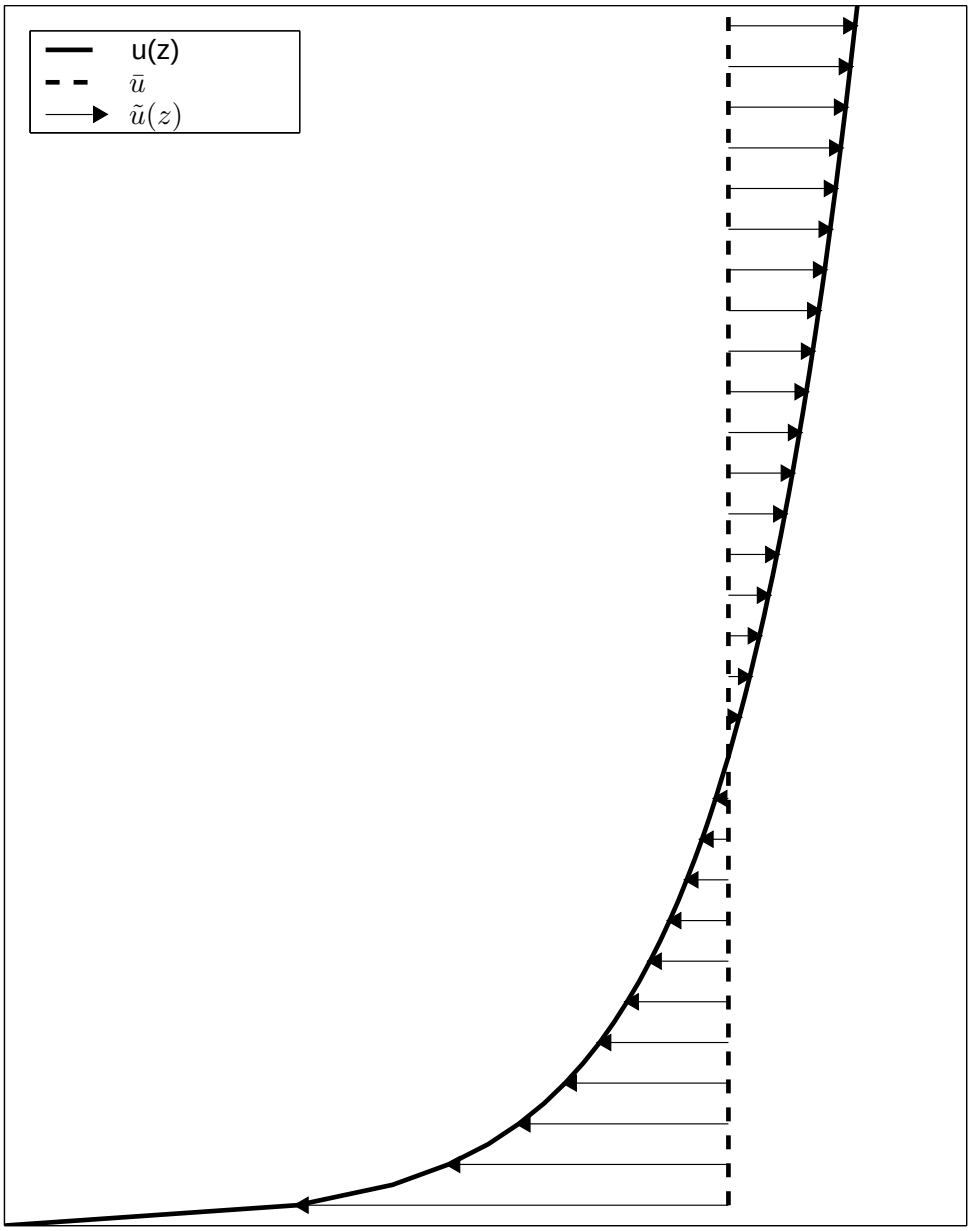

Figure 1: Cartoon showing the potential effect of depth-averaging a barotropic flow through a strong bottom boundary layer in shallow water. The thick line denotes $u(z)$, the depth-average of which is $\bar{u}$, represented as the dashed line. The arrows show the magnitude and direction of $\tilde{u}(z) \equiv u(z) - \bar{u}$.

2004). The shallow depth of the SAB (typically less than 50 m) and the magnitude of the M_2 tide found on the shelf result in significant frictional shear over much of the water column. The combined effect of strong tidal currents and the associated bottom boundary layer structure that develops in the SAB can significantly hinder clean separation of the barotropic and baroclinic velocity structures. As can be seen in Fig. 1, the depth-averaged current fails to capture the free-stream velocity, and leads to a small underestimate of the barotropic current near-surface that can be several cm/s. The effect is most acute at the base of the water column; overestimate of the barotropic current by $\bar{u}_z(t)$ near-bottom could potentially be tens of cm/s. Depth-averaging through veering within the tidal bottom boundary layer further confounds the separation of barotropic and baroclinic velocity structures by introducing errors in estimates of barotropic tidal phase and orientation.

To quantify the ability of EOF analysis to isolate a barotropic signal in shallow water, the EOF method is applied to mid-shelf tidal currents synthesized using a purely barotropic formulation of vertical structure, and the results are compared to those using depth-averaging methods. The analysis is repeated for measured current data acquired in a mid-shelf location in the SAB. Interpretation of the analysis and potential sources of error are presented, and practical considerations of the methods are discussed.

2.2 Methods

The CEOF technique (e.g., *Davis*, 1976; *Horel*, 1984; *Barnett*, 1985; *Preisendorfer*, 1988; *Kaihatu et al.*, 1998) serves as a separation of variables in space and time. Here it is applied to the complex time series $\psi(z,t) = u(z,t) + iv(z,t)$, where u and v are the eastward and northward positive components of velocity and $i = \sqrt{-1}$. The eigenvalue problem is solved for the complex covariance matrix formed from the time-varying portion of $\psi(z,t)$; the eigenvectors $\phi_j(z)$ describe independent vertical modes and the eigenvalues, λ_j, give the variance associated with each mode. Temporal variability of the jth vertical mode at depth level m, ϕ_{jm}, is given by the projection of the data onto that mode:

$$a_j(t) = \sum_{m=0}^{M-1} \psi_m(t)\phi_{jm} \tag{2.2.1}$$

where m is the modal index, less than or equal to the number of vertical levels M. Time series of the jth mode profile $\hat{\psi}_j$ can be reconstructed simply as a spatial time series:

$$\hat{\psi_j}(z,t) = a_j(t)\phi_j^*(z). \tag{2.2.2}$$

where * denotes the complex conjugate.

Kaihatu et al. (1998) argue that this CEOF formulation converges faster than real-valued EOF analysis by component, but loses some meaning of the vector projection, citing *Preisendorfer*'s caution that directionality can become ambiguous in the eigenvalue search. In this application to the SAB, the principal axes of the flow are well-defined, and representation of the rotary tidal currents does not require independence of the along- and cross-shore components of flow. That the CEOF coefficients are complex yields a more intuitive physical interpretation than the 2-dimensional spatial problem; the vertical profile of a given mode retains its shape, but dilates and contracts in the horizontal as it rotates over a tidal cycle. Similarly, the limitation that the CEOF method can only represent two dimensions simultaneously is not a concern for this application.

For this application to the SAB, the barotropic tide is dominant and has been shown to contain the bulk of the variance of the currents. It is then assumed that the lowest vertical mode $\hat{\psi}_0(z,t)$ captures the structure of the barotropic tide and of other motions associated with free surface tilt and friction. The sum of the higher modes $\hat{\psi}_j(z,t)$ from $j = 1$ to $J = M - 1$ are interpreted to represent baroclinic motions.

2.3 Application to synthetic and measured current profiles

Part of the SABSOON/SEACOOS network of real-time observational towers in the SAB, the R6 tower is located near the 32 m isobath approximately 60 km offshore of Savannah, Georgia (Fig. 2). The combined effects of strong tides, wind stress, and shallow depth yield a frictionally dominant system, where the surface and bottom frictional boundary layers can potentially merge.

To estimate the barotropic and internal tidal structure, CEOF and depth-averaging methods are applied to synthetic and measured time series of current profiles at R6. Synthetic tidal current profiles for this mid-shelf location are constructed using a purely barotropic formulation (described below) resulting in a known vertical structure and internal tidal currents of zero magnitude. Measured ADCP data from the month of October 2002 are chosen as a second case study for comparison of the performance of depth-averaging and CEOF estimates of barotropic and baroclinic tidal currents. The observations were acquired under well-mixed conditions, which minimizes the internal structure in the measured currents. Monthly averaged winds at R6 were weakly downwelling-favorable towards the southwest, characteristic of autumn, and cross-shore monthly mean currents suggest little cross-shelf exchange. Co-located wind measurements over October 2002 reflect the passage of synoptic-scale atmospheric storms through

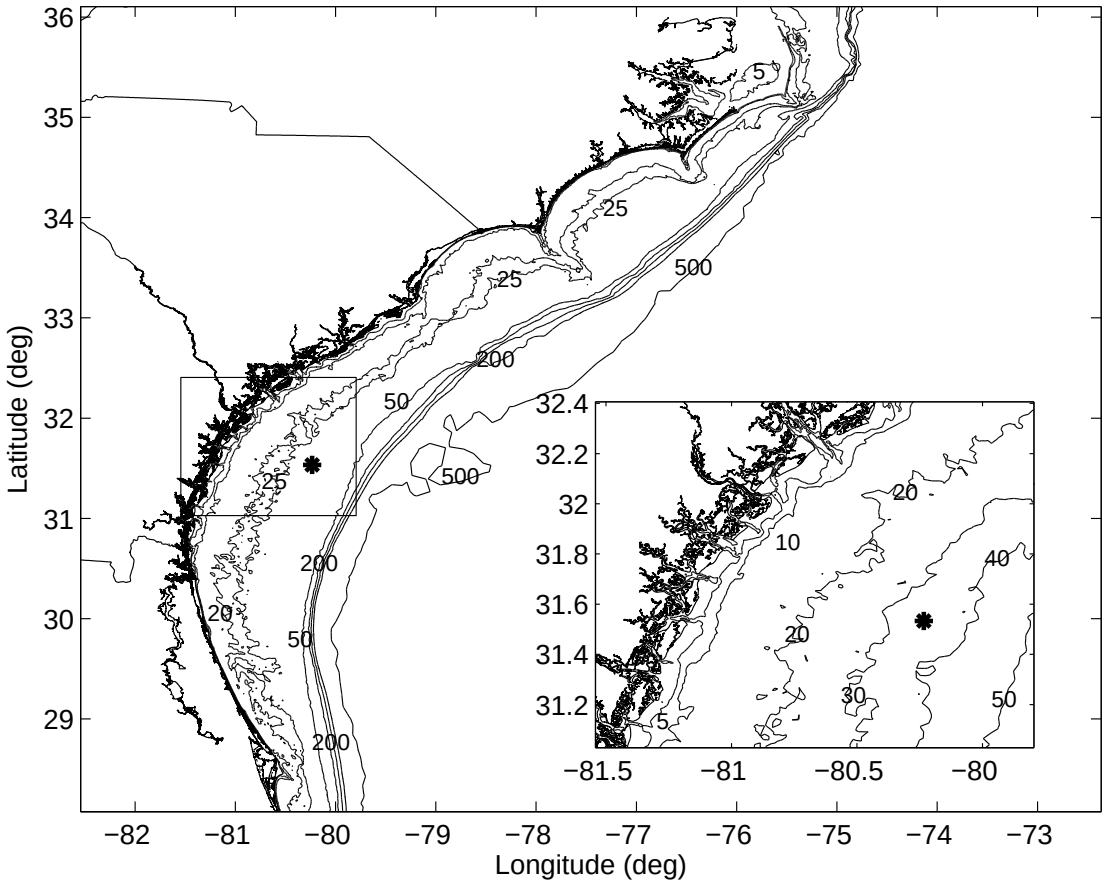

Figure 2: Bottom topography of the South Atlantic Bight, with location of the R6 tower indicated by the asterisk.

the region every 5-8 days, yielding a well-mixed mid-shelf region with slight surface cooling, consistent with typical autumn conditions (*Weber and Blanton*, 1980).

The barotropic tide is the dominant signal in the observations and precise estimates of bottom boundary layer structure are necessary to examine any potential internal tide, as $\tilde{u}(z)$ can be on the order of several to tens of cm/s, with a vertical structure that could easily be mistaken as arising from a baroclinic process. Barotropic tidal dynamics are relatively well-understood in the SAB, and the discrete frequencies at which the tides occur allows a clear interpretation of the successes and failures of each method in removing the barotropic signal. For these reasons, tidal analysis is used to compare the CEOF and depth-averaged estimates of the barotropic tide for synthetic and ADCP-measured currents.

2.3.1 Synthetic tidal data

Idealized profiles of tidal currents at the R6 tower are chosen as a simple representation of barotropic flow at the mid-shelf location. Amplitudes and phases of the depth-averaged M_2 tide are calculated using the South Atlantic Bight tidal database derived from the shelf-wide observational and modeling study of *Blanton et al.* (2004). A reasonable vertical structure is then computed using the analytical solution to a linear eddy viscosity model given and described by *Soulsby* (1990), using frictional parameters derived from a fit to tidal currents measured above the log layer. The roughness length z_0 was chosen to be 0.06 m based on observational estimates of 0.02-0.10 m derived from independent ADCP measurements and a linear one-dimensional turbulence closure model (*Muglia et al.*, 2003). Using this value of z_0 and eddy viscosity profiles estimated under unstratified autumn conditions, $\hat{u}_*$ was chosen to be 0.099 m/s. The free stream boundary condition to the solution is adjusted such that the integral over the resulting profile from the z_0 to the surface matches the depth-averaged current in the database. Time series over the month of October 2002 were then constructed from the resulting vertical profiles, with one hour temporal resolution and 1-m increments from 3.5 to 27.5 m above the bottom, matching those of the ADCP records analyzed in the following section.

The resulting synthetic time series of vertical profiles of the M_2 tidal currents are then decomposed into empirical vertical modes through CEOF analysis. The CEOF analysis is expected to recover the full signal $\psi(z,t)$ in its gravest mode, as its temporal variability is independent of its shape in the vertical; energy in higher modes indicates error in the analysis. Time series of each reconstructed mode $\hat{\psi}_j(z,t)$ are fit to the astronomical tide at each depth level using the least-squares analysis of *Pawlowicz et al.* (2002). Defining $\bar{\psi}_z(t)$ to be the vertical depth-average of $\psi(z,t)$ and $\tilde{\psi}(z,t) \equiv \psi(z,t) - \bar{\psi}_z(t)$ to be the complex number analogue of $\tilde{u}(z,t)$ shown in Figure 1, tidal analysis is repeated for the estimates

of barotropic and baroclinic current structure using depth-averaging methods. Tidal ellipses of $\psi(z,t)$, $\hat{\psi}_j(z,t)$, and $\tilde{\psi}(z,t)$ are then compared at each depth level. For brevity, the (z,t) dependence is omitted in the description below but is implied unless otherwise specified.

The tidal ellipses and the 95% confidence intervals about the ellipse parameter estimates derived from the least-squares fit to the original signal ψ, $\tilde{\psi}$ are examined (Fig. 3), and the first two EOF modes $\hat{\psi}_0$ and $\hat{\psi}_1$. All tidal ellipses are normalized to the semi-major axis of the near-surface synthetic ellipse. The lowest mode, $\hat{\psi}_0$, contains more than 99.998% of the variance of the input signal; $\hat{\psi}_1$ represents 0.001% of the variance, and is the only other mode with computable variance. Both $\hat{\psi}_1$ and $\tilde{\psi}$ show a 180° phase difference between the upper and lower layer, but the $\tilde{\psi}$ ellipses (Fig. 3c) are two orders of magnitude larger than those of $\hat{\psi}_1$. While $\tilde{\psi}$ represents only 2% of the variance of ψ as a bulk measure over the water column, evaluating at z=3.5 m above the bottom, $\tilde{\psi}$ accounts for 11% of the variance of ψ. This near-bottom variance in $\tilde{\psi}$ corresponds to a M_2 semi-major axis amplitude of 4.78 cm/s, which is statistically significant and would suggest the presence of an internal tide despite the purely barotropic formulation used to synthesize the time series.

The linear eddy viscosity model used to provide a realistic vertical profile is frequency dependent. The vertical scale of the bottom boundary layer depends on the difference between the tidal frequency and that of the local inertial frequency. To examine CEOF performance in recovering barotropic vertical structure of a signal containing multiple tidal frequencies (each with slightly different boundary layer scales), time series were synthesized with the five most significant tidal constituents on this part of the shelf (Blanton et al., 2004): M_2, N_2, S_2, K_1, and O_1. Near-surface synthetic semi-major axes specified by the synthetic signal are given in the first two columns of Table 1. The depth-average $\bar{\psi}_z$ underestimates the M_2 semi-major and semi-minor axes by 3.98 and 1.58 cm/s, respectively, near surface; near-bottom overestimates (not shown) are 8.4 and 2.9 cm/s. Comparable to the single-frequency analysis, $\hat{\psi}_0$ contains 99.999% of the variance of the multiple frequency synthetic record. The bulk of the remainder of the variance lies in $\hat{\psi}_1$, and is not significant; confidence intervals about the $\hat{\psi}_1$ calculated semi-axes lengths are 1-2 orders of magnitude smaller than could be practically measured for typical ADCP configurations used to measure velocity over the water column on the shelf.

Using synthetic velocity data generated for a shallow water shelf, CEOF analysis recovers the known vertical structure of the barotropic tide at a single frequency into the lowest mode. The CEOF technique is a significant improvement over depth-averaging methods, which suggest the presence of baroclinic tidal motions in the synthetic signal where none were prescribed by the purely barotropic formulation. This successful estimation of a zero amplitude baroclinic current is repeatable with synthesis of multiple

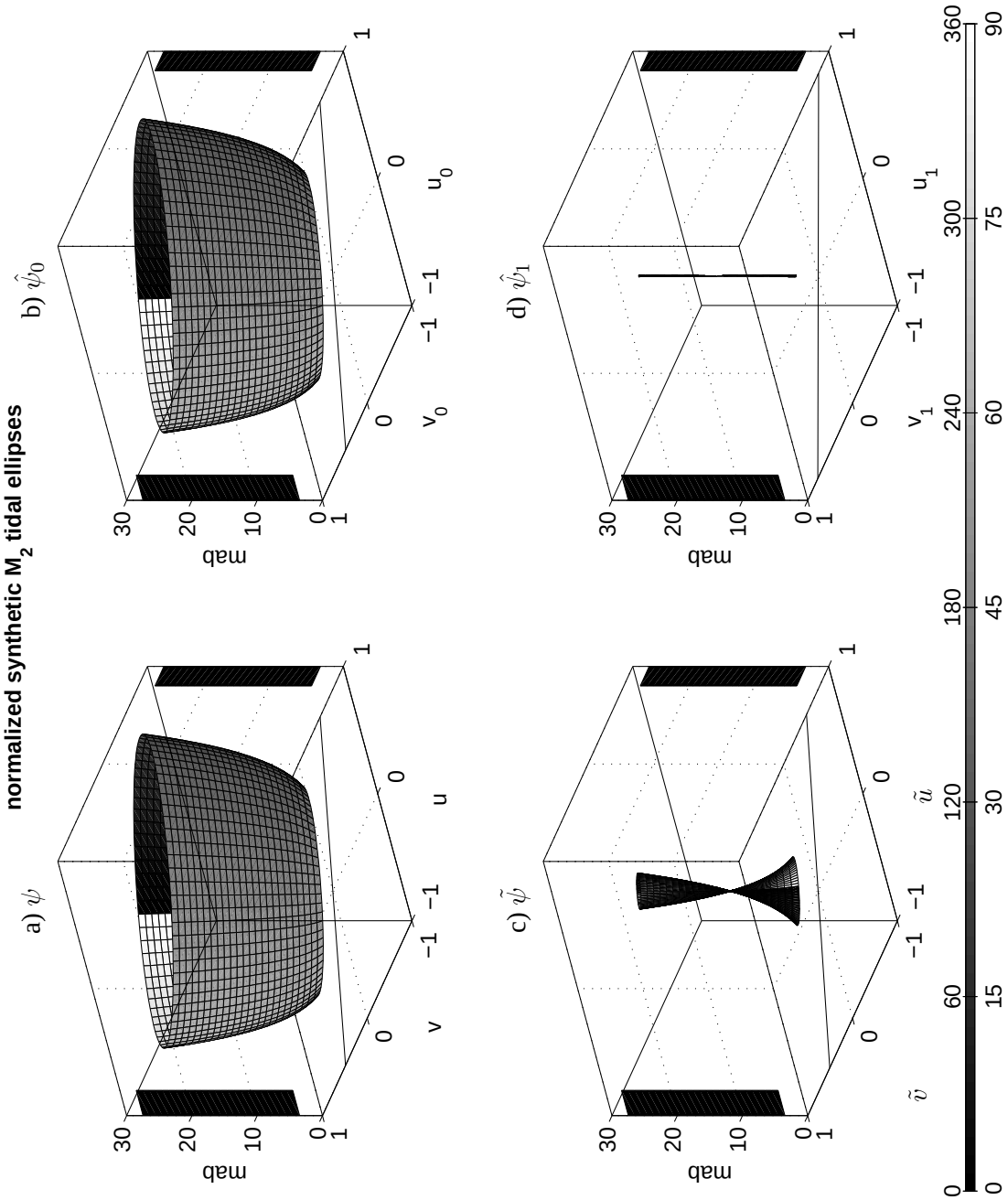

Figure 3: Normalized M_2 tidal ellipses and 95% confidence intervals (CIs) about calculated ellipse parameters for synthetic M_2 input: a) the original signal $\psi(z,t)$, b) $\hat{\psi}_0(z,t)$, c) $\tilde{\psi}(z,t)$, and d) $\hat{\psi}_1(z,t)$. Ellipse phase is contoured along the ellipse on the upper color scale. Near-surface ellipse orientation is shown as a thin line for reference; vertically-averaged semi-major and semi-minor axis CIs about the near-surface ellipse are shown as thick lines, and orientation and phase CIs are contoured on the left and right corners of the plot, respectively, using the lower color scale. Ellipse semi-axes and CIs are normalized by the semi-major axis of the near-surface ellipse of the original signal shown in a. All ellipses are plotted on the same scale for emphasis.

tidal frequencies with slightly varying vertical structures.

2.3.2 R6 data

Having shown that CEOF analysis can represent in its gravest mode a frictionally modified barotropic tide comprising multiple frequencies with slightly varying but known vertical structure, the analysis is repeated for data measured by an ADCP over the same time period at the same location. The structure of any internal tide present in the measured data is not known a priori, but the generally well-mixed conditions under which the observations were collected suggest that baroclinic tidal motions cannot be supported. Thus, as in the previous section, $\tilde{\psi}$ and $\hat{\psi}_1$ are not expected to represent an internal tide but rather a measure of error of the estimates of the barotropic tide given by $\bar{\psi}_z(t)$ and $\hat{\psi}_0$, respectively, using depth-averaging and CEOF methods. Hourly unfiltered data are used as input.

The lowest CEOF mode, $\hat{\psi}_0$, captures 99.36% of the variance over the month, with $\hat{\psi}_1$ and $\hat{\psi}_2$ containing 0.55% and 0.06%, respectively. The variance in $\hat{\psi}_2$ and higher modes is small enough that $\hat{\psi}_1$ can be interpreted as the EOF estimate of baroclinic current structure in ψ. Four-day time series of the u- and v-components of ψ at z=3.5 meters above bottom (mab, Fig. 4) suggest M_2 tidal currents of the order of 25-30 cm/s occur near-bottom. Time series of the tidal fits to the estimates of baroclinic currents formed by depth-averaging and CEOF methods, $\tilde{\psi}$ and $\hat{\psi}_1$, differ by an order of magnitude. Near-bottom $\tilde{\psi}$ is directed opposite the near-bottom measured velocity, and is largely anticorrelated with ψ. Variability of $\hat{\psi}_1$ is less tidal than that of $\tilde{\psi}$; the 29 tidal constituents resolved in a 30-day time series account for approximately 30% of the variance in $\hat{\psi}_1$ and 70% of the variance of $\tilde{\psi}$.

M_2 tidal ellipses of ψ (Fig. 5a) are oriented cross-shore, and are reproduced to within 2 cm/s by the $\hat{\psi}_0$ ellipses (Fig. 5b). Confidence intervals about $\hat{\psi}_0$ represent between 2.4-4.1% of the semi-axes lengths and are less than 4° for orientation and phase. Tidal ellipses of the $\tilde{\psi}$ (Fig. 5c) have a trend in the vertical similar to that of the synthetic data – the near-bottom semi-axes reflect the presence of the frictional boundary layer, with about twice the magnitude of near-surface values (4.18 vs 2.12 cm/s semi-major axis speeds, respectively). The $\tilde{\psi}$ ellipses (Fig. 5c) near-surface lie within 10° of the orientation of the full-signal ellipses, with a 180° phase difference surface to bottom. The phases of ψ vary less than a degree over the water column, but $\tilde{\psi}$ M_2 phase changes about 10° over the deepest 5 m.

In contrast, the $\hat{\psi}_1$ M_2 ellipses (Fig. 5d) are nearly rectilinear, with semi-major axis 20° counter-clockwise of the orientation of that of ψ and largest values near surface (max u_{major}=1.18 cm/s, max u_{minor}=0.014 cm/s). In the mean, $\hat{\psi}_1$ semi-major and -minor axes are approximately one and two orders of magnitude smaller than those of the values for $\tilde{\psi}$. The 95% confidence intervals indicate $\hat{\psi}_1$

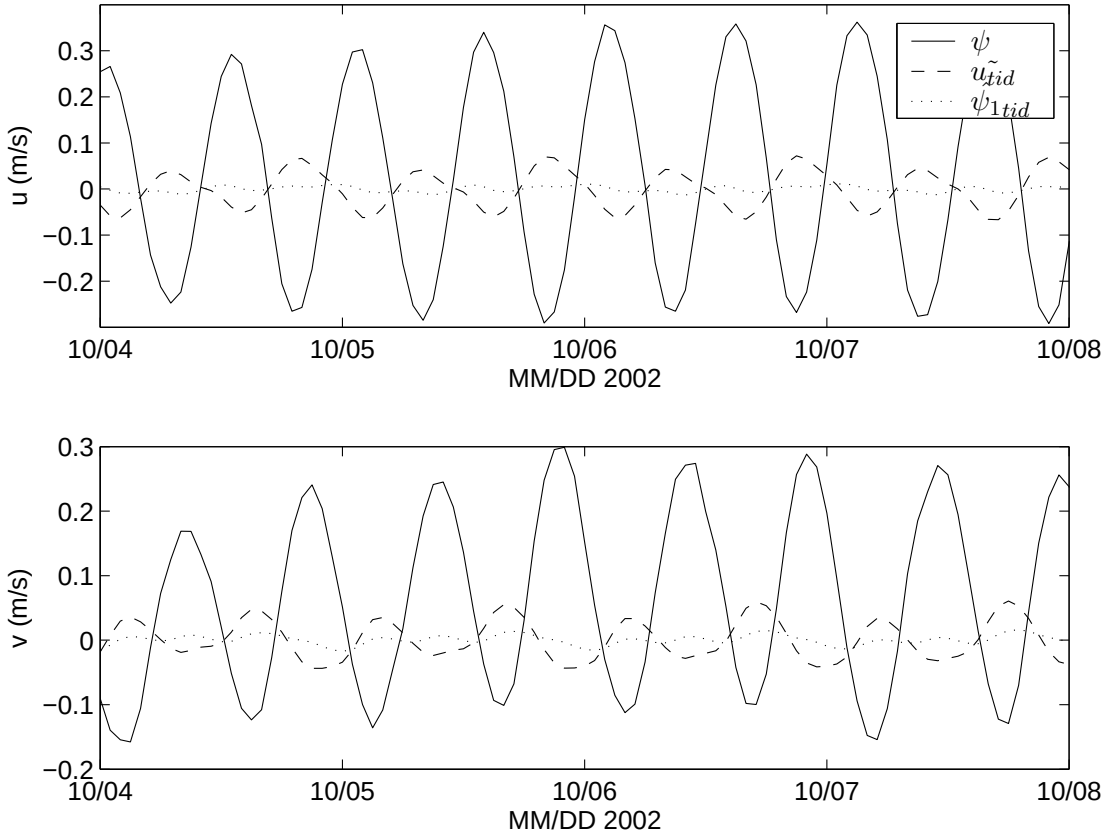

Figure 4: Time series of the u- and v-components of $\psi(z,t)$ (solid line), and the tidal fits to $\tilde{\psi}(z,t)$ (dashed line), and $\hat{\psi}_1(z,t)$ (dotted line) at z=3.5 m above the bottom, over a 4-day period in October 2002.

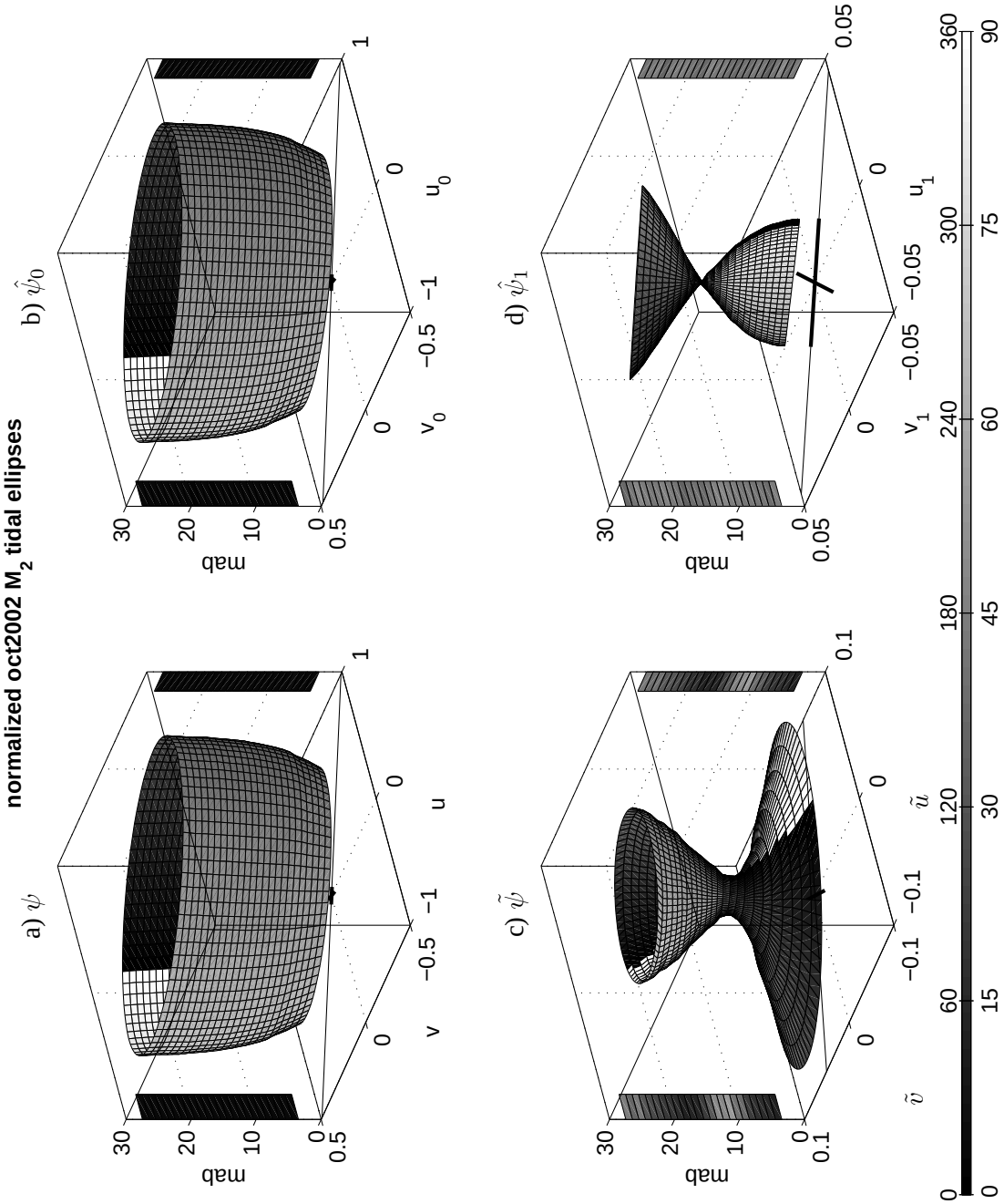

Figure 5: M_2 tidal ellipses and ellipse parameter errors for October 2002 data: a) the original signal $\psi(z,t)$, b) $\hat{\psi}_0(z,t)$, c) $\tilde{\psi}(z,t)$, and d) $\hat{\psi}_1(z,t)$, following the same convention as Fig. 3. Ellipse semi-axes and semi-axis errors are normalized by the semi-major axis of the near-surface ellipse of the synthetic signal shown in Fig.3a. Note the difference in scale from Fig. 3.

to be not significantly different from zero. The lack of energy in higher empirical modes suggests that M_2 internal tidal motions are not present in the data, which conflicts with the prediction using depth-averaging methods that baroclinic M_2 tidal currents in the measured data are of the order of several cm/s.

Comparison of $\tilde{\psi}$ given synthetic and measured time series as input currents supports the hypothesis that bottom boundary layer dynamics are responsible for the energy in $\tilde{\psi}$. The shape and magnitude of the profiles of M_2 semi-major and semi-minor axes of $\tilde{\psi}$ given synthetic and measured time series are compared (Fig. 6). The similarity in shape and size of the profiles of M_2 ellipse parameters calculated for measured data and a purely barotropic formulation substantiates the assumption that the relatively well-mixed water column should not be able to support baroclinic tidal motion. Since friction (modified by rotation) is the only source of shear in the *Soulsby* (1990) formulation of the synthetic ψ, this resemblance of $\tilde{\psi}$ for measured data to $\tilde{\psi}$ for a purely barotropic synthetic profile indicates that the variance in $\tilde{\psi}$ of measured current data is likely due to bottom boundary effects.

The diurnal tides are significantly less energetic than the semidiurnal tides on the SAB (Table 1), but the height of the bottom boundary layer associated with a tidal current is inversely proportional to the difference between the local inertial frequency, f, and tidal frequency (Soulsby, 1990). At this latitude, K_1 and O_1 lie at frequencies which approach the singularity at the inertial frequency ($0.96f$ and $0.89f$, respectively), and the effects of bottom friction on the diurnal tide can theoretically reach to nearly the height of the water column. K_1 tidal ellipses of ψ (Fig. 7a) are larger in magnitude than predicted by the tidal database of *Blanton et al.* (2004). However, the magnitude and shape of $\hat{\psi}_0$ in the vertical are in closer agreement to the expected vertical profile of the diurnal tide at this latitude. Further, in comparison to ψ, the tidal fit to $\hat{\psi}_0$ is significantly improved, with smaller confidence intervals about the semi-axes, inclination, and phase (Fig. 7b). The K_1 tidal fit to $\tilde{\psi}$ is not smooth in either the vertical or phase (Fig. 7c), and 95% confidence intervals about the ellipse magnitudes indicate that the fits to the $\tilde{\psi}$ and $\hat{\psi}_1$ are not significant. Confidence intervals about $\hat{\psi}_1$ ellipse phase are smaller than those for the $\tilde{\psi}$, but errors in orientation are larger due to the more circular shape.

Analysis of the O_1 constituent present in ψ (Fig. 8a) yields a pronounced increase in signal strength relative to *Blanton et al.* (2004), but with a distinct conical shape to the tidal ellipses with depth. Confidence intervals about ellipse orientation and phase for all O_1 tidal ellipses are large because of the ambiguity in orientation of a nearly circular ellipse. Tidal analysis of $\hat{\psi}_0$ recovers a signal that more closely resembles a frictional boundary layer associated with the barotropic tide (Fig 8b). Near-bottom, the magnitude of O_1 is greater than the tidal analysis of the ψ indicates. However, the difference be-

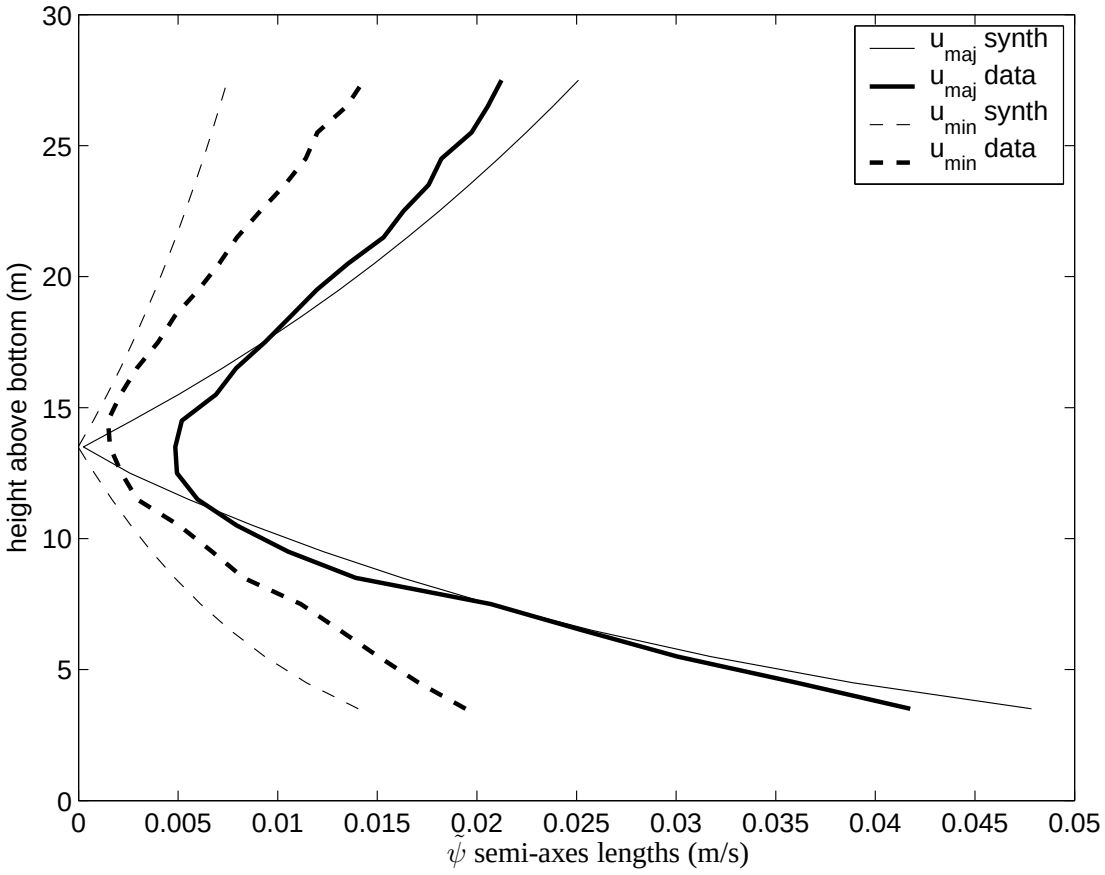

Figure 6: Profiles of M_2 ellipse semi-axes lengths calculated for synthetic (thin lines) and measured (thick lines) representations of $\tilde{\psi}(z,t)$. The solid and dashed lines indicate the semi-major and semi-minor axes u_{maj} and u_{min} in m/s.

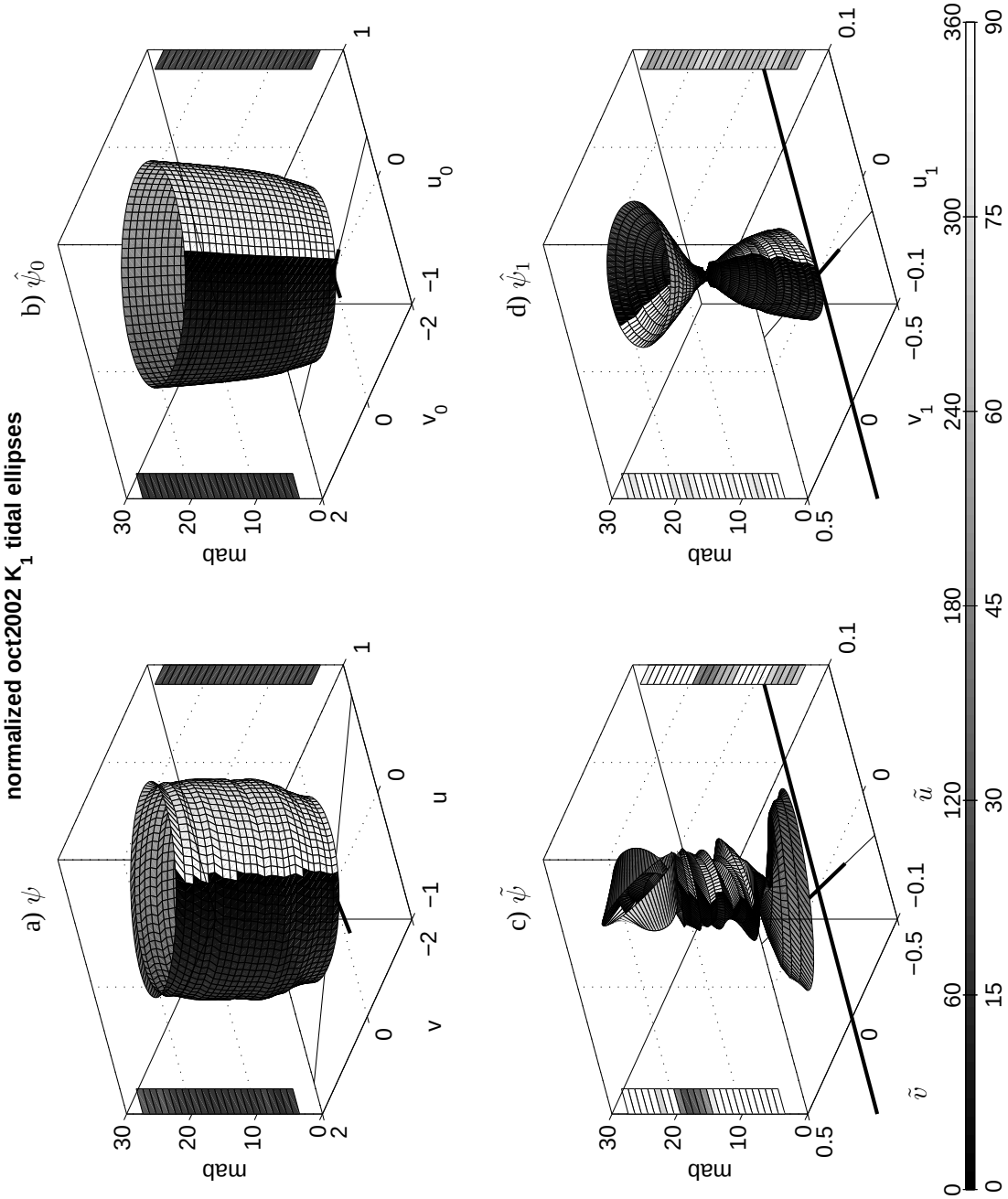

Figure 7: K_1 tidal ellipses and ellipse parameter errors for October 2002 data: a) the original signal $\psi(z,t)$, b) $\hat{\psi}_0(z,t)$, c) $\tilde{\psi}(z,t)$, and d) $\hat{\psi}_1(z,t)$, following the same convention as Fig. 3. Ellipse semi-axes and semi-axis errors are normalized by the semi-major axis of the near-surface ellipse of the synthetic K_1 signal shown in Table 1.

tween the profiles of the $\hat{\psi}_0$ and ψ ellipses suggest a superposition of internal and external modes at this frequency. Both the $\tilde{\psi}$ and $\hat{\psi}_1$ ellipses are of statistically significant magnitudes (of the order of 1-2 cm/s) and have similar profile shape in the vertical (Figs. 8c,d), but near-surface, $\hat{\psi}_1$ is more consistent.

Summarizing this section, CEOF analysis yields an estimate of barotropic tidal currents that includes the frictional boundary layer structure primarily associated with barotropic tidal dynamics; depth-averaging methods assume any vertical variability in the measured velocity time series is due to baroclinic motion. Tidal analysis of $\tilde{\psi}$ suggests significant internal tidal currents at the M_2 and O_1 frequencies, whereas analysis of $\hat{\psi}_1$ indicated significant internal tidal variability only at the O_1 frequency. The estimates of barotropic tidal motion using depth-averaging and EOF methods produce conflicting predictions of the frequencies at which there is meaningful baroclinic variability.

2.4 Discussion

In both idealized shallow water records of tidal currents and field-measured currents, CEOF analysis provides a better estimate of the barotropic tide than depth-averaging methods, and thus can allow more accurate representation of internal tides in measured data in shallow water. The representation of the barotropic tide as a depth-averaged signal cannot account for the modification of the barotropic tide by bottom friction. When the internal tidal structure is estimated by subtracting the depth-average from the original signal, frictional effects can be misinterpreted as arising from the baroclinic tide, for example, the M_2 signal in $\tilde{\psi}$ for both the synthetic and measured datasets. Estimates of barotropic tidal currents using CEOF analysis can retain in $\hat{\psi}_0$ this frictional boundary layer as part of the barotropic tide, providing a more accurate representation of internal structure in higher modes.

Though the data and time frame used here for comparison of CEOF and depth-averaging methods were primarily chosen to minimize potential internal tidal variability, both methods of separating the surface and internal tides identify an unanticipated internal structure given the well-mixed conditions. At this latitude (31.4° N), diurnal tidal frequencies fall into the inertial/near-inertial band, and the tidal and near-inertial processes can be harmonically indistinguishable given a time series of this length. While the strength and vertical structure of $\hat{\psi}_0$ at O_1 and K_1 are consistent with that of barotropic tidal currents, the signal in $\hat{\psi}_1$ suggests an inertial response. The mode-1 shape of the diurnal/near-diurnal variability may be attributed to inertial oscillations near a coastal boundary rather than the baroclinicity of the mass field (*Rippeth et al.*, 2002; *Davies and Xing*, 2003). CEOF analysis separates the signal into modes that allow interpretation of the diurnal band as dominated by a tidal signal apparent in

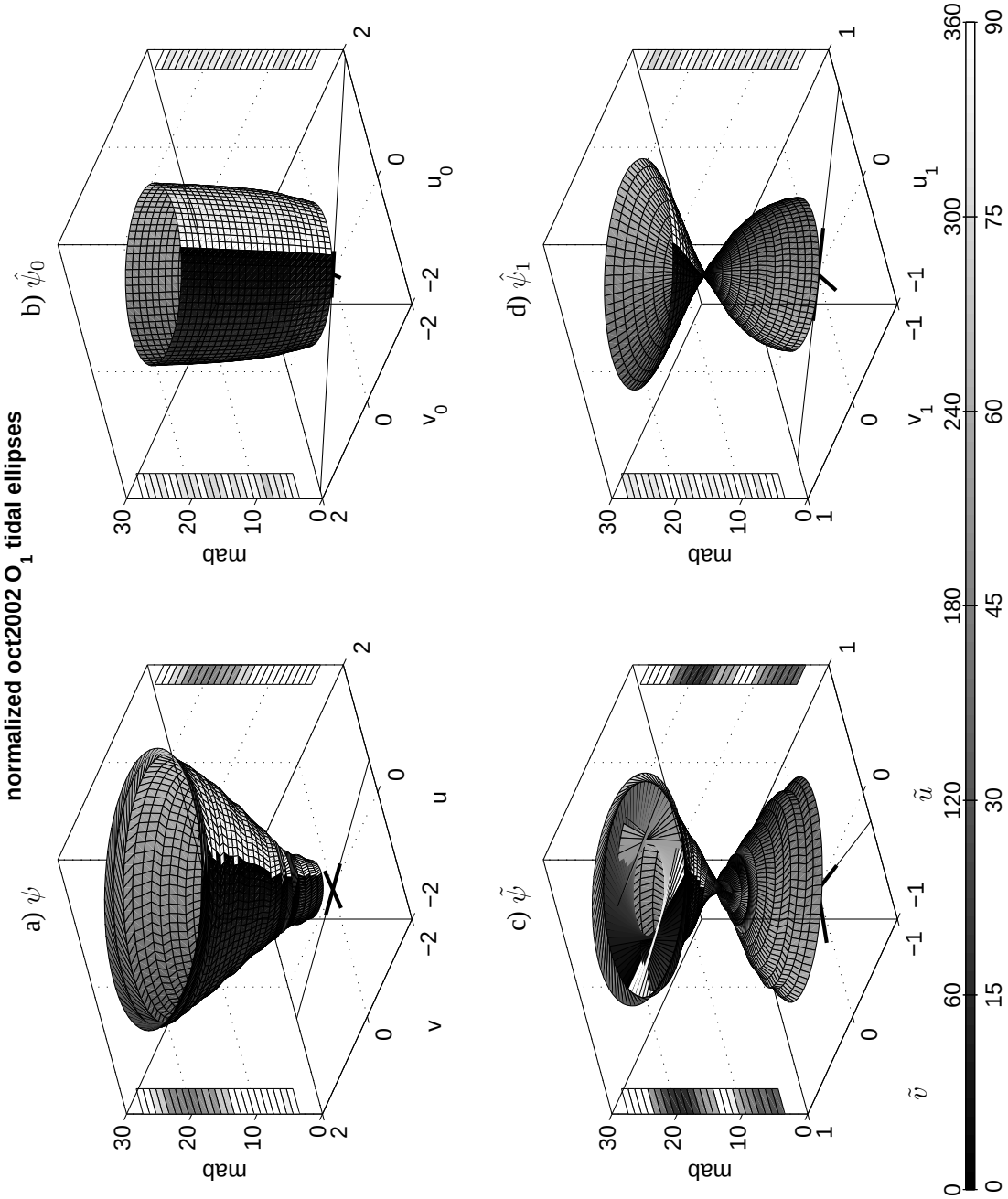

Figure 8: O_1 tidal ellipses and ellipse parameter errors for October 2002 data: a) the original signal $\psi(z,t)$, b) $\hat{\psi}_0(z,t)$, c) $\tilde{\psi}(z,t)$, and d) $\hat{\psi}_1(z,t)$, following the same convention as Fig. 3. Ellipse semi-axes and semi-axis errors are normalized by the semi-major axis of the near-surface ellipse of the synthetic O_1 signal shown in Table 1.

$\hat{\psi}_0$ and wind-forced inertial/near-inertial oscillations apparent in $\hat{\psi}_1$. While the variance in $\hat{\psi}_1$ is less than 1% of the total variance, the signal represents currents of 2-3 cm/s, approaching or exceeding the magnitude of $\hat{\psi}_0$ in the diurnal band. The unpredicted energy in $\hat{\psi}_1$ in the diurnal band indicates that the CEOF method correctly separates into independent modes two processes that are indistinguishable via harmonic analysis. Potential forcing by diurnal sea breeze and near-resonant response is beyond the scope of this analysis but is currently being explored.

Both CEOF and depth-averaging methods agree in predicting significant energy at O_1 that is not explained by the barotropic tide, and an inertial response is a plausible physical mechanism to explain the presence of increased diurnal energy at this latitude. However, separating the barotropic and baroclinic tidal currents using depth-averaging methods suggests an energetic M_2 internal tide of 2-5 cm/s which is not predicted by CEOF analysis. The resemblance of $\tilde{\psi}$ for measured data to the synthetic barotropic signal supports the notion that bottom boundary layer structure associated with the barotropic tidal dynamics can mistakenly be interpreted to result from an internal tide when depth-averaging is employed in shallow water. The present results suggest that CEOF analysis allows for a better representation of the vertical structure of internal waves and tides in energetic shallow water environments.

As with any empirical method, however, careful consideration must be given to the applicability of the method and particularly to interpretation of the results. The analysis above interprets the lowest CEOF mode to be the barotropic tidal motion modified by bottom friction, with the higher orthogonal modes indicating energy in the baroclinic tide. While the empirical modes are by definition orthogonal to each other and that the input velocity can be represented by the linear sum of the modes, barotropic and baroclinic dynamics are not linearly independent. When nonlinear friction is important over much of the water column, there can be significant coupling of the barotropic and baroclinic tidal signals. The structure of the bottom boundary layer is set by the sum of barotropic and baroclinic velocities, but the analysis assumes each will be independently modified by friction. In this coupling of barotropic and baroclinic tidal dynamics by nonlinear friction, a challenge can arise in separating barotropic and baroclinic modes when the amplitudes of the modes are comparable and thus both contribute significantly to the frictional response. Semidiurnal internal tidal currents in the SAB are not expected to be comparable to the 30-40 cm/s barotropic tidal current signal, but the analysis above predicts $\hat{\psi}_1$ to be of the same order as $\hat{\psi}_0$ at the O_1 frequency. Here, the two signals at O_1 have been interpreted as arising from non-tidal and tidal dynamics and the total energy in the higher modes is much less than that of $\hat{\psi}_0$, but the degree to which the coupling of barotropic and baroclinic modes hampers their separation using CEOF analysis remains unclear.

The CEOF method allows for the analysis of inertial oscillations or internal tidal motions that may or may not be phase- or frequency-locked to barotropic processes. In contrast, removing a depth-average of a tidal current imposes direction and phase information on the resultant estimate of baroclinic currents. Near-surface, $\bar{\psi}$ underestimates the barotropic flow by several cm/s in the SAB, which results in a near-surface $\tilde{\psi}$ that is in phase with $\bar{\psi}(t)$. Near-bottom, where the overestimate of the barotropic currents can be tens of cm/s, depth-averaging casts a 180° phase difference between $\bar{\psi}(t)$ and near-bottom $\tilde{\psi}$.

The CEOF method's assumption of independence of vertical and temporal variability can break down when vertical structure is dependent on time or frequency content. Analysis of synthetic tidal data containing multiple tidal frequencies successfully recovered these slightly varying vertical structures into the lowest mode. Application of the method to several years' worth of ADCP currents measured on the SAB in water depths ranging from 15 to 45 m (not shown) yields similar results as those presented here for a mid-shelf location – the boundary layer structure of barotropic currents is contained in the lowest mode, allowing for a more accurate estimate of the internal structure. However, practical experience with multi-year time series over this spatial array suggests particular consideration be paid to the time scales over which the character of the profiles may change. In the SAB, seasonal stratification appears to be the most important control. Time series lengths greater than 3 months tend to yield a decomposition in which the gravest mode can no longer fully describe the barotropic tide, and part of the variance is shunted to a higher mode. This result is consistent with observational estimates of bottom boundary layer thickness that suggest that the height of the bottom boundary layer changes as the seasonal stratification varies (Muglia et al., unpublished). Experimentation with input time series length can be a useful indicator of validity of the assumption that the lowest mode fully contains the barotropic tide. Significant change in structure advises shorter input time series length, with a minimum given by the Rayleigh criterion for the frequency resolution of interest.

An estimate of the error in neglecting slight differences in vertical structures among the dominant semidiurnal, M_2, and the other major constituents can be calculated using *Soulsby*'s linear eddy viscosity model over a range of tidal frequencies and latitudes. The depth-averaged normalized difference between the vertical structure of M_2 and tidal frequencies between 0.75 and 2.25 cpd is examined (Fig. 9), assuming that the frequencies compared have the same magnitude of free-stream velocity maximum. Errors are greatest at the local inertial frequency, where the singularity in the *Soulsby* (1990) formulation gives a boundary layer of infinite vertical extent. Increasing the northern latitudinal bound of Fig. 9 would reveal a second error maximum at the latitude where the M_2 tide becomes critical (74.48° N). For this application, the depth-averaged normalized error is as large as 11% for K_1, but the CEOF approach

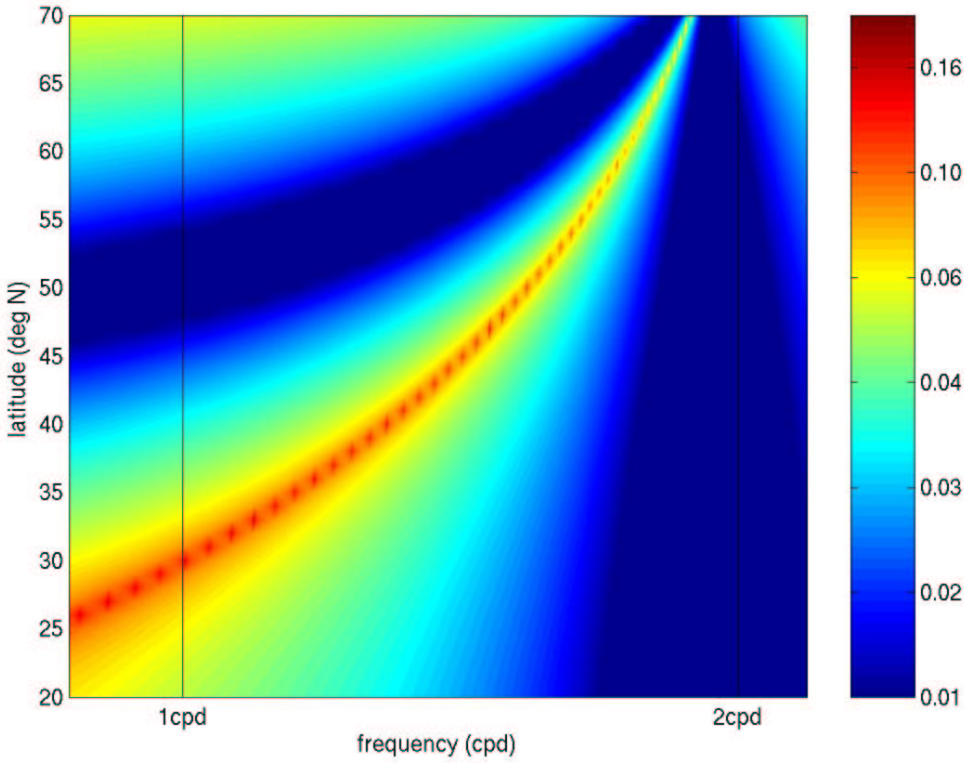

Figure 9: Normalized bulk error in assuming the vertical structure of M_2 for tidal currents of a given frequency over a range of latitudes. The error estimate is formed by vertically averaging the magnitude of the vector difference between normalized tidal current profiles relative to M_2 using the linear eddy viscosity model of Soulsby (1990).

is able to aggregate all synthetic tidal frequencies into a single mode (Table 1), which suggests some degree of flexibility in application of the method, even at a latitude where expected error is large.

2.5 Summary

A CEOF method of separating the barotropic and baroclinic tidal velocity structures is shown to be a significant improvement over assigning the depth-averaged current to be the barotropic component in shallow water. The representation of baroclinic tidal motions as the difference between velocity profiles and a depth-average cannot account for frictional shear in the bottom boundary layer and results in an overestimate of internal tidal motions that can resemble a bottom-trapped internal tide. CEOF analysis reduces the error in removing a synthetic barotropic signal modified by friction. Application of the method to measured data suggests similar advantages over depth-averaging. Whereas the analysis of $\tilde{\psi}$

suggests multiple possible internal modes of motion at tidal frequencies, the EOF method unambiguously separates a potentially wind-forced structure (i.e., near-inertial motion) from the barotropic tide despite the overlay in frequency space. The successful application of the method to unfiltered data measured in an energetic shallow water environment of the SAB constitutes a significant test of the method, and suggests that CEOF analysis can be a valuable tool for the investigation of internal waves, inertial motions, and tides on continental shelves and in other shallow water environments.

Table 1: Synthetic near-surface tidal ellipse parameters for the five largest tidal constituents for the specified input signal $\psi(z,t)$ (left), the depth-average of the 30-day synthesized current $\bar{\psi}_z(t)$ (above right), and of the lowest CEOF mode $\hat{\psi}_0(z,t)$ (below right). The 95% confidence intervals about the ellipse parameter estimates for $\bar{\psi}_z(t)$ and for $\hat{\psi}_0(z,t)$ are given.

Tidal Constituent	$u_{major}(cm/s)$ ψ	$\bar{\psi}_z$ $\hat{\psi}$	$u_{minor}(cm/s)$ ψ	$\bar{\psi}_z$ $\hat{\psi}$	Incl (deg) ψ	$\bar{\psi}_z$ $\hat{\psi}$	Phase (deg) ψ	$\bar{\psi}_z$ $\hat{\psi}$
M_2	38.15	33.77 $\pm$ 3.60 38.16 $\pm$ 7.3e-05	-13.31	-11.74 $\pm$ 1.28 -13.27 $\pm$ 2.1e-04	153.87	154.01 $\pm$ 0.10 154.06 $\pm$ 0.15	280.48	280.16 $\pm$ 0.24 280.18 $\pm$ 0.24
N_2	8.30	7.35 $\pm$ 0.78 8.31 $\pm$ 1.4e-05	-2.88	-2.54 $\pm$ 0.28 -2.87 $\pm$ 4.7e-05	152.34	152.48 $\pm$ 0.10 152.52 $\pm$ 0.15	264.54	264.22 $\pm$ 0.23 264.24 $\pm$ 0.23
S_2	4.34	3.84 $\pm$ 0.41 4.34 $\pm$ 1.1e-05	-1.43	-1.26 $\pm$ 0.14 -1.42 $\pm$ 2.4e-05	152.22	152.36 $\pm$ 0.10 152.41 $\pm$ 0.15	307.42	307.09 $\pm$ 0.24 307.11 $\pm$ 0.24
K_1	1.94	1.72 $\pm$ 0.18 1.94 $\pm$ 9.9e-06	-0.95	-0.84 $\pm$ 0.09 -0.95 $\pm$ 1.5e-05	135.40	135.57 $\pm$ 0.12 135.62 $\pm$ 0.17	111.42	111.23 $\pm$ 0.13 111.25 $\pm$ 0.13
O_1	1.37	1.21 $\pm$ 0.13 1.37 $\pm$ 6.7e-06	-0.68	-0.60 $\pm$ 0.07 -0.68 $\pm$ 9.9e-06	133.24	133.39 $\pm$ 0.11 133.44 $\pm$ 0.16	117.78	117.58 $\pm$ 0.14 117.60 $\pm$ 0.14

CHAPTER 3. Sea breeze/land breeze near the resonant critical latitude in the Georgia Bight

3.1 Introduction

Inertial response of the ocean to wind forcing is widely described in the literature (e.g., *Pollard and Millard*, 1970), but previous studies generally have focused on either low frequency variability in the wind or a wind impulse forcing the surface ocean. Near 30°N or S, the local inertial and diurnal frequencies coincide, and an inertial response of the atmosphere or the surface ocean is resonant with diurnal forcing. The sea breeze/land breeze (SBLB) system is the mesoscale atmospheric circulation that develops in response to diurnal variability in horizontal temperature gradients in the atmosphere at the land-sea interface. Studied in many coastal regions due to its profound effects on coastal meteorology and potential to transport pollutants (*Simpson*, 1994), SBLB may be enhanced at 30°N or S, the critical latitude for diurnal/inertial resonance.

SBLB is typically confined to a short distance from the coastline, 40-80 km (e.g., *Simpson*, 1994). However, *Clarke* (1955) tracked a sea breeze front propagating nearly 300 km inland from the southern coast of Australia near 31°S. There is observational evidence that the SBLB system of the Texas-Louisiana coastline, an east-west coastline at about 30°N, may extend on the order of hundreds (*Nielsen Gammon*, 2001) up to 1000 km across the Gulf of Mexico to the Yucatan Peninsula (S. DiMarco, pers. comm.). These estimates of the extent of SBLB variability near 30°N or S suggest that resonance may significantly amplify the scale of SBLB near the critical latitude.

In a comprehensive spectral analysis of the National Data Buoy Center STDMET data set, *Stockwell et al.* (2004) found increased inertial energy at all latitudes, but particularly near 30°N/S, and suggest that diurnal winds may serve as a significant source for energy transfer from the atmosphere into the ocean near these critical latitudes. *Skyllingstad et al.* (2000) describe an increased efficiency of mo-

mentum and energy transfer from resonant wind forcing into the ocean's surface boundary layer. Ocean observations and modeling studies in the northwestern Gulf of Mexico (*Daddio et al.*, 1978; *Chen and Xie*, 1997; *DiMarco et al.*, 2000) and off the coast of Namibia (*Simpson et al.*, 2002) report increased inertial/diurnal energy, but a large-scale comparison of the wind forcing and the coastal ocean response has not been described for a location with near-resonant interaction between SBLB and the coastal ocean response.

Significant non-tidal diurnal/inertial currents have been observed in the Georgia Bight (*Edwards and Seim*, 2008a), defined here as the embayment bounded by Cape Romain, SC and Cape Canaveral, FL. The response to SBLB wind forcing and potential mechanisms for internal wave generation in the Georgia Bight may differ from the idealized cases represented by *Davies and Xing* (2003), as the coastline is not straight and the SBLB generated across it may not be spatially uniform. Knowledge of the SBLB system in the Georgia Bight is critical to understanding the potentially shelf-wide wind forcing near the resonant frequency.

In this paper, SBLB theory is examined to first provide a context for the description of the offshore structure and variability of SBLB in the Georgia Bight, with particular attention to potential changes in SBLB structure through the critical latitude. Using a combination of observed and modeled wind fields, the spatial patterns of diurnal wind variance in the Georgia Bight are compared to those predicted by SBLB theory. Fitting SBLB ellipse parameters to the diurnal variability in the observations, three case studies during summers 2006 and 2007 are investigated more closely. Finally, the timing of SBLB with respect to the diurnal heating cycle is examined, compared to SBLB theory, and assessed as a potential mechanism for generation of near-inertial internal waves in the coastal ocean of the Georgia Bight.

3.2 Theory of the sea breeze/land breeze

Linear sea breeze theory is a useful and attractive framework for description of SBLB structure and for comparison with observations and numerical models. The governing equations for the SBLB system are:

$$\frac{\partial u}{\partial t} + u\frac{\partial u}{\partial x} - fv = -\frac{1}{p}\frac{\partial p}{\partial x} + \mathcal{F}(u) \tag{3.2.1}$$

$$\frac{\partial v}{\partial t} + u\frac{\partial v}{\partial x} + fu = -\frac{1}{p}\frac{\partial p}{\partial y} + \mathcal{F}(v) \tag{3.2.2}$$

$$\frac{\partial w}{\partial t} + u\frac{\partial w}{\partial x} = -\frac{1}{p}\frac{\partial p}{\partial z} + \mathcal{F}(w) + b \tag{3.2.3}$$

$$\frac{\partial b}{\partial t} + u\frac{\partial b}{\partial x} + N^2 w = \mathcal{D}(b) \tag{3.2.4}$$

$$\frac{\partial u}{\partial x} + \frac{\partial w}{\partial z} = 0 \tag{3.2.5}$$

where (u, v, w) correspond to wind speeds in the cross-shore, alongshore, and vertical directions (x, y, z), and pressure p, and buoyancy b vary in three dimensional space and time. Buoyancy is directly proportional to potential temperature θ, and is equal to $g\beta\theta$, where β is the thermal expansion coefficient. The Coriolis parameter is f, and the Brunt Vaïsälä frequency, N, is the ambient stratification in the atmosphere given by the vertical change in air density ρ_o: $N^2 \equiv -\frac{g}{\rho_o}\frac{\partial \rho_o}{\partial z}$ ($\equiv g\Gamma\beta$, where β is the thermal expansion coefficient and Γ is the adiabatic lapse rate). The functions $\mathcal{F}$ and $\mathcal{D}$ represent frictional and diffusive processes acting on (u, v, w) and b, respectively.

Several studies of SBLB in the literature estimate the strength and horizontal extent of SBLB with various scalings of the above equations, with different representations of friction, and consider the effect of latitude on the system. All scalings are based on linear formulations that neglect advection in the momentum and buoyancy equations, though *Walsh* (1974) considered the influence of a mean cross-shore flow U. Estimates of scale for these models are given by the Rossby radius of deformation, empirical calculations based on model simulations (*Ueda*, 1983; *Niino*, 1987), or considering the wave properties of the solutions with $\mathcal{F}$=0 for the inviscid case (*Rotunno*, 1983) and $\mathcal{F} = r$ for linearized friction (*Dalu and Pielke*, 1989). Table 2 summarizes these models and their estimates of α, the ratio of the horizontal and vertical scales of sea breeze.

Walsh (1974) observed that horizontal scale δ increased with increasing stratification, and proposed that δ might be analogous to the Rossby radius, NH/f, where H is a vertical scale. Assuming that H scales as the diffusion length $(\kappa/\omega)^{1/2}$ for SBLB at the diurnal frequency ω, *Niino*'s interpretation of *Walsh* (1974) suggested that $\delta = N(\kappa/\omega)^{1/2}/f$. The equivalent aspect ratio, $\alpha \equiv \delta/H = N/f$, suggests a maximum at the equator for constant N. However, *Walsh*'s non-hydrostatic model, which assumes that the atmosphere exchanges heat and momentum on the same scale (i.e., the Prandtl number $Pr \equiv \nu/\kappa = 1$), showed a maximum offshore extent at the inertial latitude. *Niino*'s simple assumption of scale based on the Rossby radius alone does not adequately describe the *Walsh* (1974) model results.

Table 2: Scaling the horizontal extent of SBLB: Aspect ratio of SBLB given by the Rossby radius of deformation and four linear theories of SBLB. Assumptions of each model and its dynamics are also given for reference.

	Model dynamics	$\alpha \equiv \delta/H$
Horizontal scale set by Rossby radius	Rotation $\approx$ buoyancy	$R_o/H = N/f$
Ueda (1983)	Linear, non-hydrostatic $\mathcal{F} = \nu\nabla^2, \mathcal{D} = \kappa\nabla^2$	$0.669(N/\omega)^{0.774} Pr^{1/4}$
Niino (1987)	Linear, non-hydrostatic, $Pr = 1$ $\mathcal{F} = \nu\nabla^2, \mathcal{D} = \kappa\nabla^2$	$N\frac{F(f)}{\omega}$
Rotunno (1983)	Linear, hydrostatic, inviscid ($Pr = 0$) $\mathcal{F} = r, \mathcal{D}$ periodic function of ΔT	$N\lvert\frac{1}{(f^2-\omega^2)}\rvert^{1/2}$
Dalu and Pielke (1989)	Linear, hydrostatic, $Pr = 1$ $\mathcal{F} = r, \mathcal{D}$ periodic function of ΔT	$\lvert\frac{N^2+r^2}{f^2+r^2-\omega^2}\rvert^{1/2}$

Ueda (1983) extended the *Walsh* (1974) formulation of the problem by allowing Pr to vary. The empirical scaling of the analysis gave $\delta = 0.936(N/\omega)^{0.774}$, and the vertical scale $H = 1.40Pr^{-1/4}$, scaling δ and H with stratification and friction rather than latitude. Combining these estimates of scale, the aspect ratio α can be expressed as $0.669(N/\omega)^{0.774}Pr^{1/4}$. *Niino* (1987) also took an empirical approach, considering a linearized non-hydrostatic implementation of the SBLB model with $Pr = 1$. By noting that the non-hydrostatic solution was confined close to the coastline, and rescaling the non-dimensional equations of motion with a measure of stratification, *Niino* (1987) found that δ is directly proportional to N. Aspect ratio α then is given by $\alpha = N\frac{F(f)}{\omega}$, where $F(f)$ is an empirically derived function of latitude. The variability of F with latitude suggests a maximum of horizontal scale at the tropics and a steep drop-off in horizontal scale near the critical latitude (see *Niino*, 1987, Fig. 9).

Rotunno (1983); *Dalu and Pielke* (1989) based their estimates of horizontal scale on the linearized equations of motion, considering the aspect ratio and horizontal scale implied by a wave-like solution. The derivation of horizontal scale relies on the dispersion relation. Defining a linear friction coefficient to be r and assuming no variation in the y-direction, the equations of motion reduce to a 4th order equation for w. Assuming a wave-like solution and recognizing that $N \approx 10^{-2}s^{-1} \gg \omega$, the dispersion relation implies an aspect ratio of $\alpha = \left\{\frac{(N^2+r^2)}{|f^2+r^2-\omega^2|}\right\}^{1/2}$, or a horizontal scale $\delta = H\left\{\frac{(N^2+r^2)}{|f^2+r^2-\omega^2|}\right\}^{1/2}$.

For the inviscid ($r = 0$) case considered by *Rotunno* (1983), δ reduces to $NH|(\omega^2 - f^2)|^{-1/2}$, the internal Rossby radius of deformation. The value of δ with diurnal forcing is infinite at the critical latitude, 30°N or S, where the form of the solution changes from a propagating wave equatorward of the critical latitude to a trapped disturbance poleward of the critical latitude. *Rotunno* (1983) suggested that the imposition of friction would give a finite horizontal scale at 30°, which is shown by *Dalu and*

Pielke (1989) with the addition of linear friction as above.

Thus, the horizontal scale of motion is set by the relative importance of friction, stratification, and latitude even in a relatively simple theoretical framework. Figure 10 shows α/N as a function of latitude for the references cited above. The Rotunno curve corresponds to $r = 0$, and in the case where $r = \omega$, δ collapses to the Rossby radius predicted by *Niino*'s analysis of *Walsh* (1974). Increasing the importance of friction relative to rotation with intermediate values of $0 < r < \omega$ moves the latitude of maximum horizontal scale equatorward to the latitude that corresponds to $r + f$. At $r > \omega$, rotational effects are increasingly damped by friction; maximum δ lies at the equator, with reduced horizontal scale at all latitudes.

The modeling studies of *Yan and Anthes* (1987) and *Arritt* (1989) investigate the effect of latitude on the development of SBLB through numerical simulations, and consider the sea breeze and land breeze phases separately. *Arritt* (1989) found that the scale of sea breeze was generally well-predicted by the *Rotunno* (1983) theory, but that the offshore extent reached a maximum on the order of 100 km between 20 and 30°(most similar to the $r = 0.5\omega$ case in Fig. 10). Observational estimates of δ derived from kinematic sensible heat flux ($= \overline{w'T'}$), the land-sea temperature gradient, the base state and environmental lapse rate of potential temperature show that the extent of sea breeze decreases with latitude (*Steyn*, 2003). However, the mid-latitude range examined does not pass through the critical latitude into the tropics. *Yan and Anthes* (1987) report a maximum horizontal extent of sea breeze in the tropics, but find that the land breeze near 30°has an enhanced horizontal extent and is stronger than that north or south of the critical latitude. The authors suggest that, near 30°, the Coriolis force may augment or dominate the pressure gradient that produces land breeze.

Any potential change in SBLB phase with latitude may be a consequence of the importance of the Coriolis effect in producing the land breeze. *Yan and Anthes* (1987) did find significant changes in the time of arrival of the land breeze, with land breeze arriving later toward the equator. Neglecting friction, *Rotunno* (1983) predicted fundamental changes in SBLB dynamics at the critical latitude, including a 180°change in phase at 30°. Poleward of the critical latitude, SBLB behaves like a trapped disturbance and is directly forced by the diurnal heating cycle, with sea breeze winds in phase with the temperature gradient that develops during the day. At tropical latitudes, SBLB may propagate freely as an atmospheric internal wave, and the equations of motion imply that sea breeze winds are 180°out of phase with forcing. *Rotunno* (1983) recognized the peculiarity of this aspect of the solution, suggesting that the addition of friction would cause the arrival of sea breeze to be slightly delayed at lower latitudes but would largely remove the change of phase with latitude. However, the models of *Walsh* (1974); *Ueda*

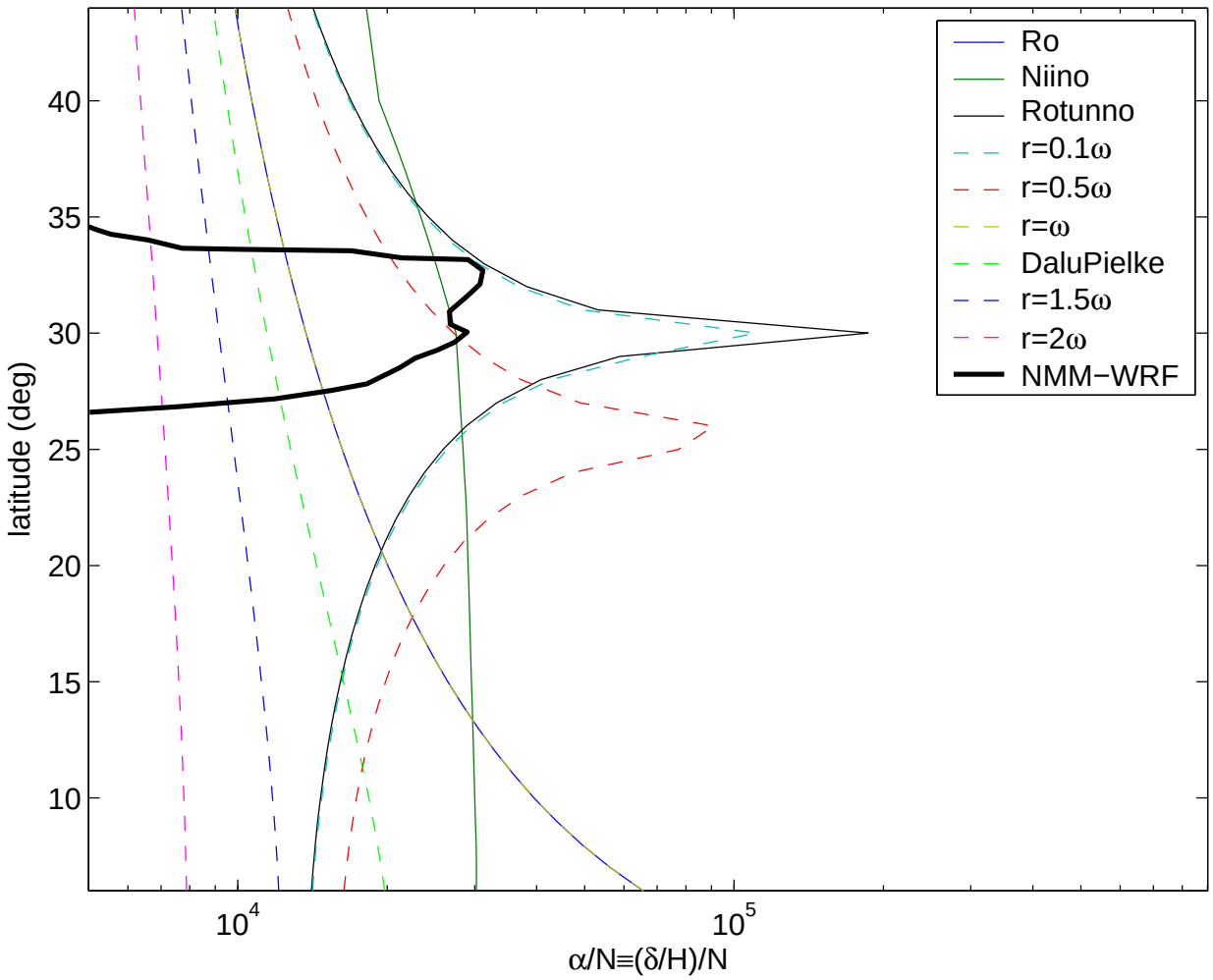

Figure 10: The aspect ratio, horizontal extent δ over the vertical scale H, of SBLB with horizontal scales given by R_o, the linear theories of *Niino* (1987); *Rotunno* (1983); *Dalu and Pielke* (1989), and the generalized linear theory presented above. *Rotunno*; *Dalu and Pielke* correspond to the general linear case ($r = 0, 1.2\omega$, respectively). The estimates of $\delta(r = \omega)$, dashed gold, collapses to the Rossby radius (blue). Aspect ratio for SBLB using the NMM-WRF model is an order of magnitude smaller than the estimates from linear theory assuming a vertical scale (κ/ω) and N=0.01 s^{-1}.

(1983); *Niino* (1987), which include frictional effects, give no change in phase of SBLB relative to the diurnal heating cycle as latitude is varied.

None of the linear models of SBLB theories differentiates between the landward and seaward extents of sea breeze or land breeze, despite the significant differences in the relative importance of friction and perhaps heat transfer across the land-sea interface. As pointed out by *Dalu and Pielke* (1989), the scale of SBLB is determined by the relative importance of latitude, friction, and stratification. *Nielsen Gammon* (2001) suggested that the simpler, inviscid *Rotunno* (1983) model might be sufficient to describe the seaward extent of SBLB, while a model with more complete dynamics and a better representation of friction, such as that of *Niino* (1987), might be more appropriate for the region near and landward of the coastline.

It is worth noting that the horizontal extent derived from each of these models is independent of the land-sea temperature difference ΔT, but the dynamics suggest that the velocity scale will increase as larger ΔT induces greater pressure gradients. *Dalu and Pielke* (1989) found that sea breeze wind speed is proportional to the temperature forcing and increases equatorward: $\tilde{u} = Q_o/(f^2 + r^2)$, where Q_o is the change in the diabatic forcing function at the coastline, proportional to ΔT. Taking $r = 0$ reduces $\tilde{u}$ to Q_o/f^2 for the inviscid case, but *Rotunno* (1983) predicted a horizontal velocity proportional to $N^{-1}(f^2 - \omega^2)^{-1/2}$, with no reference to the diabatic heat forcing. *Niino* (1987) implied that $\tilde{u}$ scales as $g\beta\Delta T/N$, proportional to the temperature difference, but variability with latitude is not specified. *Ueda* (1983) did not vary ΔT and found a velocity scale $\tilde{u} = 0.406(\omega/N)Pr^{-2/3}$ that is independent of latitude, as was the estimate of horizontal scale.

An alternate estimate of the scale of SBLB wind velocity can be derived by considering the sea breeze front to propagate onshore as a gravity current with velocity $u_{front} = \kappa(gH\Delta T/T)^{1/2}$ (*Simpson*, 1994). However, away from the non-hydrostatic region of the front, rotation must be considered and is anticipated to be significant near the critical latitude (e.g., *Yan and Anthes*, 1987). Comparison of the propagation speed of SBLB and the SBLB wind speeds to these various scalings of $\tilde{u}$ can give an estimate of the importance of the Coriolis force to the SBLB dynamics in the Georgia Bight.

3.3 SBLB in the Georgia Bight

The structure and variability of the SBLB system in the Georgia Bight are largely undescribed by the literature, and the few general descriptions of the SBLB system in the literature have been focused on its landward extent. Various studies report sea breeze front penetration of at least 100-150 km inland into

Georgia (*Williams*, 1969; *Buckley and Kurzeja*, 1997b,a; *Weber*, 2003; *Kurzeja et al.*, 1991). Further north, *Frysinger and Lindner* (2003) and *Crouch* (2006) describe sea breeze front progression 20-40 km into South Carolina. Though *Crouch* (2006) notes periodic incursions on the order of 80-120 km, *Weber* (2003) suggests that bursts of SBLB can be observed as far inland as Raleigh, NC (225 km) and Augusta, GA (200 km).

Tunney (1996) has provided the only estimates of seaward extent of sea breeze in the Georgia Bight through development of a sea breeze forecast system in Wassaw Sound in advance of the 1996 Olympic Games sailing competitions. Under very idealized conditions, sea breeze is found to propagate 75 km inland, but 110 km offshore. Land breeze was found to be weak, with less than 12 km extent seaward or landward, an order of magnitude less than that of sea breeze. However, the model focused on forecasting ability under different prevailing wind conditions, and considered the evolution of the SBLB system for only two days. Neither observational studies nor realistic regional scale modeling has been conducted in the Georgia Bight, where the applicability of linear SBLB theory can be assessed near the critical latitude.

Linear theory provides a framework for comparison for the analysis of SBLB that follows. Figure 11 summarizes the predictions of *Rotunno* (1983); *Walsh* (1974); *Yan and Anthes* (1987), as applied to the Georgia Bight. The magnitude and offshore extent of SBLB winds are greatest near the critical latitude. A maximum rotational effect will be observed at 30°N, resulting in a more elliptical rather than rectilinear trace of the diurnal winds as the SBLB ellipses become more inertial (*Haurwitz*, 1947). Coastline curvature may serve to focus land breeze on the shelf, depending on the horizontal extent of SBLB relative to the radius of curvature of the Georgia Bight. The potential change in phase at 30°suggested by *Rotunno* (1983) is noted by the lightly shaded arrows.

Coastline curvature may enhance interaction with synoptic scale winds, which, in opposition to or aligned with SBLB circulation, will serve to inhibit or extend propagation of SBLB (*Estoque*, 1962; *Arritt*, 1989). SBLB may also self-interact due to coastline curvature. If the horizontal extent of SBLB is comparable to the radius of curvature of the Georgia Bight, SBLB may extend far enough from the coastline to interact with SBLB from across the Bight.

Coastline curvature may also be a significant control on not only the SBLB system, but also the coastal ocean's response. If the land breeze and sea breeze converge/diverge over the continental shelf, the pycnocline may be depressed and elevated at or near the diurnal frequency, which may generate near-inertial internal waves. Sea and land breeze are known to converge or diverge due to coastline curvature, with significant correlation to nocturnal thunderstorm occurrence (*Neumann*, 1951) – sea

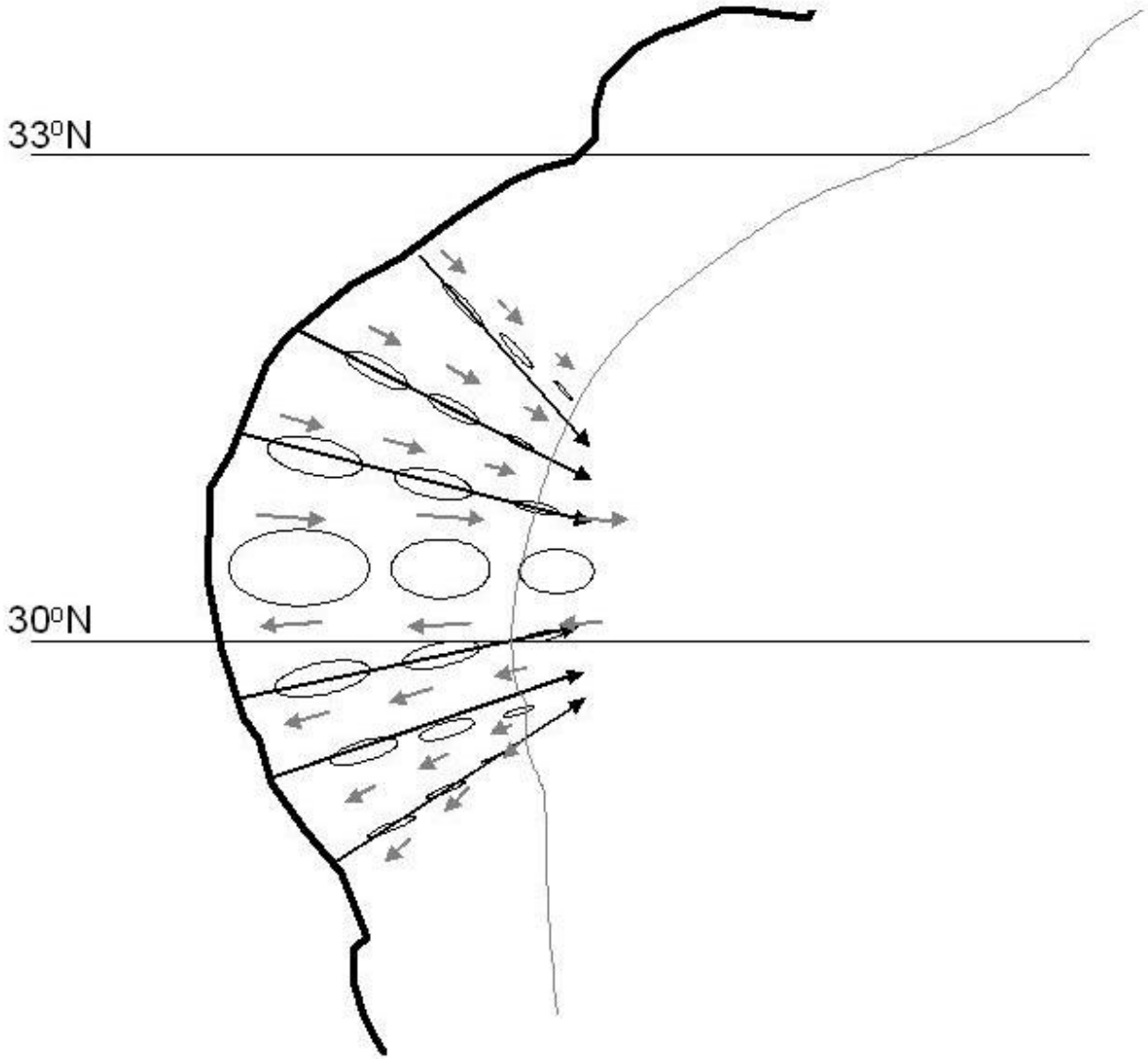

Figure 11: Cartoon of SBLB theory: a maximum of sea breeze magnitude and offshore extent at 30°N, with a minimum of ellipticity as the sea breeze ellipses become more inertial. Land breeze may converge over the shelf (bold arrows), and linear theories disagree as to changes in phase as latitude passes through the critical latitude (gray arrows). The 50 m isobath is shown for reference.

breeze convergence over the Florida peninsula is probably the earliest and best-studied example of this phenomenon (e.g., *Byers and Rodebush*, 1948). *Arritt*'s (1989) numerical model agrees with *Neumann*'s (1951) premise that concave/convex coastlines can cause convergence/divergence of the land breeze, if the radius of curvature of the coastline is smaller than the length scale of the seaward extent of land breeze. The radius of curvature of the Georgia Bight is on the order of 250 km, so coastline curvature may cause SBLB in the Bight to converge and diverge over much of the shelf. This effect may be enhanced if δ is comparable in magnitude to the radius of curvature of the embayment (*Neumann*, 1951). A climatology of when and where SBLB converges and diverges will enable a better understanding of the coastal oceanography.

3.4 Description of model, observations

The paucity of offshore meteorological observations is a significant obstacle in describing and verifying the seaward extent and offshore structure of the SBLB system in the Georgia Bight. Therefore, the SBLB system is described using a combination of analysis of observed and modeled winds. Wind observations in the Georgia Bight are collected at coastal stations maintained by the National Data Buoy Center (NDBC) buoys, Coastal-Marine Automated Network (C-MAN) stations, and at several towers on the shelf as part of the South Atlantic Bight Synoptic Offshore Observing Network (SABSOON, *Seim*, 2000) array (Fig. 12). The compilation of measurements is used to describe the along- and cross-shore variability in SBLB wind energy over the Georgia Bight north through the Carolina capes system. Wind measurements at NDBC buoy 41008 (33.5 km offshore, 15 m water depth) and SABSOON towers R2 and R6 (62.7/81.6 km offshore, 25/32 m water depth) are used to consider a quasi-cross-shore transect of SBLB structure and variability on shorter length scales.

The observations are not sufficient to completely describe the along- and cross-shore structure of SBLB in the Georgia Bight, and the description of large-scale features of the SBLB system relies on analysis of diurnal variability of near-surface wind fields given by the operational forecasting model Non-hydrostatic Mesoscale Model – Weather Research and Forecasting system (NMM-WRF). The National Center for Environmental Prediction's NMM, implemented via WRF, replaced the previous regional scale operational model, Eta, on June 20th, 2006. The model relaxes the hydrostatic condition, splitting the nonhydrostatic corrections to the hydrostatic dynamics using a hybrid pressure-sigma vertical coordinate system. Operational 60-hour forecasts and reanalysis fields are published on the NOAA Operational Model Archive Distribution System (NOMADS) server every 6 hours at 12 km resolution

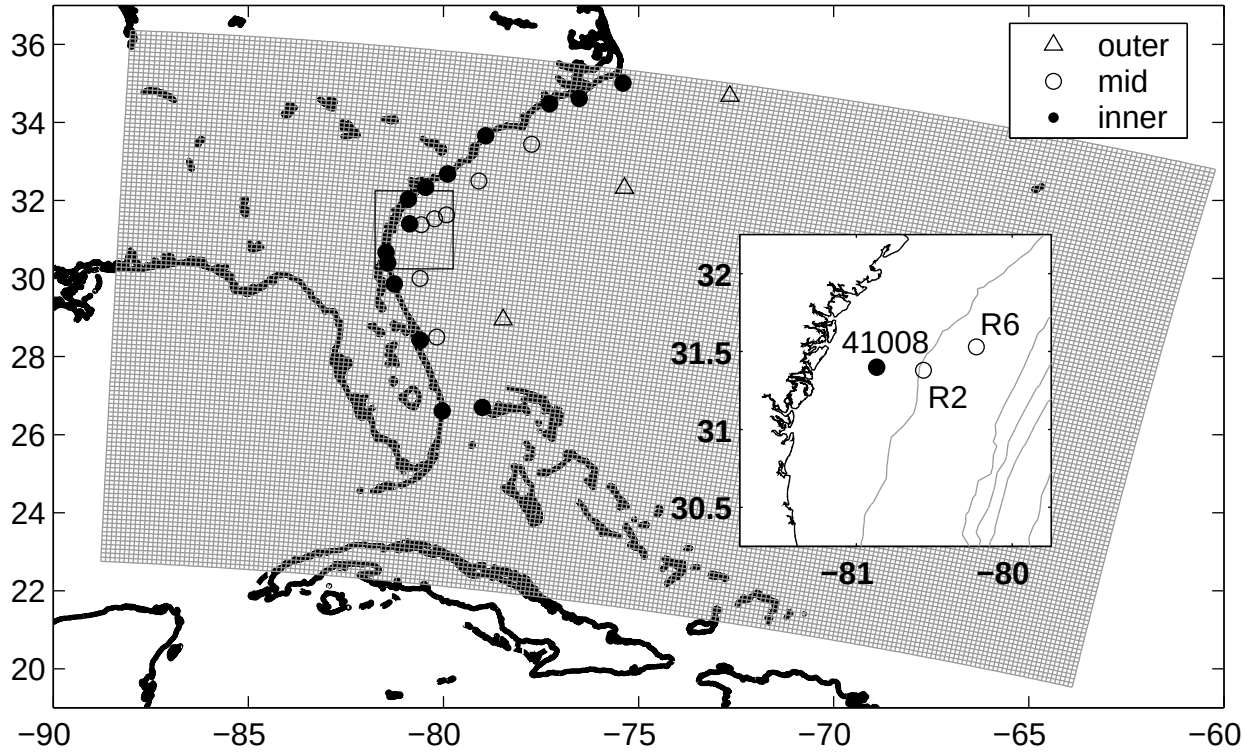

Figure 12: Map of the South Atlantic Bight, the NMM-WRF subgrid for diurnal analysis, and locations where observations are available. The observations are not necessarily coincident in time, but are coded by shape to give their location on the shelf, decreasing in number with distance offshore. The inset map shows the locations of the Gray's Reef buoy (41008) and the R2/R6 SABSOON towers, with the 25, 50, 100, 200, and 500 m isobaths for reference.

on the NCEP-218 grid spanning the continental United States. Further details of NMM-WRF model physics, data assimilation scheme, and computed fields are given by *Skamarock et al.* (2005).

With limited horizontal and temporal resolution in the reanalysis fields, the model cannot be expected to fully resolve SBLB. However, NMM-WRF is one of the few sources of operational winds available on regional scales. Higher resolution numerical weather prediction models are available and have demonstrated skill over land, but skill is not often assessed with comparable rigor offshore due to lack of measurements, particularly at distances greater than 100 km offshore. For many operational systems, larger-scale weather systems provide the basis of comparison, but knowledge of higher frequency wind variability contained by the wind forcing of the modeled ocean is essential, particularly near the resonant frequency.

A sub-grid of the NCEP-218 Lambert grid (Fig. 12) is used for further analysis and comparison to observations in the Georgia Bight. To isolate SBLB winds, the analysis is restricted to summer months after the June 2006 upgrade, when the importance of SBLB is expected to be greatest. Diurnal variability in the Eta model, operational from 1993-2006, is erroneously large in comparison to observations over the continental shelf. The diurnal spurious signal may be attributed to less sophisticated model physics, particularly those represented by the surface heat exchange module.

Figure 13 compares time series of unfiltered observed and NMM-WRF model reanalysis 10-m horizontal winds at three locations on the shelf of the Georgia Bight over two 10-day periods (Aug 02-12 2006 and July 05-15 2007). Observed near-surface winds contain significant diurnal variability, and although the standard deviation of model misfit is comparable to the magnitude of diurnal winds, 1.17-3.24 m/s, the diurnal variation of the model winds is visually coherent with the observations. The observed winds are filtered to admit an 8-hr frequency band about the diurnal (D1=20-28 hours) using a 4th order Butterworth filter; filtering of model winds requires a much higher order high-pass filter (8-10th order) to isolate diurnal variability. D1 wind variance computed as monthly estimates over July-September 2006 and 2007 in the observations ranges from 1.2-2.3 $m^2 s^{-2}$, representing 35-91% of the total variance of the unfiltered signal in the Georgia Bight.

The NMM-WRF model misfit suggests reduced model skill offshore, but even this level of skill represents a significant improvement relative to the Eta model. Comparison over 10-12 day Eta forecasts yield Eta model error twice that of the NMM-WRF, and spatial patterns that don't appear to reflect physical processes (Fig. 14). Diurnal variability is slightly underestimated by the NMM-WRF model at all locations except near Cape Canaveral and Cape Hatteras, but the level of error in the NMM-WRF model is deemed acceptable for the purposes of analyzing spatial patterns of SBLB in the Georgia Bight.

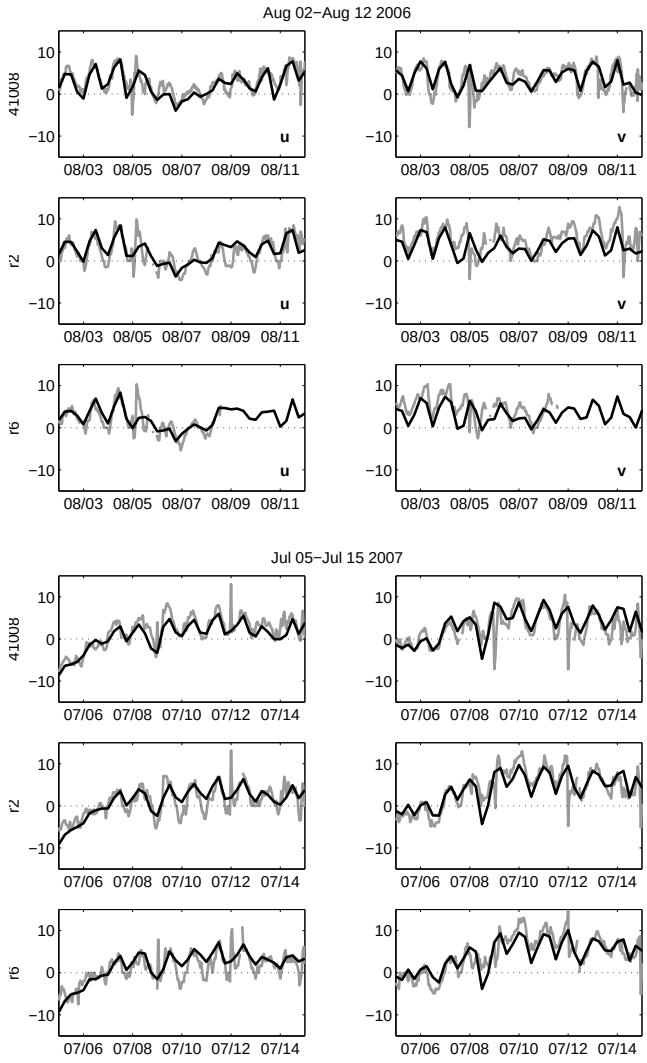

Figure 13: Time series of unfiltered NMM-WRF model (black) and observed (gray) winds at three locations on the inner to mid-shelf of the South Atlantic Bight for two 10-day periods of comparison. The model tracks generally observations and the diurnal variability contained within, with a slight underestimate of diurnal variance, but is an improved predictor of offshore winds compared to the Eta model.

3.5 Summer SBLB

Patterns of diurnal variance in the Georgia Bight are examined using the filtered winds from the reanalysis stage of the NMM-WRF model, and compared to the predictions of horizontal extent of SBLB from linear theory. Three 10-day periods are chosen as SBLB case studies, which are described in greater detail through available observations on the shelf. Trends and patterns in the phase of sea breeze winds with respect to the diurnal heating cycle allow for further comparison to linear theory.

3.5.1 Structure of SBLB

Figure 14 shows the diurnal variance of 10 m horizontal wind field over the model sub-grid, calculated over summer months 2006 and 2007. The filtering may admit non-SBLB sources of diurnal variability in the atmosphere, and no attempt is made to separate out the various sources of diurnal winds. In terms of internal wave generation in the coastal ocean, the dynamics that force the surface ocean near the resonant frequency are irrelevant. The diurnal variability in the model is generally confined to the region closest to the coastline, consistent with the pattern expected for SBLB, and is taken as evidence that SBLB is the dominant source of diurnal variability during this time period.

The filtered model winds show enhanced diurnal variance within tens of kilometers of the coastline, but augmented variance is apparent near 30°N on both the Georgia Bight and the small portion of the Gulf of Mexico contained by the sub-grid. However, the strongest diurnal variance and greatest extent offshore for all summer months occur in the Georgia Bight, where SBLB winds of 1-2 m/s extend 250 km offshore. Figure 15 shows the zonal maximum of diurnal variance in the NMM-WRF model winds as a function of latitude, computed by month. The maximum of diurnal variance coincides with the critical latitude at 30°N for all months save September 2007, when SBLB variability is minimal at all locations. The cross-shore maximum of diurnal variance lies just offshore of the coastline, on the inner shelf, which is consistent with the augmentation of land breeze winds through coastline curvature focusing, or may simply reflect the change in friction at the land/sea interface. The strength and distribution of diurnal variance in the Georgia Bight and the South Atlantic Bight vary from month to month, but the spatial patterns suggesting maximal strength and offshore extent of SBLB in the Georgia Bight persist for all summer months.

Forming the horizontal extent of diurnal winds as a function of latitude with an ensemble average over summer monthly estimates allows for comparison to linear SBLB theory. At each latitude, the horizontal extent is calculated as the zonal distance between the coastline and the point where diurnal

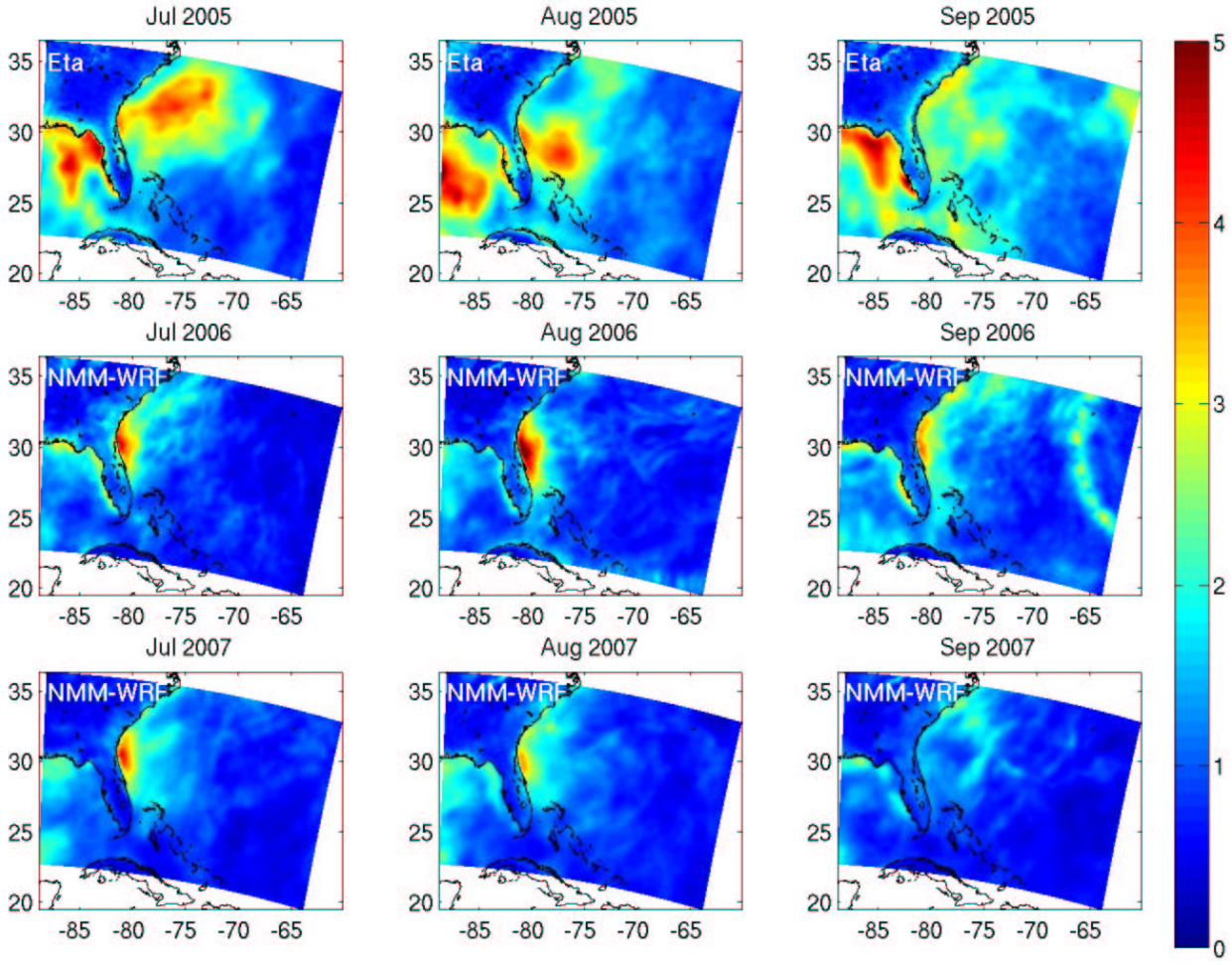

Figure 14: The upper row shows diurnal variance (m^2s^{-2}) computed by month for the Eta model over summer months 2005, and indicates spurious diurnal variability over much of the coastal ocean. Patterns of diurnal variance in the NMM-WRF model forecasts (lower panels) by month for the summer months of 2006 and 2007 show a local maximum of variance near 30°N may be augmented by the effects of coastline curvature, which may push the maximum slightly offshore.

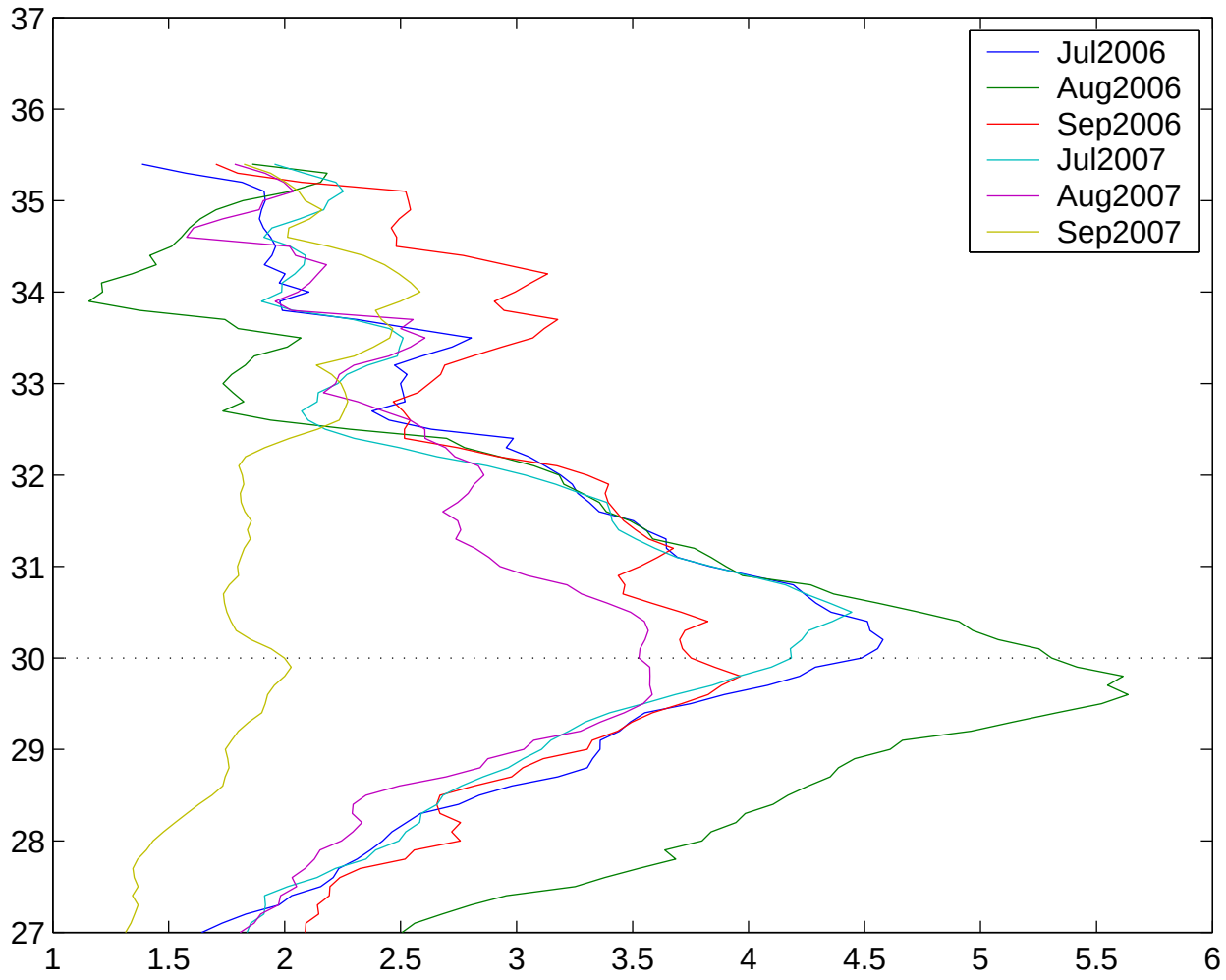

Figure 15: The zonal maximum of diurnal variance in the NMM-WRF model is shown by latitude for the six month-long periods in Fig. 14. The largest SBLB winds coincide with the critical latitude.

variance falls below a threshold value, chosen to be 1.5 m^2s^{-2}. The value of $\alpha/N \equiv \delta/(HN)$ is obtained by using typical values for the vertical scale H=1000 m and background stratification N=0.01 s^{-1}. The resulting estimate of α/N from the NMM-WRF model diurnal variance is an order of magnitude smaller than predicted by linear theory (Fig. 10), which could reflect an overestimate of the vertical scale H. Recalculation of α/N with an alternate choice of vertical scale based on the onshore depth of the circulation cell, 300-500 m (*Tunney*, 1996), yields better comparison to theoretical estimates.

The large maximum is qualitatively comparable to the sharp maxima found by the generalized linear theory when the relative importance of friction is small ($0 \leq r \leq \omega$), but the geographic view of variance patterns (Fig. 16) highlights the degree to which SBLB is enhanced in the Georgia Bight. Contours of D1 variance in the NMM-WRF model winds over summer months 2006-2007 highlight the maximum SBLB winds near 30°N, and SBLB variance greater than 2 m^2s^{-2} extends over 100 km past the shelfbreak, taken to be the 100 m isobath. The SBLB system of the Carolina Capes suggests that coastline curvature focuses SBLB in Long and Onslow Bays, the two smaller embayments just north of the Georgia Bight. D1 wind variance exceeds 2 m^2s^{-2} just offshore of these small bays, consistent with a focusing/defocusing of land breeze/sea breeze winds by coastline curvature.

The horizontal extent of SBLB is small over the Carolina Capes relative to the scale of SBLB in the Georgia Bight, where the radius of curvature of the Georgia Bight, 250 km, is comparable to the observed seaward penetration of appreciable diurnal winds. Though not the focus of this study, the SBLB variance in the eastern Gulf of Mexico is smaller than in that found in the Georgia Bight, suggesting that the effect of coastline curvature is significant. This result suggests that divergence and convergence of SBLB may be considerable, as the SBLB system of the Georgia Bight may self-interact on the shelf.

3.5.2 Case studies

Three 9-11 day periods during summers 2006 and 2007 serve as case studies and are used to describe SBLB in the Georgia Bight, its temporal variability, and the processes that influence its along- and cross-shore structure. The frequency of synoptic activity decreases significantly in summer, from 3-5 days period in fall and spring to 8-10 days in summer, as the Bermuda High moves southward and dominates the weather patterns over much of the SAB (*Weber and Blanton*, 1980). Aug. 1-12 2006, Aug. 17-26 2006, and July 5-15 2007 are chosen as time spans when SBLB can develop over longer time scales between synoptic storms that pass through the region.

Prevailing winds are 4-7 m/s from the SSW at all locations for the three periods considered, and

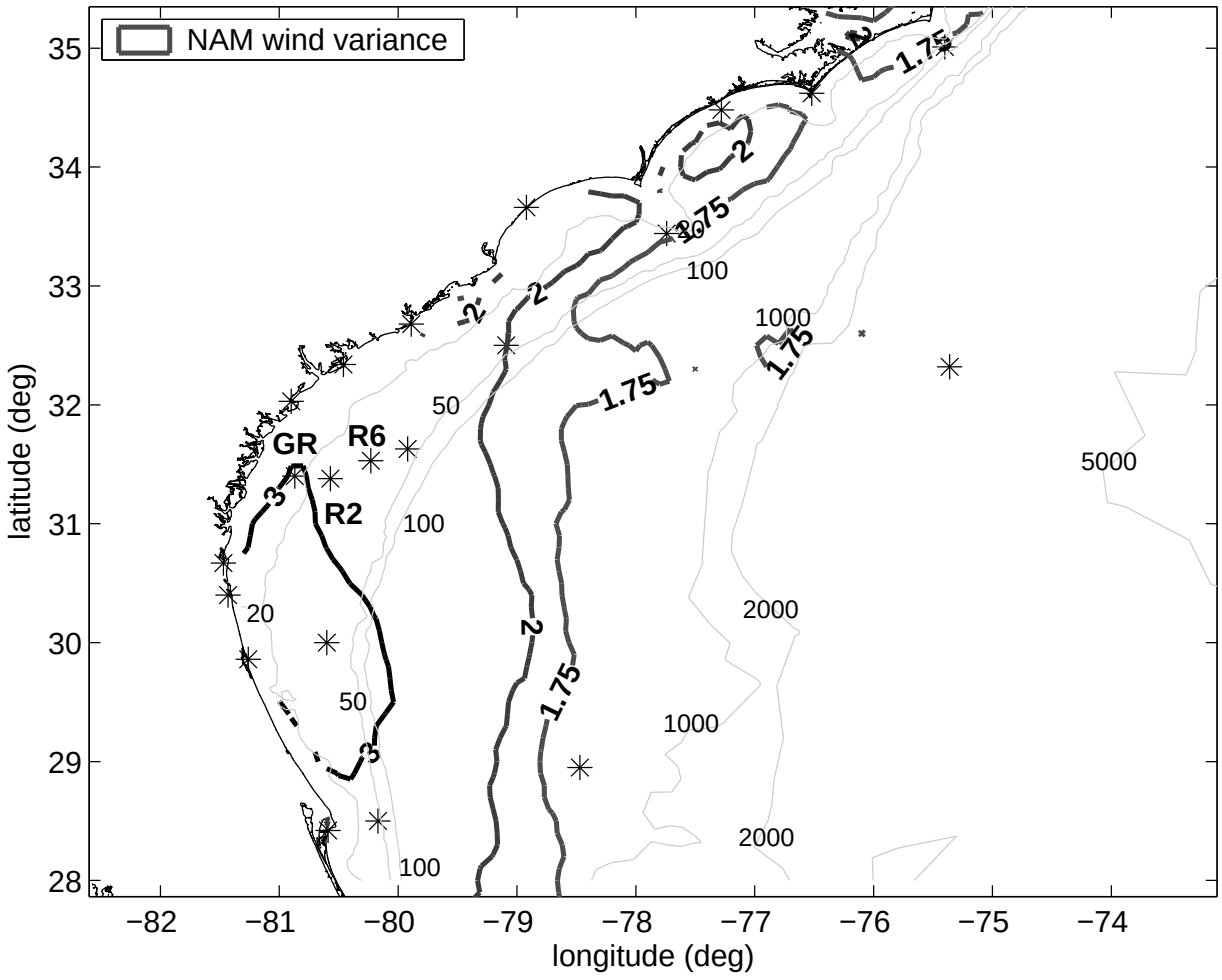

Figure 16: Contours of diurnal variance (m^2s^{-2}) computed over summer months 2006-2007 show a maximum of SBLB variance near 30°N, and enhanced extent of SBLB in the Georgia Bight.

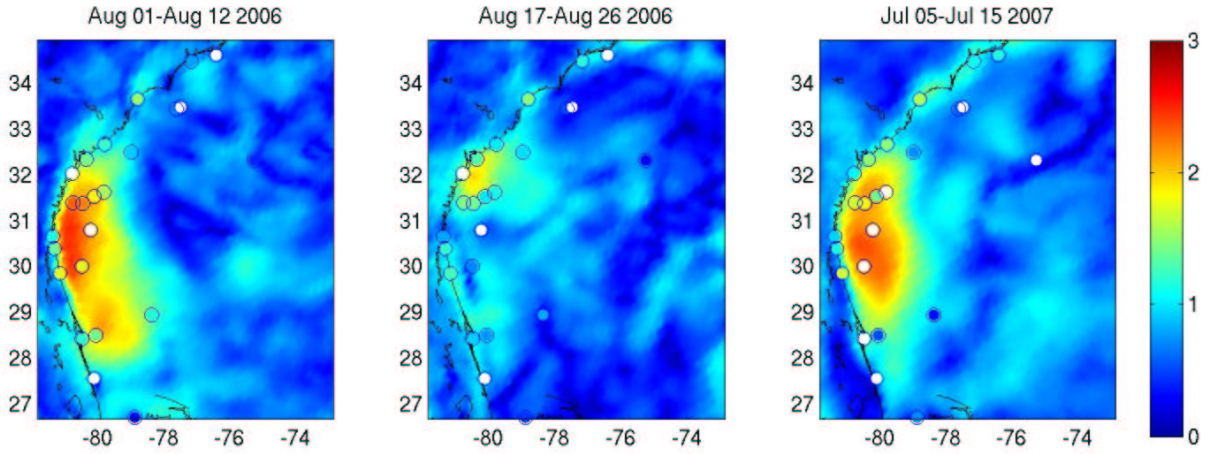

Figure 17: Diurnal variance in the modeled winds show similar patterns of spatial variability as that computed from the observations (circles) for three 9-11 day periods of well-developed sea breeze. Missing data are represented by white circles.

are predicted to inhibit the short term (<2 day) development of SBLB by 10-20% compared to calm conditions (*Tunney*, 1996, δ =70-80 km vs 90 km). Time series of observed and model winds are shown for two of these periods in Figure 13, and indicate that the major source of variance in the wind measured offshore is at the diurnal frequency, with little synoptic variability. The tail end of a front is visible in the time series on July 5-6, but prevailing winds typical of summer resume within a day.

Figure 17 shows the variance of modeled and observed winds computed over the three case study time periods. Observed and modeled estimates of diurnal variance are in general agreement on both the magnitude and spatial patterns. Though the details of the spatial patterns in observed and model diurnal variance differ, each of the three periods shows a local maximum of diurnal variance in the Georgia Bight near 30-31°N, in agreement with the longer-term analysis. The offshore extent of diurnal winds is greater in the Georgia Bight compared to regions to the north or south, where the D1 variance is enhanced in the area immediately surrounding the coastline.

The temporal resolution of the model reanalysis fields (6hr) is not sufficient to describe SBLB orientation, elliptical shape, or phase, and observations can provide this finer description of the SBLB system and its temporal variability. Figure 18 shows best-fit ellipses to the D1 filtered wind observations over two month-long time series in 2006 and 2007. Diurnal wind is generally oriented cross-shore, with a wind speed approaching 5 m/s at its maximum over the inner shelf at Gray's Reef (Fig. 12), but wind ellipse size, ellipticity, orientation, and shape vary on a 7-10 day time scale, consistent with the synoptic

time scale of summer in the Georgia Bight.

The three observation locations form a quasi-cross-shore transect, and can be used to describe the cross-shore structure of SBLB. Generally, SBLB magnitude decreases with distance offshore. The persistent counter-clockwise change in ellipse orientation with distance offshore can be attributed to small changes in the cross-shore direction, as the line of stations is not strictly aligned cross-shore. Figure 18 shows cross-shore coherence to be variable in time; 2007 SBLB is generally coherent, with a slight decrease of diurnal wind offshore. However, 2006 SBLB is more variable in space and time, with less organized structure of the diurnal ellipses.

A geographic view of D1 wind ellipses in the Georgia Bight for August 17-26, 2006 is shown in Figure 19, highlighting the horizontal and temporal variability of SBLB on relatively small length and time scales. Ellipse orientation off the Florida and South Carolina coasts has a bimodal distribution, most noticeable off the northern coast of Florida where SBLB is oriented alongshore as frequently as cross-shore over the 10-day time series. Diurnal winds off the Georgia coast are largely aligned with the cross-shore direction for the same time period. When SBLB significantly changes orientation, the changes off South Carolina's and Florida's coasts do not necessarily correspond. These changes in SBLB orientation over short time scales may indicate periods of time when SBLB is not locally generated or has interacted with the prevailing wind.

3.5.3 Phase

The timing of SBLB with respect to the diurnal heating cycle allows for comparison to linear theory, particularly to the unusual change in phase at 30°found by *Rotunno* (1983), a phenomenon not observed in reality. A close examination of phase may also reveal patterns that explain the coastal ocean's response to SBLB wind forcing near the resonant latitude. In particular, changes in SBLB phase over the shelf, with latitude and/or distance offshore, may be a source of horizontal gradients of diurnal wind that may generate near-inertial waves.

Figure 20 shows the May-August 2007 average of D1 filtered wind, evaluated at three-hour intervals over a SBLB cycle. In the mean, sea/land breeze winds are strongest at the coastline between at about 6pm/am local time and are oriented within 10°of cross-shore. Change in phase with distance offshore is clearest as sea/land breezes relax, near 00:00 and 12:00, respectively, with up to 110°($\approx$7.3 hr) lag in temporal phase from the coastline to mid-shelf.

A more careful calculation of phase with respect to latitude and distance offshore yields estimates of offshore propagation of the SBLB circulation cell's influence. Phase is chosen as the time at which

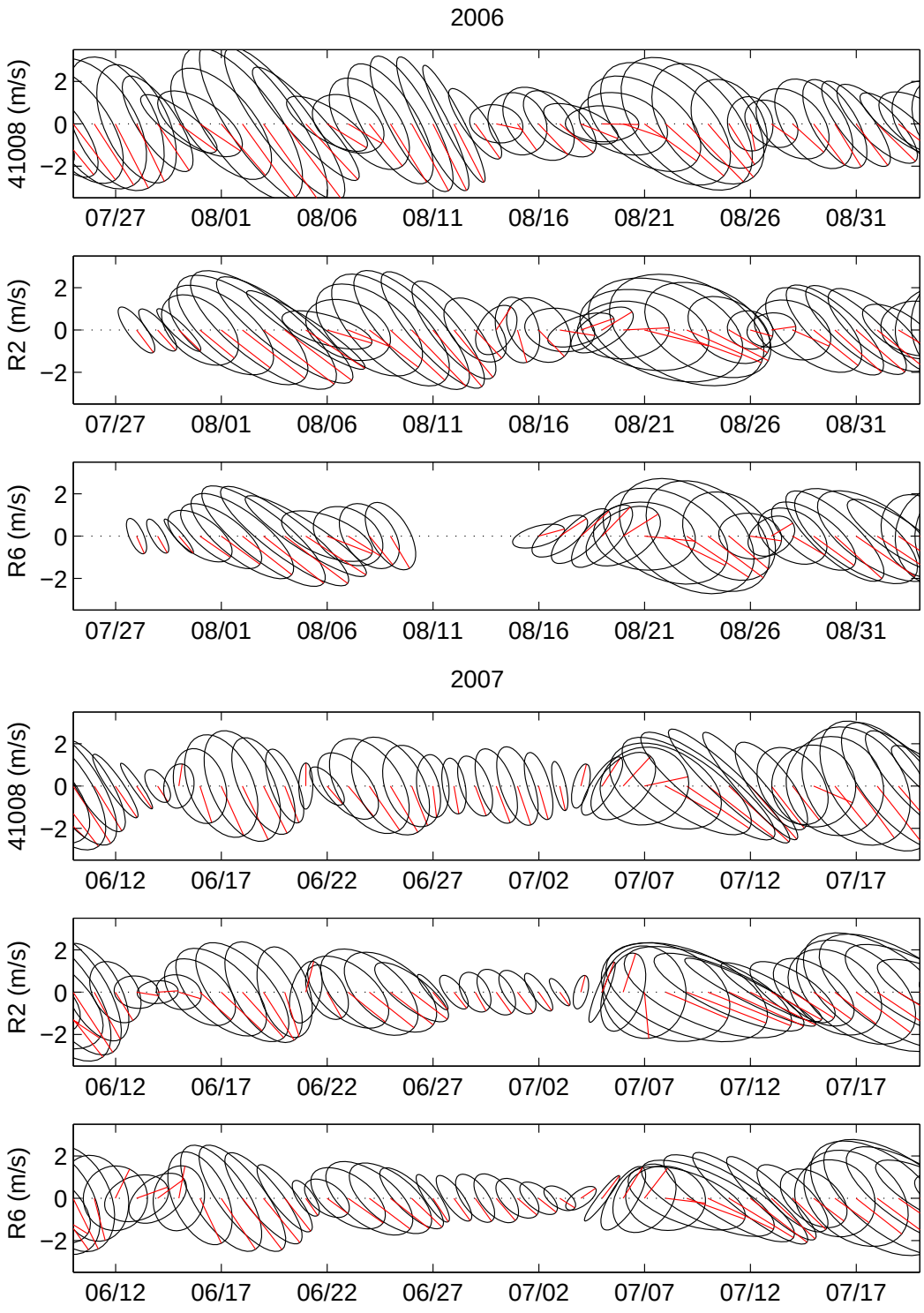

Figure 18: Best-fit ellipses to the diurnal wind show periods where sea breeze appears to be disorganized (upper panels, July/Aug. 2006), with significant change in ellipse magnitude, shape, and orientation with distance offshore along a quasi-cross-shore transect. In contrast, a month-long time series in June/July 2007 is generally coherent and near-uniform (lower panels). Red lines connect the ellipse major axis and the ellipse center on the time axis.

the diurnal wind is aligned with the daily wind ellipse orientation, regardless of the wind ellipse's angle with respect to the cross-shore direction. Phase of diurnal wind at mid-shelf locations (see Fig. 12) lags that of the inshore ("inner") stations by 2-4.5 hours, corresponding to offshore propagation speeds of 5-9 m/s. This estimate of propagation speed is on the same order as values estimated from land-based observations in Georgia (0.6-4.2 m/s, *Williams*, 1969) and southern Australia near 31°S (4-9 m/s, *Clarke*, 1955), the local modeled estimates of 2.4-4.2 m/s found by *Tunney* (1996), and the global estimate of *Gille et al.* (2005) (2-15 m/s, equatorward of 30° N/S). The internal gravity current speed u_{front} is estimated as 8 m/s, taking typical values from *Simpson* (1994) (T=300 K, ΔT=5 K, H=1000 m, κ=0.62). This estimate of propagation speed is consistent with the range of observed propagation speeds in the Georgia Bight.

Though *Gille et al.* (2005) did not observe a trend in phase with respect to latitude, analysis of the observations presented here suggests a weak dependence on latitude. Taken as a bulk estimate over summers 2006 and 2007 between 27 and 36°N, SBLB winds near the coastline reach a maximum at about 06:00/18:00 local time in the Georgia Bight at 31.5°N, but arrive 20 minutes later with each degree northward. This finding is consistent neither with *Rotunno*'s (1983) linear theory nor with no change in latitude (*Ueda*, 1983; *Niino*, 1987), and the trend is opposite of that noted by *Yan and Anthes* (1987). However, both linear theories assume straight coastlines and neither considers SBLB interaction with other SBLB systems or synoptic winds. With significant variability in ellipse orientation over synoptic time scales, the time at which SBLB winds are aligned with the cross-shore changes by up to 4 hours over several days (Fig. 19). These large changes in orientation and phase may reflect the influence of non-local SBLB systems, the relaxation of SBLB to synoptic winds, or the combination of both effects. Any zonal changes in SBLB phase are likely modified by coastline curvature, and it is difficult to separate the effects of latitude, coastline curvature, and non-local SBLB, all of which may contribute to divergence and convergence of SBLB on the shelf.

3.6 Discussion

Comparison to linear SBLB theory provides a framework for interpreting the scale of SBLB and SBLB wind speed in the Georgia Bight. Inviscid linear theory (*Rotunno*, 1983) explains the patterns of offshore extent of SBLB energy and its maximum wind speed with latitude better than models with more complete dynamics. The maximum of SBLB variance for the east coast of the southeastern United States lies in the Georgia Bight. However, the maximum horizontal extent of SBLB is not focused on a

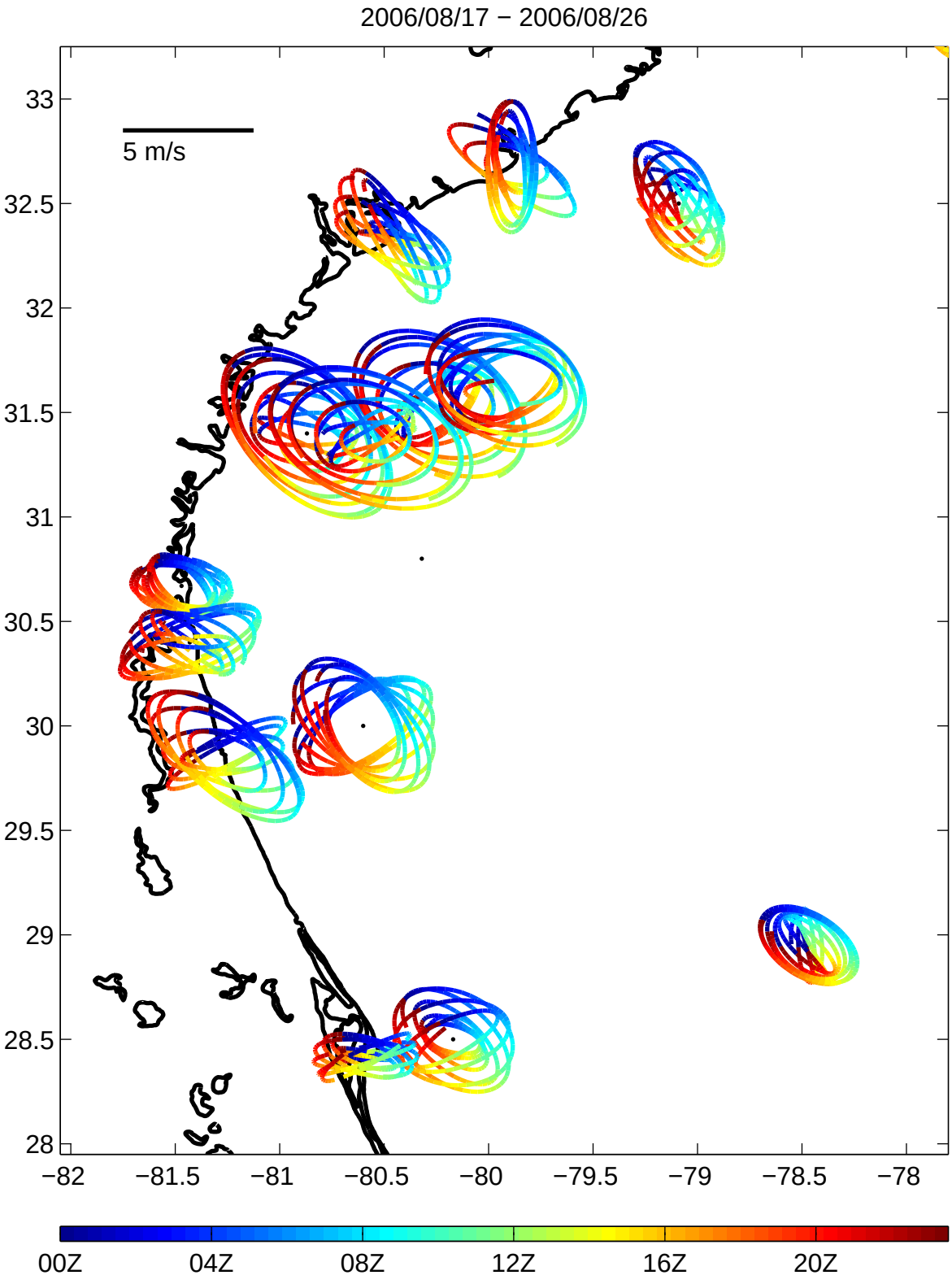

Figure 19: Diurnally filtered wind observations from August 17-26 2006 indicate a bimodal distribution of SBLB ellipse orientation off the Georgia and South Carolina coastlines, even over relatively short time scales. Color represents the time of day, with the extremes of the colorbar corresponding to 8pm EDT, just before sea breeze winds reach a maximum over the inner to mid-shelf.

latitude but rather centered on the Georgia Bight itself, where the radius of curvature of the embayment is comparable to the horizontal scale of SBLB. It is proposed that coastline curvature may be primarily responsible for the latitudinal variations of horizontal scale of SBLB in the Georgia Bight. The spatial patterns of D1 variance off the Carolina Capes are consistent with enhanced SBLB due to coastline curvature, but near 30°N, the effects of latitude may increase the scale of SBLB to allow the interaction as far as 250 km offshore. Offshore extent of SBLB and the magnitude of SBLB winds are smaller in the eastern Gulf of Mexico near 30°N than the Georgia Bight. The difference between an east-west and north-south coastline may reflect the orientation of the coastline, the radius of curvature, or its angle with respect to the prevailing winds.

As discussed in Section 3.2, in the absence of coastline curvature, the horizontal scale of SBLB is set by the relative importance of friction, stratification, and latitude. Though only the inviscid theory predicts a maximum horizontal extent near the critical latitude at 30°N or S, some of the relevant modeling work with more complicated dynamics agree (*Walsh*, 1974; *Yan and Anthes*, 1987), and others find a maximum of SBLB scale in the tropics (*Niino*, 1987; *Dalu and Pielke*, 1989) or at an intermediate latitude (*Arritt*, 1989). Though the physics and implementations of the various models differ, the degree to which these differences in predicted horizontal extent could potentially be explained with the treatment of friction remains an open question.

The maximum SBLB wind speed observed in the Georgia Bight is 5-6 m/s, smaller than the observed offshore propagation speed of the SBLB front. The propagation speed of the front is consistent with that of an internal gravity current, but away from the front, SBLB winds become more elliptical as rotation becomes more important to the dynamics, particularly near 30°. The ability of inviscid theory to predict the latitude of maximum horizontal extent and SBLB winds implies that, over the coastal ocean, the effect of friction is small relative to rotation in the Georgia Bight. The change in roughness from land to sea may explain the faster SBLB propagation and wind speeds over the ocean relative to the *Tunney* (1996); *Williams* (1969) result, and the asymmetry of landward/seaward extent and propagation seen by *Tunney* (1996).

That the effect of friction is minimal over the coastal ocean compared to that over land is not surprising; however, the ability of the linear SBLB theory to describe spatial patterns of seasonal estimates of diurnal wind variance is unexpected, particularly because the temporal variability on short time scales can be significant. Coastline curvature and interaction of SBLB across the Georgia Bight or with large scale flow contribute to the temporal variability of SBLB structure, with several periods where the orientation of SBLB is clearly not in response to local temperature gradients.

The linear SBLB models referenced require that the landward and seaward extents of SBLB are symmetric with respect to the coastline. The offshore horizontal extent of SBLB in the Georgia Bight presented here is 1.2-6 times the estimates of onshore propagation from land-based observations (e.g., *Williams*, 1969; *Kurzeja et al.*, 1991; *Weber*, 2003; *Crouch*, 2006), which may reflect the difference in friction over land versus the coastal ocean. However, the offshore propagation speed of SBLB derived from observations is shown to be consistent with theory and observations near the critical latitude. Determination of horizontal extent and propagation speed from offshore and land-based observations over the same time period, using the same metric of δ, would be a useful comparison to *Tunney*'s 1996 modeling work, which shows significant asymmetry in the horizontal extent and propagation speed of SBLB landward and seaward.

One consequence of the enhanced horizontal extent of SBLB is the change in phase with large distances cross-shore where the SBLB is still significant. Propagating at 8 m/s, SBLB originating at the coastline will arrive 250 km offshore about 8.7 hours after its generation. Though decreased in magnitude at this distance offshore, SBLB can be nearly 180° out of phase at its maximum extent relative to the coastline.

The summer-long, monthly, or 10-day estimates of SBLB variance shown during summer months do not indicate a diurnal signal associated with the Gulf Stream. During summer, the water on the shelf of the Georgia Bight approaches Gulf Stream temperatures, and the sea surface temperature (SST) gradient across the Gulf Stream is at an annual minumum. In spring and fall, SST gradients across the north wall of the Gulf Stream are at a maximum, and the atmospheric circulation cells induced at the sharp SST gradient *Sweet et al.* (1981); *Hsu* (1984) may be affected by the diurnal heating cycle. However, the patterns of diurnal variance in the observed and modeled winds suggest no discernible influence of the Gulf Stream on SBLB circulation in the Georgia Bight during summer months.

The spatial and temporal variability of the SBLB system will have significant implications for determining the coastal ocean response to forcing near the resonant frequency over the entire shelf (and beyond). At times, the signal is coherent over much of the shelf; a near-uniform wind field may generate near inertial internal waves in the "coastal boundary layer" set by the coastal boundary and stratification, with internal wave propagation offshore, as described by *Davies and Xing* (2003). However, in the Georgia Bight, horizontal variability of SBLB winds appears to be significant. In this case where resonant wind forcing is allowed to vary in space and time, near-inertial internal waves may be generated in regions of horizontal divergence and convergence of the SBLB wind field.

Estimates of mean divergence of the D1 wind field is shown in Figure 20, calculated between unique

pairs of observations separated by less than 200 km. The average diurnal wind speed and direction are taken as a season average over May-August 2007 at 3 hr intervals. Divergence/convergence are generally strongest off the Florida and South Carolina coasts, and reach a maximum of 6-8$\times 10^{-4}$ s^{-1}. The change in phase across the shelf is visible from the snapshots of mean SBLB wind over 24 hours. In particular, at 12:00 local time, the sea breeze circulation cell remains confined to the coastline. Mid-shelf winds have rotated southward alongshore, and the diurnal wind diverges on the inner to mid-shelf. At 00:00 local time, the land breeze is developing near the coast, while mid-shelf winds are aligned with the alongshore, leading to convergence of the diurnal wind field. Coastline curvature may enhance the interaction of SBLB across the Georgia Bight or with large scale flow, but change in phase across the shelf is visible from the snapshots of mean SBLB wind, and may be a more persistent source of energy that can displace the pycnocline.

Assuming that diurnal/inertial currents are in phase with the diurnal wind forcing and are on the order of a few percent of the forcing wind speed, the continuity equation implies that up/downwelling velocities are on the order of $-h(\nabla_H \cdot \gamma \mathbf{u_{wind}})$, where h is the depth of wind mixing, $\mathbf{u_{wind}}$ is the horizontal wind velocity, and γ is an efficiency factor set to 0.025. The distance h is chosen to be 15 m based on a representative depth of the surface layer of diurnal/inertial currents, implying that a local divergence/convergence of 1×10^{-4} s^{-1} would force an upwelling/downwelling velocity of 0.38 mm s^{-1}. Integrated as a half-sine over 12 hours, pycnocline displacement due to up- or downwelling of this magnitude is about 10 m.

The scale of the divergence and convergence is on the order of the resolution of the observations, which suggests that the observations under-resolve SBLB and its horizontal gradients. The NDBC and SABSOON networks are designed to provide frequent, high-quality observations to forecasters, scientists, and other end-users, but are primarily designed to collect observations on synoptic and larger scales. Land-based meteorological observing systems have been used to characterize fine details of SBLB systems. Achieving comparable offshore observing systems is unlikely, but sub-synoptic scale variability in the atmosphere can be significant near the coast, and has important implications for the coastal oceanography.

3.7 Summary

Enhanced non-tidal diurnal currents have been observed near the critical latitude in the Georgia Bight, and SBLB is a likely source of shelf-wide wind forcing near the resonant frequency. The offshore

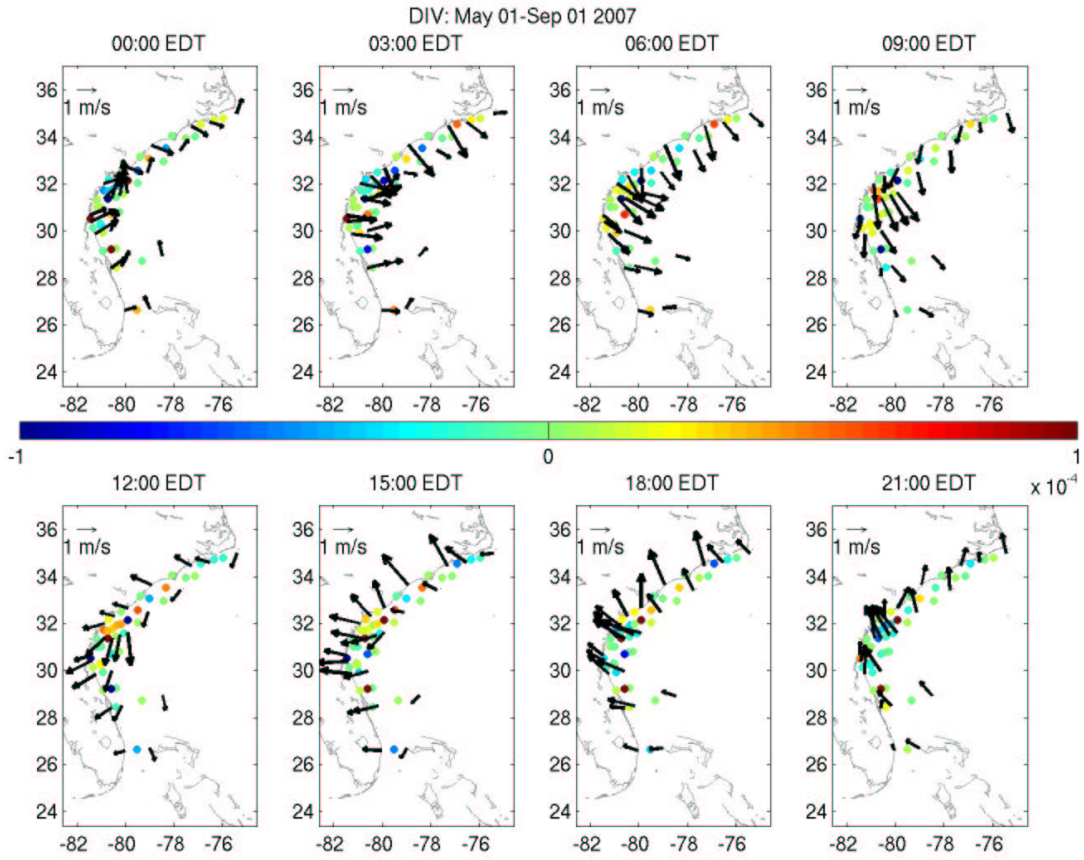

Figure 20: Mean diurnal wind speed and direction by time of day, calculated over May-August 2007 at 3-hour intervals (local time). Dots indicate the local divergence (s^{-1}) of diurnal wind, taken between pairs of observation locations fewer than 200 km apart. The offshore phase lag is most visible at 00:00 and 12:00 EDT, but the considerable divergence and variability suggest that the observations are under-resolved compared to the scale of SBLB.

structure of SBLB in the Georgia Bight is characterized using a combination of observed and modeled winds. This first description of the offshore structure of SBLB in the Georgia Bight finds that SBLB winds can exceed 1-2 m/s at least 250 km offshore, almost an order of magnitude greater than the general offshore extent of SBLB predicted by *Simpson* (1994). The latitudinal variability of SBLB offshore from long-term averages is consistent with inviscid linear SBLB theory, with a maximum of SBLB wind variance at 30°N. Coastline curvature appears to enhance the offshore extent of SBLB over the entire embayment. Comparison of SBLB horizontal and velocity scales implies that the effects of rotation near the critical latitude are significant while those of friction are not significant in the Georgia Bight. The change in phase of SBLB with cross-shore distance results in divergence and convergence of the diurnal wind field, which may lift and depress the pycnocline tens of meters at the diurnal frequency.

CHAPTER 4. Coastal ocean response to SBLB in the Georgia Bight: Structure and variability

4.1 Introduction

Inertial oscillations (IOs) are ubiquitous in the ocean, and are often described as a slab-like anticyclonic circular excursion of the near-surface layer in response to a wind impulse. Near a coastal boundary, however, conservation of mass requires a compensating flow at depth, resulting in anticyclonic inertial oscillations in the lower layer 180° out of phase with those in the upper layer (e.g., *Millot and Crépon*, 1981). This vertical structure is manifested as a combination of pure inertial oscillations and near-inertial internal waves, and has been observed in lakes (*Malone*, 1968), shallow water embayments (*Millot and Crépon*, 1981), marginal seas (*Jacobs et al.*, 2001), semi-enclosed seas (*Chen et al.*, 1996; *Lewis*, 2001; *Jarosz et al.*, 2007), and continental shelves (*Simpson et al.*, 2002; *Rippeth et al.*, 2002; *Maas and van Haren*, 1987).

Many models (*Millot and Crépon*, 1981; *Kundu et al.*, 1983; *Orlic*, 1987; *Tintoré et al.*, 1995; *Lewis*, 2001; *Knight et al.*, 2002) have considered the development and vertical structure of near-inertial currents in response to a wind impulse of energy. However, near 30°N or S, the diurnal sea breeze/land breeze (SBLB) and local inertial periods coincide, and SBLB can force a resonant response in the coastal ocean. This diurnal/inertial resonance has been observed on the Catalonian shelf (*Rippeth et al.*, 2002), the southern coast of Namibia (*Simpson et al.*, 2002), along the northwest Gulf of Mexico (*Daddio et al.*, 1978; *Chen et al.*, 1996; *Chen and Xie*, 1997; *DiMarco et al.*, 2000; *Lewis*, 2001), and in the DeSoto Canyon in the northern Gulf of Mexico (*Jarosz et al.*, 2007).

The vertical structure of near-inertial motions on continental shelves near the critical latitude is generally well-described by the response to a wind impulse. One-dimensional point models (e.g., *Millot and Crépon*, 1981; *Kundu et al.*, 1983; *Orlic*, 1987; *Tintoré et al.*, 1995; *Chen and Xie*, 1997; *Lewis*,

2001; *Simpson et al.*, 2002; *Knight et al.*, 2002) are able to capture the development, strengthening, and vertical structure of IOs in the coastal ocean. However, a greater degree of complexity is required to describe the generation and propagation of near-inertial internal waves (NIIWs, *Davies and Xing*, 2003). Under spatially uniform periodic wind forcing at the inertial frequency, inertial oscillations develop across a stratified coastal ocean in response to local wind, and near-inertial internal waves are generated due to internal pressure gradients set up at the coastal wall. Isopycnal surfaces are elevated or depressed in response, and near-inertial internal waves propagate offshore. While inertial oscillations are generated over much of a flat shelf profile, the swath where NIIWs are generated is confined to a narrow region near the coast termed the coastal boundary layer (CBL) by *Davies and Xing* (2003).

When the pycnocline no longer intersects the coastal wall, further modeling studies with surface and bottom fronts suggest that the frontal boundaries mimic the role of the coastline (*Davies and Xing*, 2002; *Xing and Davies*, 2004; *Davies and Xing*, 2005). NIIW are generated at frequency $f_{eff} = f + \zeta/2$ to first order, where ζ is the relative vorticity (*Mooers*, 1975). In effect, the coastline or the presence of surface or bottom fronts causes local divergence or convergence of the near-surface currents in the same way as a spatially varying wind field would, generating NIIW that radiate away.

The coastal response to SBLB can be near-resonant with the wind forcing near the critical latitude, but the SBLB system itself is near resonance with the diurnal thermal gradients that force the wind circulation. *Edwards and Seim* (2008b) found that SBLB is enhanced near the critical latitude in the Georgia Bight, defined as the region bounded by Cape Romain and Cape Canaveral; the structure of summer SBLB is reproduced in Figure 21. The greatest SBLB winds lie near 30°N, but the the horizontal extent of SBLB winds is enhanced over all of the Georgia Bight, extending at least 250 km offshore, and appears to be modified by coastline curvature. The Gulf Stream is a potential source of diurnal energy (*Alliss and Raman*, 1995), but no Gulf Stream signal was found in the modeled wind pattern during summer months. The SBLB wind field in the Georgia Bight diverges and converges at the diurnal frequency largely from the cross-shore propagation of SBLB each day and night.

Thus, the wind which forces the coastal ocean near the resonant inertial frequency in the Georgia Bight varies significantly in space and with time, but models in the literature forced by spatially invariant wind fields can be used as a framework for consideration of more complex wind forcing. The cross-shore response to a cross-shore wind impulse is predicted to grow to some distance L offshore that is several times Rossby radius of deformation ($R_o = \sqrt{(gH/f)}$, f is the Coriolis parameter, g is the acceleration of gravity, and H is water depth), beyond which the response decreases (*Lewis*, 2001). However, the frequency of the wind forcing is important in setting the cross-shore structure (*Craig*, 1989). *Davies*

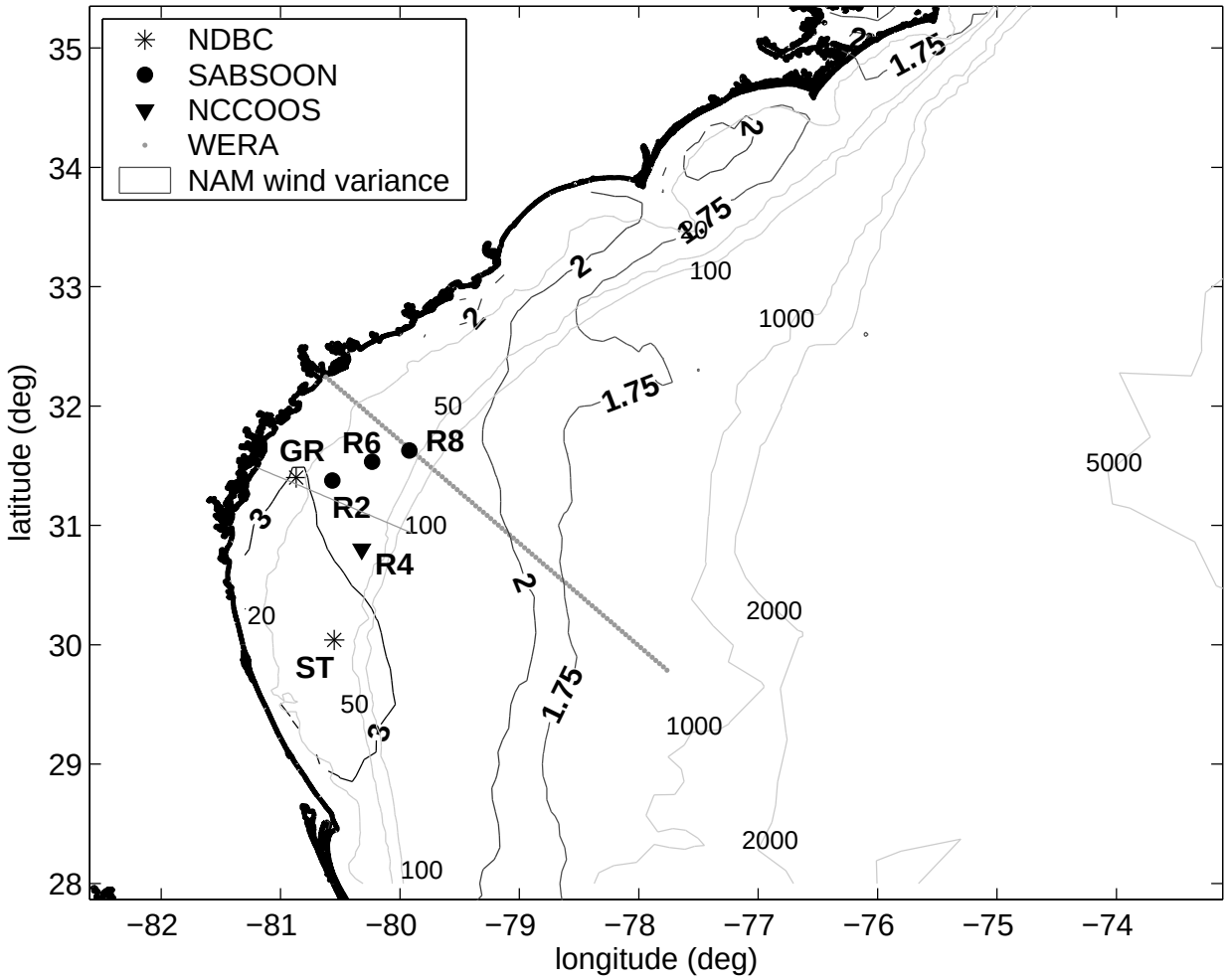

Figure 21: Map of the Georgia Bight, showing locations of SABSOON/NCCOOS data locations at the R2, R4, R6, and R8 towers, NDBC buoys 41008 (GR) and 41012 (ST), and the transect over which WERA surface currents are measured. Contours of SBLB variance (m^2s^{-2}) from *Edwards and Seim* (2008b) are given as a reference. The maximum SBLB wind lies at 30°N, but the horizontal extent of SBLB winds enhanced over the entire latitudinal range of the Georgia Bight, relative to that off Florida and the Carolinas' coast. The light cross-shore transect is used to evaluate the effects of stratification and friction using climatology.

and Xing (2004) show that the offshore-decreasing influence of bottom friction over a sloping shelf causes the inertial current magnitude to increase with distance offshore under periodic cross-shore wind stress at resonant and non-resonant frequencies. The maximum response lies tens of km offshore, but alongshore flow in the upwelling favorable direction enhances the inertial current maximum and moves it onshore (*Davies and Xing*, 2004).

Observations in the western and northern Gulf of Mexico support the prediction of increasing diurnal/inertial energy with distance offshore near the critical latitude, but other mechanisms have been invoked to explain the cross-shore structure of diurnal-inertial energy. In the western Gulf of Mexico, near-inertial energy increases slowly to a maximum value at the shelfbreak and drops off steeply offshore (*Chen et al.*, 1996); this pattern is set by the surface pressure gradient set up by the wind and the vertical gradient of wind stress (*Chen and Xie*, 1997). In the DeSoto Canyon region in the northern Gulf of Mexico, near-inertial energy continues to increase past the shelfbreak to at least the 1500 m isobath, located 125 km offshore (*Jarosz et al.*, 2007). The offshore maximum of diurnal/inertial energy is primarily attributed to the proximity of the turning latitude (30°N) to the shallowest locations (100 m), but could potentially be trapped near-inertial energy through interaction with mesoscale shear (*Jarosz et al.*, 2007).

The observational studies of near-resonant diurnal/inertial currents in the literature, though generally limited in time (*DiMarco et al.*, 2000) or space (*Simpson et al.*, 2002), provide a valuable framework for comparison with the spatial patterns in the Georgia Bight. The year-long study with significant coverage over the DeSoto Canyon region by *Jarosz et al.* (2007) demonstrates the influence of resonant wind forcing, and suggests that stratification may enhance the response in the upper ocean. However, the tidal dynamics of the Georgia Bight differ significantly from those of the Gulf of Mexico, where tides are small, and the diurnal/inertial motions dominate the energy spectrum. In contrast, the Georgia Bight is a broad shallow shelf over which the barotropic M_2 tide is amplified significantly (*Redfield*, 1958), and the bottom boundary layer associated with energetic barotropic tidal motions can occupy a significant fraction of the water column.

In the analysis of SBLB-forced motions in the Georgia Bight, two larger scientific questions arise: what controls the effectiveness of conversion of diurnal-inertial kinetic energy from the atmosphere into the coastal ocean, and what processes interact with the forced diurnal/inertial motions, and do those process redistribute the wind input energy vertically or horizontally on the shelf? The goal of this study is to answer the former by describing the shelf response to near-resonant forcing by SBLB, and characterize the alongshelf, cross-shelf, and vertical structure on seasonal and interannual time scales. The results are

compared to the horizontal and vertical structure predicted by models and observed estimates, and are considered in the context of the local dynamics to assess the roles of forcing, stratification, and friction. A companion paper, *Edwards and Seim* (2008c), approaches the second question by considering the interaction of shear and stratification over shorter time scales, and how baroclinic motions may mediate the transfer and redistribution of diurnal/inertial energy on the shelf near the critical latitude.

Seven years of observations on the shelf of the Georgia Bight are described, along with the methods used to separate the energy in the non-tidal diurnal currents from the barotropic near-diurnal signal, which is too close to separate harmonically. The vertical, along-, and cross-shore structure of the distribution of diurnal/inertial energy on the shelf is described, and the interaction of wind forcing, stratification, and friction is considered in determining the coastal response to SBLB near the critical latitude. The implications for mixing on the shelf of the Georgia Bight are considered in a discussion section.

4.2 Description of observations and methods

The coastal ocean's response to near-resonant forcing of SBLB in the Georgia Bight is examined using multi-year records of observations of winds and currents on the shelf. Complex EOF (CEOF) analysis is used to separate the internal structure from the barotropic currents. Applied by season to minimize the effect of changing stratification on the vertical structure of the barotropic tidal currents, the method also distinguishes the barotropic tide from the non-tidal processes in the diurnal/inertial frequency band, a separation not possible through spectral methods, as the Rayleigh criterion would require time series of over a year, longer than the time scale of non-tidal diurnal/inertial variability. Intermittency of the non-tidal phenomenon favors the use of non-stationary time series analysis. Thus, a combination of CEOF and cross wavelet methods are used to describe the variability of non-tidal energy in the diurnal/inertial band.

4.2.1 Observations

Observations of winds and currents on the shelf of the Georgia Bight are available through four main sources, summarized in Table 3. The South Atlantic Bight Synoptic Offshore Observing Network (SABSOON, *Seim*, 2000) has instrumented several offshore towers in the Georgia Bight with Acoustic Doppler Current Profilers (ADCPs) and meteorological packages (Fig. 21), providing offshore meteorological and ocean data at high vertical and temporal resolution (up to 6 min) since 2000. These

Table 3: Availability of measurements of currents on the shelf of the Georgia Bight. Water depth, temporal and spatial resolution, data coverage over 2000-2008, and availability of co-located winds are listed for ADCP data available through SABSOON, NC-COOS, and NDBC and for WERA HF radar data from Skidaway Institute of Oceanography.

	Station name	Water depth (m)	Δt	$\Delta z/\Delta x$ (m)	Data coverage	Total days coverage	Winds
SABSOON	R2	25	6 min	0.5-1	Jul. 2002-Dec. 2007	1468.0	$\surd$
	R6	32	6 min	0.5-1	Apr. 2000-Jun. 2003 May-Jul 2005 Mar.-Jun. 2006	1147.3	$\surd$
	R8	45	6 min	1	Jul. 2004-Jul. 2006	338.9	$\surd$
NC-COOS	R4	41	10s-1hr	0.5-2	Apr. 2005-Jul. 2007	714.2	
NDBC	GR	16	1hr	1	Dec. 2005-Sep. 2006	292.9	$\surd$
	ST	39	1hr	2	Sep. 2005-Mar. 2007 Aug.-Sep. 2007	508.9	$\surd$
SkIO	WERA	10-1000	0.5hr	4.15 km	Apr. 2006-Jul. 2007 Oct. 2007-Feb. 2008	477.8	

long-term records allow the compilation of a climatology of mean winds and currents over the shelf over long time scales, but also of SBLB and associated diurnal/inertial energy in the ocean.

The North Carolina Coastal Offshore Observing System (NCCOOS) has supplemented these data with repeated deployments of bottom-mounted ADCPs near SABSOON towers. The multiple deployments near the R4 tower provide a nearly continuous record of ADCP measurements on the mid- to outer shelf for over 2 years. Shorter term ($<$2 months) observations of currents are available at other locations on the shelf, but are not used in this study.

Surface currents from a long-range, shore-based HF radar system augment the description of diurnal/inertial surface currents. The WERA system, maintained by the Skidaway Institute of Oceanography and the University of South Carolina, provides half-hourly surface currents over much of the shelf of the Georgia Bight (*Shay et al.*, 2008). Processed surface currents along a cross-shelf transect which coincides with the R8 tower (Fig. 21) are used to describe the cross-shore variability near the critical latitude.

Two National Data Buoy Center buoys, located at Gray's Reef (GR, 41008) and offshore of St. Augustine (ST, 41012), are each outfitted with a downward-looking ADCP and a meteorological package that measures winds. The ADCP configuration appears to be significantly improved from earlier implementations (*Seim and Edwards*, 2007), and the instruments provide crucial estimates of diurnal/inertial variability on the inner shelf (GR, 41008) and on the mid-to outer shelf near 30°N due east of St. Augustine, FL (ST, 41012).

Unfortunately, observations of the mass field on the shelf for the 7 year period of analysis are limited and seldom continuous in the vertical dimension, but a general description of the mass field can be deduced from the three shelf regimes defined by *Atkinson et al.* (1983), spanned by the observations. GR lies on the inner shelf, characterized by shallow water depths (<20 m) and the influence of the river input to the coastal ocean, termed the coastal frontal zone (CFZ, *Blanton*, 1981). The mid-shelf region (e.g., R6, 32 m water depth) is dominated by wind and tidal processes, and is seldom influenced by river discharge. R2 (25 m water depth) straddles the inner and mid-shelf regions, and may be influenced strongly by both tides and intermittent intrusions of fresh water. R8, R4, and ST lie on the mid- to outer shelf, where dynamics are significantly affected by the presence of the Gulf Stream. The increased water depth and reduced influence of bottom friction allows thermal stratification to develop near surface, and periodic intrusions and filaments of the Gulf Stream contribute to density stratification on the outer shelf.

4.2.2 Methods

Two major methods of isolating non-tidal diurnal/inertial variance are used in the following analysis, the details of which are given below. Cross wavelet transform (XWT) techniques are applied to the vertical modes that result from complex empirical orthogonal function (CEOF) analysis of the measured currents. Alternately, measured observations (winds and currents) and baroclinic currents (as identified through CEOF) are filtered to isolate the diurnal band.

CEOF+XWT, variance-preserving formulation

CEOF and cross wavelet analyses are combined into a new method of assessing variance from different physical processes as a function of frequency and time, and are applied here to measured ADCP data on the shelf of the Georgia Bight. The CEOF technique described in *Edwards and Seim* (2008a) is applied to the complex time series $\psi(z,t) = u(z,t) + iv(z,t)$, where u and v are the eastward and northward positive components of velocity and $i = \sqrt{-1}$. The analysis decomposes the observations into independent vertical modes $\phi_j(z)$ with temporal variability $a_j(t)$ given by the projection of the data onto that mode:

$$a_j(t) = \sum_{m=0}^{M-1} \psi_m(t)\phi_{jm} \tag{4.2.1}$$

where m is an index less than or equal to the number of vertical levels M. Time series of the jth mode profile $\hat{\psi}_j$ are reconstructed by mode:

$$\hat{\psi_j}(z,t) = a_j(t)\phi_j^*(z) \tag{4.2.2}$$

where * denotes the complex conjugate.

The time series of modal amplitude given by $a_j(t)$ describes the time variability of mode j, but the temporal variance in each mode $\hat{\psi_j}(z,t)$ depends on the product of $a_j(t)$ and $\phi_j(z)^*$. If instead, each vertical mode is normalized by its depth-averaged magnitude, the time-varying modal coefficients will fully contain the variance of the $\hat{\psi_j}(z,t)$. Normalizing $\phi_j(z)$ with respect to its depth-averaged magnitude $\overline{|\phi_j|}$, the normalized vertical modes $\xi_j(z)$ are given by

$$\xi_j(z) = \frac{\phi_j(z)}{\overline{|\phi_j|}}. \tag{4.2.3}$$

and Equation 4.2.2 can be recast in terms of $\xi_j(z)$ and the time series of modal amplitude $b_j(t)$:

$$\hat{\psi_j}(z,t) = b_j(t)\xi_j^*(z) = a_j(t)\phi_j^*(z) \tag{4.2.4}$$

$$b_j(t) = \overline{|\phi_j|}\, a_j(t). \tag{4.2.5}$$

Because $b_j(t)$ refers to the normalized vertical modes, $b_j(t)$ obtained from measurements at different locations and periods of analysis may be directly compared.

Cross wavelet analysis (*Torrence and Compo*, 1998; *Grinsted et al.*, 2004) is used to describe the frequency content of the complex time series $b_j(t)$ for each mode. The cross wavelet transform is formed by the continuous wavelet transforms of the real and imaginary parts of $b_j(t)$. The continuous wavelet transform of a scalar time series x_n of length N and time step δt is given by its convolution with a mother wavelet function Ψ that is scaled and translated in time (see *Kumar and Foufoula-Georgiou*, 1997; *Torrence and Compo*, 1998, for an excellent review of theory and application of wavelet analysis). The resulting spectrum is a complex function of scale s (analogous to frequency), and is normalized by s to compare wavelet spectra of disparate data:

$$W_n^x(s) = \sqrt{\frac{\delta t}{s}} \sum_{n'=0}^{N-1} x_{n'} \Psi^* \left[\frac{(n'-n)\delta t}{s} \right] \tag{4.2.6}$$

The mother wavelet effectively acts like a filter at different temporal and frequency scales. The Morlet wavelet, with dimensionless frequency $\omega_0 = 6$, is a standard mother wavelet for geophysical applications (*Torrence and Compo*, 1998; *Grinsted et al.*, 2004) and is used here:

$$\Psi(\eta) = \pi^{-1/4} e^{i\omega_0} e^{-\eta^2/2}. \tag{4.2.7}$$

The cross wavelet transform (XWT) of $b_j(t)$ is calculated as the product $W_{nj}^{ri}(s) = W_{nj}^{r}(s) W_{nj}^{i}(s)^*$, where the r and i superscripts refer to the real and imaginary parts of the input time series. The cross wavelet power $|W_{nj}^{ri}(s)|^2$ and phase $\tan^{-1}(\text{Im}\{W_{nj}^{ri}(s)\}/\text{Re}\{W_{nj}^{ri}(s)\})$ are calculated over all times n, giving power $|W_j(t,s)|^2$ and phase information for each vertical mode as a function of time and frequency. Using the cross wavelet Matlab package provided by A. Grinsted, $W_j^{ri}(t,s)$ is formed for each vertical mode, using default parameters recommended by *Grinsted et al.* (2004). Cross wavelet energy per unit mass $\mathcal{E}_j(t,s)$ is then recovered from the cross-wavelet power by removing the normalization of $|W_j(t,s)|^2$ by $s/\delta t$, in a fashion analogous to the formation of variance-preserving autospectra.

$$\mathcal{E}_j(t,s) \equiv \frac{s}{\delta t} W_j^{ri}(t,s) \tag{4.2.8}$$

The ability of the combination of CEOF and cross wavelet methods to give valid estimates of energy can be assessed by comparing the magnitude of the modal amplitude, $|b_j(t)|$, filtered to pass a frequency band D, to the estimates of $\mathcal{E}_j(t, s_D)$, where s_D is the range of scales corresponding to D. In particular, $|b_j(t)[\text{D}]|$ is a current speed which corresponds to the square root of $\mathcal{E}_j(t, s_D)$. CEOF and cross wavelet analysis are applied to a 100-day time series of velocity $u(z,t) + iv(z,t)$ measured on the mid- to outer shelf at R4 in 41 m water depth (Fig. 21) from April through July 2005. Over this time scale, barotropic currents are isolated in the lowest mode $\hat{\psi}_0(t)$ (*Edwards and Seim*, 2008a), and the analysis will focus on the diurnal (D1) and semidiurnal (D2) bands.

Time series of the magnitude of mode 0, $|b_0[\text{D2,D1}](t)|$ (plotted in blue, Fig. 22, upper panels), show strong modulation of the M_2, S_2, and N_2 barotropic tides in the D2 band, as well as the interaction of O_1 and K_1 barotropic tides in the D1 band. Mode 1 (lower panels) amplitude in D2 is an order of magnitude smaller than mode 0. In contrast, D1 band amplitude increases significantly in May and June to over 20 cm/s, which approaches the magnitude of semidiurnal barotropic tide ($|b_0[\text{D2}]t)|$). The differences between $|b_0[\text{D2,D1}](t)|$ and the square root of average, maximum, and summed energy of $\mathcal{E}_j(t, s_D)$ over the D2 and D1 scale-bands may be attributed to the filter characteristics of the D-band filters and spectral smoothing in cross wavelet space, but in general, the variability of the input time series is preserved by the XWT estimates of $\mathcal{E}_j(t, s_{D2,D1})$.

Thus, this combination of normalized CEOF and XWT methods retains variance in time and frequency space, and the variance-preserving formulation can give energy estimates of vertical modes as a

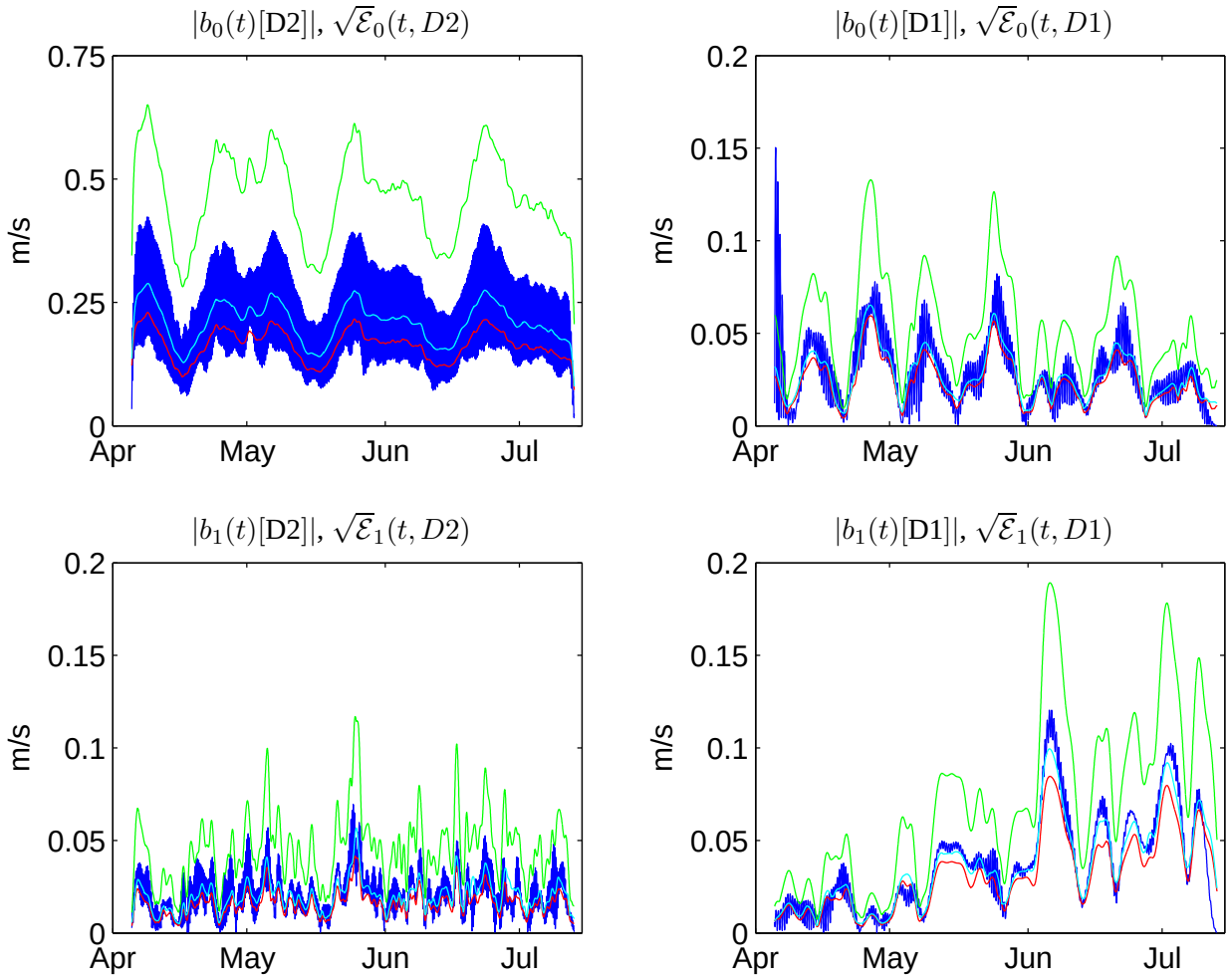

Figure 22: Magnitude of $b_j[\mathrm{D}](t)$, computed over frequency band D, and three estimates of rms speed $\sqrt{\mathcal{E}}_j(t, s_D)$ based on the scale-band-average (red), maximum (cyan), and sum (green) of energy per unit mass derived from CEOF+XWT analysis. The energy estimates over D=D2,D1 (left, right) for modes $j = 0, 1$ (upper, lower) of the ADCP data measured at R4 in 2005 confirm that the combined methods correctly retains variance through the normalized CEOF and variance-preserving XWT formulation of $\mathcal{E}_j(t, s_D)$.

function of time and frequency. This application of CEOF and XWT analyses to currents on the Georgia Bight seeks to understand processes with the same frequency, at the same location, but with different vertical scales. First using CEOF reduces the vertical dimension of measured currents to the first three vertical modes, $j = 0, 1, 2$, which contain over 99.5% of the total variance for all seasons, years, and locations. Even still, for this application to data with high vertical and temporal resolution spanning multiple years at several locations over the shelf, it is advantageous to conduct the two analyses separately, over different periods. Wavelets, like any filter, suffer from edge effects that define a "cone of influence" which changes with scale s (*Torrence and Compo*, 1998). On the other hand, the time scale of variability of stratification on the shelf determines the maximum period over which CEOF can be applied to properly separate the barotropic and baroclinic velocity structures. This practical maximum period of analysis has been empirically estimated to be about 120 days in the South Atlantic Bight (SAB *Edwards and Seim*, 2008a).

The combination of EOF and wavelet analysis has been explored in the literature, but the application described here is novel. The analyses in the literature are typically applied in the opposite order. The application of CEOF to cross-covariance matrices derived from wavelet analysis of scalar quantities (*Wang et al.*, 2000; *Pairaud and Auclair*, 2005; *Mwale et al.*, 2007) would be not be computationally feasible (*Wang et al.* (2000): 11 vertical locations, Δt=20 min over 25 days; this study: 7 horizontal locations, 15-45 vertical locations, $6 < \Delta t <$30 min over multi-year records); the application of CEOF before cross wavelet analysis as described here reduces the computational load significantly. *Waseda et al.* (2003) approach the computational load of the problem by combining the separate results of EOF analysis over large scales and 2-dimensional wavelet analysis over small scales to form an error covariance matrix for applications of data assimilation. The formulation of EOF analysis on the product of XWT analysis is intended for the case of processes at different frequencies and scales in the same location or at the same frequency but at different locations and times (*Pairaud and Auclair*, 2005).

To take best advantage of both methods, in this study, CEOF is applied by season (DJF, MAM, JJA, SON) to minimize the influence of changing stratification on the boundary layer structure of the barotropic currents (*Edwards and Seim*, 2008a), and the resulting vertical modes $\phi_j(z)$ are normalized by the methods described above. The $b_j(t_{season})$ are concatenated in time for each mode at each location and then sub-sampled to 1-hr resolution. Cross wavelet analysis is then performed on the combined record of $b_j(t)$, and estimates of $\mathcal{E}$ as a function of time, frequency, and spatial location are derived for each vertical mode.

Filtering

If CEOF is applied over a sufficiently short time scale such that the bottom boundary layer structure of the barotropic tide will not change, the gravest mode $\hat{\psi}_0(z,t)$ will fully contain barotropic velocity structure and its variability in time. The "baroclinic" velocity structure is then described by the sum of the reconstructed vertical modes $j \geq 1$.

CEOF is applied to all available ADCP data by season (DJF, MAM, JJA, SON), and the "baroclinic" portion is reconstructed: $\psi_{bc}(z,t) = u_{bc} + iv_{bc} = \sum_{j=1}^{M-1} \hat{\psi}_j(z,t)$. The diurnally varying portion of the baroclinic currents, $\psi_{bc}[\mathrm{D1}](z,t)$, is given applying a 4th order Butterworth filter designed to pass the diurnal band D1 (defined here to be 20-28 h).

Lacking the vertical dimension to separate the barotropic and baroclinic currents, the buoy wind and WERA data are simply filtered to the D1 band as above at each location. To address the frequent but short gaps in the WERA records, the data are linearly interpolated through short gaps before filtering; the filtered data corresponding to the gaps are replaced with not-a-number values for further analysis. The estimates of D1 variance that result contain both tidal and non-tidal diurnal variance. However, diurnal barotropic tidal currents in the Georgia Bight do not vary significantly over the study region (2-4 cm/s, *Blanton et al.*, 2004) and are small relative to the surface-enhanced diurnal/inertial currents observed in spring, which approach 25-35 cm/s on short time scales.

4.3 Development of a climatology: vertical, along-, and cross-shore structure

Observations of currents on the shelf of the Georgia Bight from 2000 through 2007 are used to compile a climatology of the along- and cross-shore structure of non-tidal diurnal/inertial currents in the surface ocean near the critical latitude. These estimates of the distribution of diurnal/inertial energy can be compared to the climatology of SBLB winds, found to be enhanced in the Georgia Bight due to the combined effects of the critical latitude and coastline curvature. The multi-year coverage of the data allows for assessment of monthly, seasonal, and interannual trends of diurnal variance in the vertical, along-, and cross-shore directions.

4.3.1 Vertical structure

The vertical structure of non-tidal diurnal/inertial currents is described using filtered baroclinic currents ψ_{bc} and the combination of CEOF and cross wavelet methods. Non-tidal D1 band currents are enhanced near-surface, circularly polarized, and vary on synoptic time scales from April through October. Figure 23 shows estimates of D1 variance computed by season (winter=DJF, spring=MAM, summer=JJA, fall=SON) for all available data on the shelf. The panels are arranged to mirror the location of instruments in shallower (15-32 m water depth, left) and deeper (35-40 m, right) shelf waters, with latitude increasing bottom to top.

Near-surface variance is enhanced at all locations in spring and summer, and generally increases with water depth. The summer-long estimates of D1 variance near-surface at R8 and R4 are on the order of 0.007-0.025 m^2s^{-2}, or an root mean square (RMS) speed of 8-16 cm/s as an estimate over a 3-month window. However, on synoptic time scales, the near-surface current speeds at times exceed 30 cm/s at the outer shelf locations.

Despite the deeper water location, the D1 variance at R6 is comparable to the shallower location at R2. The vertical structure of D1 currents at Gray's Reef (GR), located in 16 m water depth, exhibits different patterns of temporal variability over its short deployment. Spring variability at GR is greater than that of summer; this decrease in D1 energy from spring into summer is not seen at any other ADCP on the Georgia Bight. This result may yield clues about the relative importance of the position of the CFZ, spring freshets, and summertime heating in shallow water. Significant stratification on the inner shelf appears to be caused by spring freshets. The shallow water depth may prevent the establishment of thermal stratification in summer.

The subsurface maximum of D1 variance in the vertical corresponds to the depth at which the lower layer is 180°out of phase with the surface layer. The advent of summer brings changes to the lower level structure, particularly at the mid- to outer shelf locations, R8-R4-ST. On the seasonal time scale, the strengthening of the energy in the lower layer in summer may correspond to periods of strong stratification. If so, R8 may be subject to different sources or variability of stratification than R4 and ST; the enhanced variability in the lower layer at R8 is strongest in 2004 and 2006, while R4 and ST D1 variance are largest in summers 2003 and 2005. The interannual variability at each location suggests that the vertical structure changes from year to year, presumably in response to varying stratification. The vertical structure at R2 contains a strong subsurface maximum that is lower in the water column than seen at R6. This closer resemblance of the vertical structure at R2 to the outer shelf locations compared

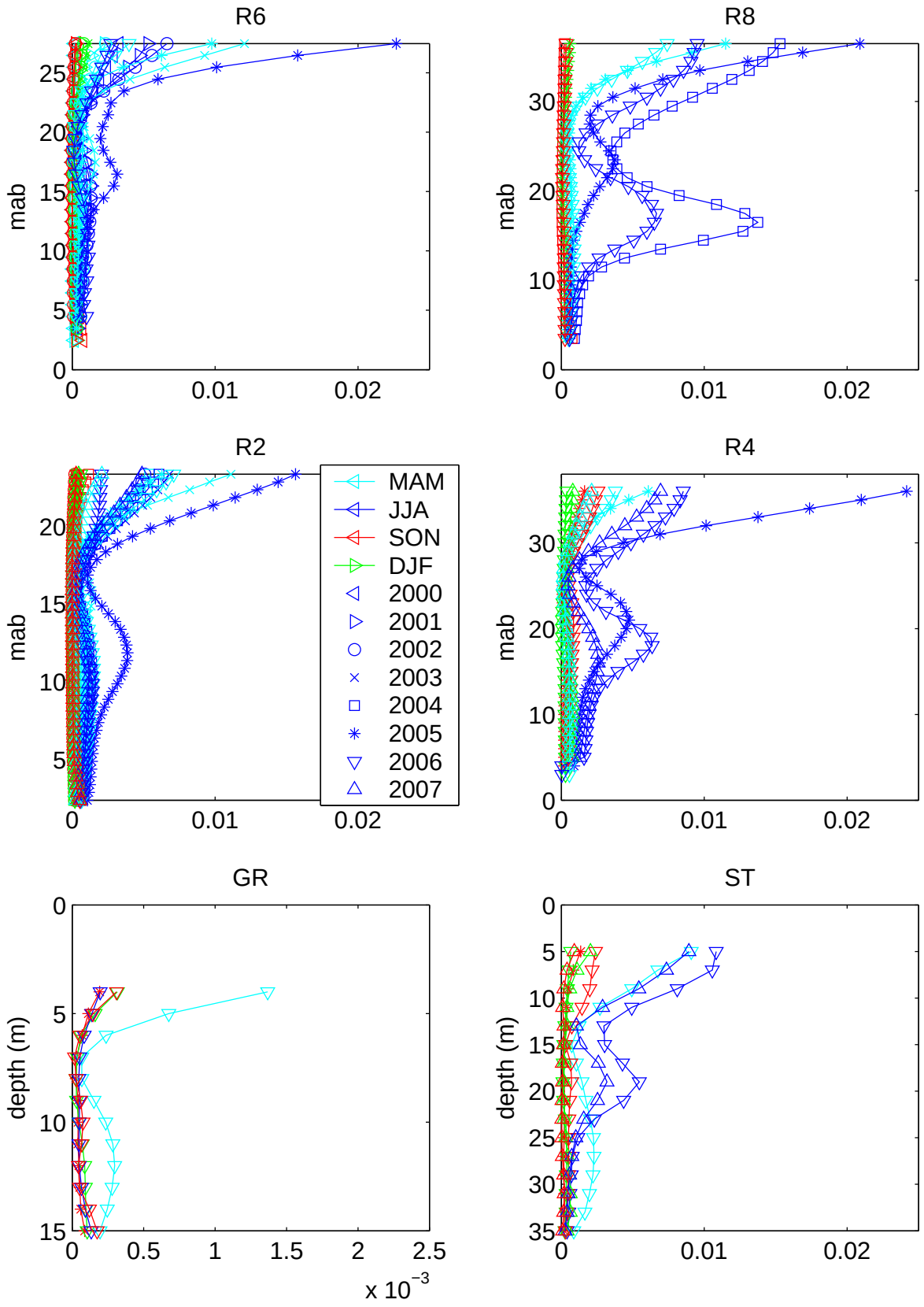

Figure 23: Estimates of D1 variance in the baroclinic currents ψ_{bc} with depth at 6 locations on the shelf, given by season (coded by color) from 2000-2007 (coded by symbol), show increased non-tidal near-surface diurnal/inertial energy at locations on the mid- to outer shelf relative to inshore ADCP measurements.

to its nearest neighbor at R6 may be related to the exception to the trend of increasing variance with distance offshore.

The combination of CEOF and cross wavelet analysis is applied to all ADCP data available on the shelf as described in Section 4.2. Only the lowest mode defined by CEOF can be directly related to a specific physical process (*Edwards and Seim*, 2008a), but *MacKinnon and Gregg* (2003b) show that EOF modes of currents observed during the Coastal Mixing and Optics (CMO) experiment on the New England shelf do correspond to the normal modes computed for measured stratification. *MacKinnon and Gregg* found the New England shelf to be dominated by mode 1 energy, with the growth of mode 2 currents corresponding to the onset of stratification and the change in the vertical position of the pycnocline. Measures of the density structure on the Georgia shelf and its variability are not available for this study to confirm the relationship between EOF and normal modes, but increases of higher mode amplitude are tentatively interpreted to arise from the shallowing of the pycnocline as stratification strengthens in the upper portion of the water column.

The D1 variance in the baroclinic currents ψ_{bc} (Fig. 23) is effectively described by the sum of modes 1 and 2, as the first three modes (0, 1, and 2) contain over 99% of the variance in ψ. Though the relative magnitudes of the modal amplitude vary in space and time, the vertical modes are qualitatively similar at all locations. At each location, the modal structure seldom varies, with zero crossings typically within a couple meters among seasons. Mode 2 is usually an order of magnitude smaller than mode 1. The annual cycle is the dominant signal for both modes (Fig. 24). Mode 1 is enhanced from spring through early fall, with increased mode 2 energy primarily during the summer months. Closer inspection reveals that the event frequency of variability in modal energy is on the order of 8-15 days.

In general, both modes are strongest on the outer shelf, but the 5-year maximum of mode 2 energy occurs at R2 and R6 in May 2003, a period of anomalously strong stratification on the shelf (*Arexta-baleta et al.*, 2006). The observations are limited to the mid-shelf through May 2003 because the ADCPs were removed for tower maintenance from June through September. Differences in the diurnal/inertial energy on the shelf between years are apparent; as seen in Figure 23, 2005 has a relatively high baseline level of D1 energy. Variability in summer 2006 is small relative to the spring and fall of the same year, particularly in mode 1. D1 motions in 2007 are much smaller than preceding years.

4.3.2 Alongshore, cross-shore structure

The along- and cross-shore structure of diurnal/inertial currents on the shelf are examined and compared to that found elsewhere in the literature (*Chen et al.*, 1996; *Chen and Xie*, 1997; *Lewis*, 2001;

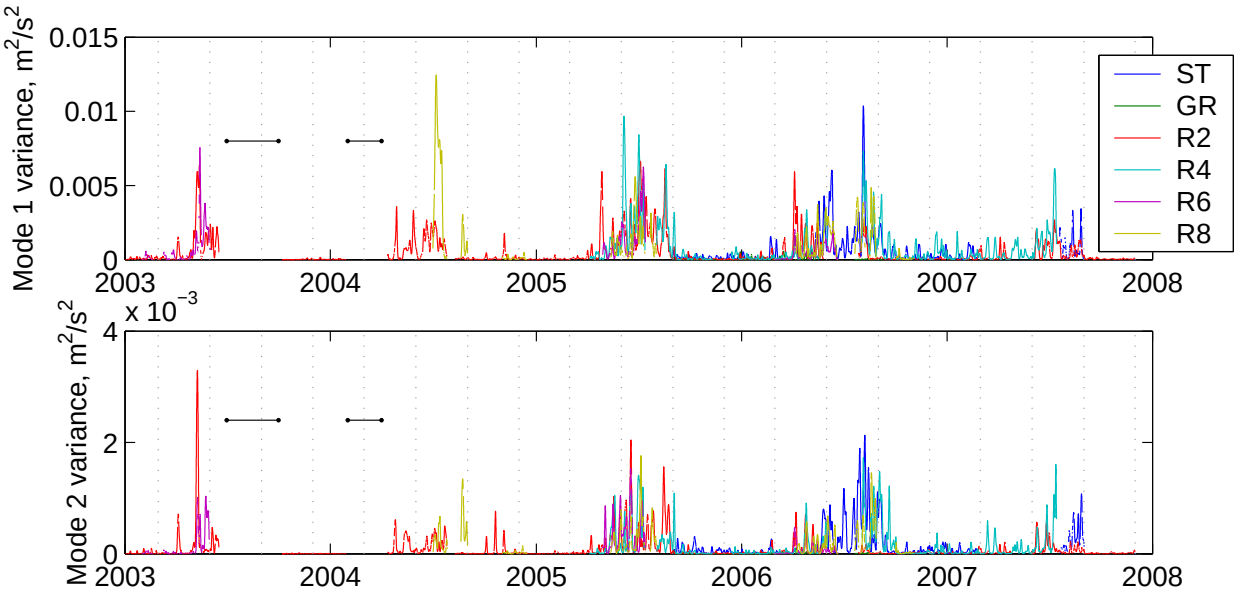

Figure 24: Time series of the max value of $\mathcal{E}_j(t, D1)$ for mode 1 (j=1, upper panel) and mode 2 (j=2, lower panel), given in m^2s^{-2}. The horizontal black lines mark periods over which no data are available due to tower maintenance.

Jarosz et al., 2007). Variability in structure in either direction may indicate or reveal mechanisms for strengthening or damping near-inertial motions. The structure of the D1 currents is compared to that of the SBLB winds.

Estimates of D1 variance in the surface currents are calculated by month for each summer month (taken here to be May-September), and summer-long D1 variance is estimated by calculating the variance over summer months over all years. The ADCPs on the mid- to outer shelf form an alongshore transect close to the 40 m isobath, ST-R4-R8, with latitude ranging from 30.04 to 31.63°N. Similarly, the line of ADCPs from Gray's Reef to R8 (GR-R2-R6-R8) complements the cross-shelf WERA transect shown in Figure 21.

Monthly alongshore transects of variance when all 3 ADCPs are operational show no significant trend in D1 variance with latitude (Fig. 25a); nor does the summer-long estimate of D1 energy (dark black line). The range of D1 variance in the alongshore direction is large relative to any potential trend with latitude/distance alongshore, with R4 variance ranging from 0.0025 m^2s^{-2} in May 2007 to 0.0375 m^2s^{-2} in July 2005. The meridional range spanned by the observations is small (250 km), and significant enhancement of D1 currents at the critical latitude is not observed over these scales.

The two cross-shore transects (Fig. 25b,c) reveal a maximum of D1 energy on the outer shelf, and

the separate estimates of D1 variance from the ADCP moorings and from the HF radar agree well at R8, where they intersect. Despite the range of energy present over the summer months, the WERA and ADCP transects show very little cross-shore change in D1 energy in the mid-shelf region (the plateau of energy level across water depths 20-35 m). Along the cross-shore transect given by GR-R2-R6-R8, the energy at R6 is comparable to or slightly weakened relative to R2 for all but one of the months when data are available.

A geographic view of the compilation of variance estimates highlights the cross-shore structure and its variability in time (Fig. 26). Monthly mean D1 variance is plotted in color, with monthly mean wind and depth-averaged currents given for reference. As seen in Fig. 25b and c, D1 variance near the outer shelf is consistently large relative to inshore locations. On the inner and mid-shelf, diurnal/inertial energy is smaller in the mean, but more widely distributed, which suggests that the upper end of the D1 variance range may be event-driven.

Mean summer flow on the shelf is generally northward, oriented alongshore, as noted by *Lee et al.* (1991), and follows the mean wind pattern in summer. Southward flow in September tracks the wind reversal that marks the beginning of mariner's fall (*Weber and Blanton*, 1980). D1 variance is relatively small in May, increases through June and July, decreases in August, and returns to low levels in September. The interannual variability in the D1 variance is notable. Comparing years, 2005 emerges as a year of greatly enhanced D1 variance over much of the shelf, with greatest D1 variance at R4 for June and July. D1 variance is relatively weak in 2007.

Despite the significant interannual variability, the spatial patterns of increasing energy with distance offshore remains through all years. The WERA data suggest a pattern of increasing variance with cross-shore distance, consistent with that found by modeling (e.g., *Chen and Xie*, 1997; *Lewis*, 2001; *Davies and Xing*, 2004) and observational (*Chen et al.*, 1996; *Jarosz et al.*, 2007) studies. However, the ADCP data do not extend far enough offshore to confirm a maximum suggested by the WERA observations rather than the continued increase to the multiples of the Rossby radius predicted by *Lewis* (2001), or the nature of the decrease on the shore- and seaward sides of the maximum for comparison to *Chen et al.* (1996).

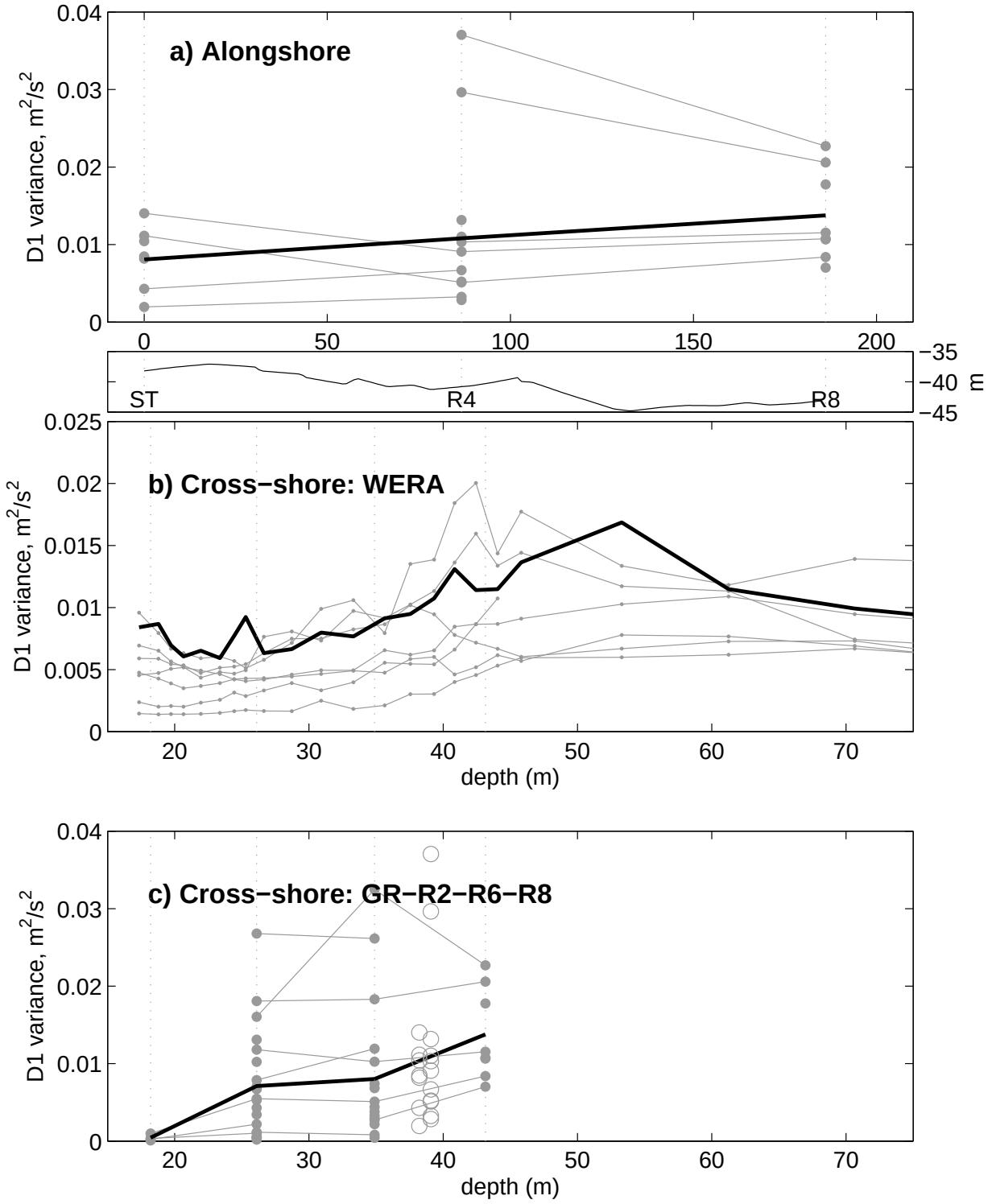

Figure 25: Monthly (May-September, gray) and summer-long (black) estimates of D1 variance with distance in km along an alongshore transect (ST-R4-R8). Variance along cross-shore WERA (middle) and GR-R2-R6-R8 (lower) transects are plotted versus water depth, as the comparison scales with water depth rather than distance offshore. The alongshore variance at ST and R4 are plotted with depth on the lower panel for comparison, and are shown as open circles.

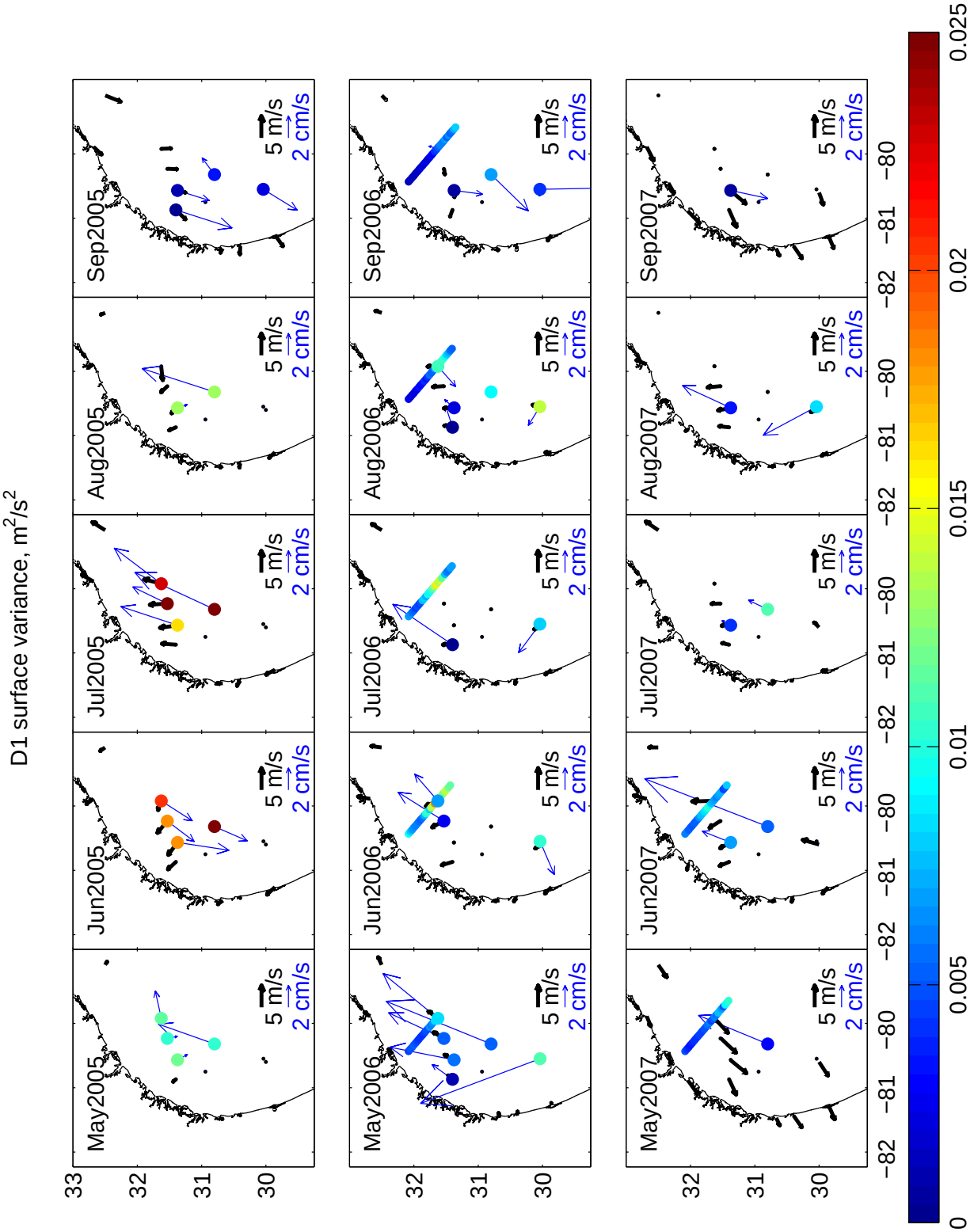

Figure 26: Mean wind (black) and depth-averaged currents ($\bar{\psi}_z(t)$) are shown with arrows, and colored dots indicate the D1 variance (m^2s^{-2}) of the measured surface currents along the WERA transect and of baroclinic surface currents $\phi_{bc}(z,t)$ for moored/buoy-mounted ADCPs. The compiled monthly data are shown for summer months (May-September) 2005-2007.

4.4 Comparison to SBLB

4.4.1 Alongshore, cross-shore structure

Comparison of the spatial structure and variability of the D1 surface currents to the patterns of SBLB in the Georgia Bight provides insight into the degree to which the surface current response is determined by wind forcing alone. *Edwards and Seim* (2008b) estimate the summertime SBLB wind variance in the NAM model reanalysis fields over summers 2006-2007, contoured in Fig. 21. Figure 27 shows the monthly estimates of D1 wind variance from winds observed at NDBC buoys and SABSOON towers. Maximum SBLB winds coincide with the critical latitude for diurnal/inertial resonance, but the offshore extent of SBLB is enhanced over the entire latitudinal range of the Georgia Bight.

The strength of the coastal ocean's response does not directly track the forcing. SBLB winds are typically strongest just off the coastline and decrease with distance offshore, while the surface currents are weak inshore, strengthen on the inner shelf, plateau on the mid-shelf, and reach a maximum in the observations furthest offshore. Maxima of SBLB horizontal extent and wind speed near and just north of the critical latitude in the Georgia Bight are not repeated in the coastal response. The surface ocean's response in the D1 frequency band does not indicate a maximum at the critical latitude along a transect of the 40 m isobath (Fig. 25a), but Figure 27 highlights the limited latitudinal range spanned by the observations relative to the length scale of SBLB circulation.

4.4.2 Phase

Edwards and Seim (2008b) propose that spatial variability of the SBLB wind field causes diurnal divergence and convergence of the wind field which may lift and depress the pycnocline at the diurnal frequency. The relative phase of SBLB and the surface currents may reveal areas of surface divergence and convergence, and indicate the degree to which the near-inertial signal is locally generated. Time series of snapshots of the SBLB wind and D1 surface currents every 6 hours over August 4-6 (Fig. 28) show that the winds and the currents are nearly aligned, with the currents leading the winds by 10-25°or so. Though the direction of the SBLB wind varies in space, the direction of D1 surface currents is largely uniform across the entire shelf. There may be some surface divergence between R4 and ST when the magnitude of SBLB slackens at 00:00 and 12:00 local time.

Significant differences in phase of the wind and the surface current could indicate that NIIW at a location were not locally generated, but more likely reflect the difference between the diurnal forcing and the inertial response of the ocean (indicated by the currents leading the forcing). One measure of

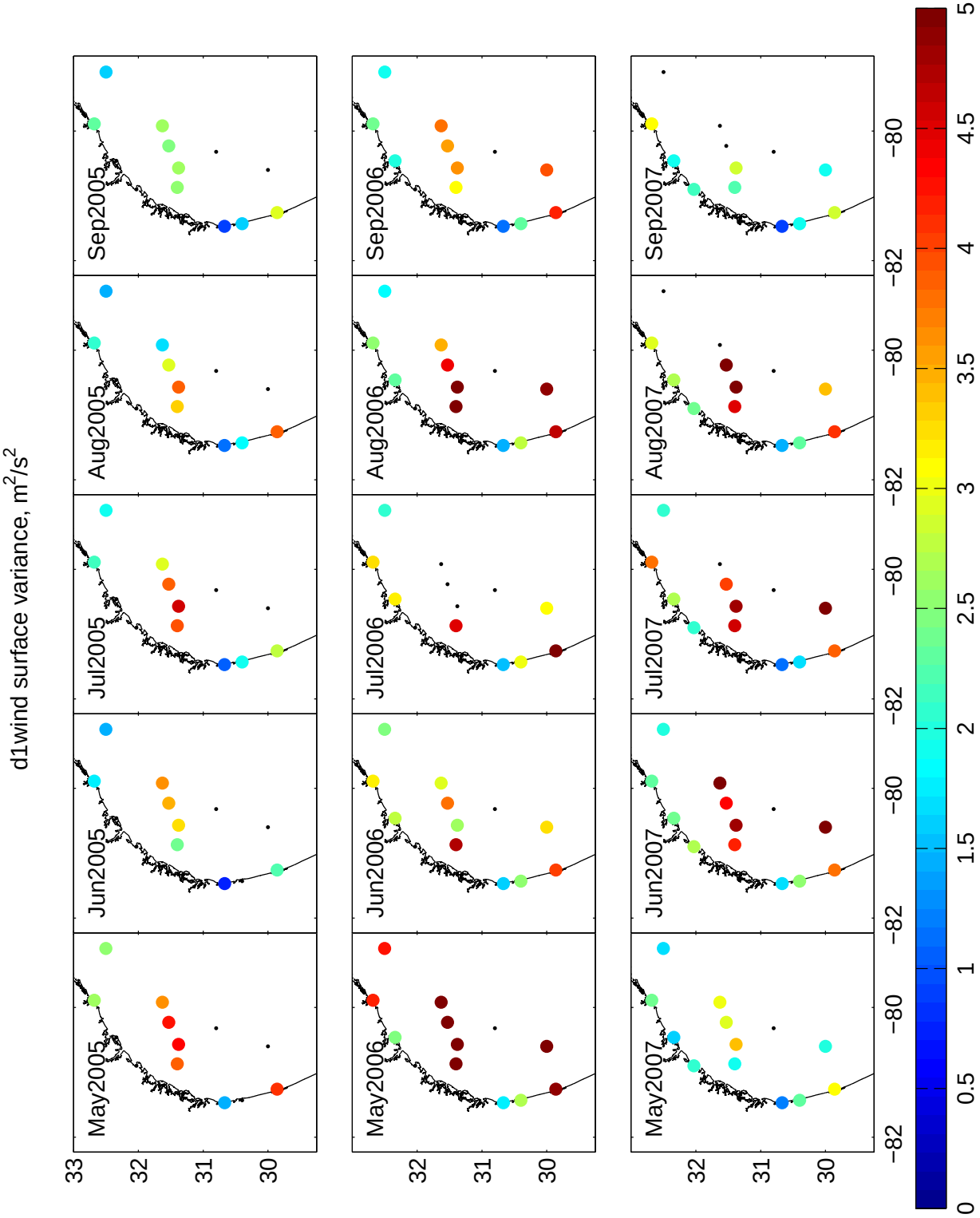

Figure 27: D1 wind variance by month where winds are available, in m^2s^{-2}, compiled for summer months (May-September) 2005-2007. The patterns in the D1 current variance do not generally match those of the D1 wind variance.

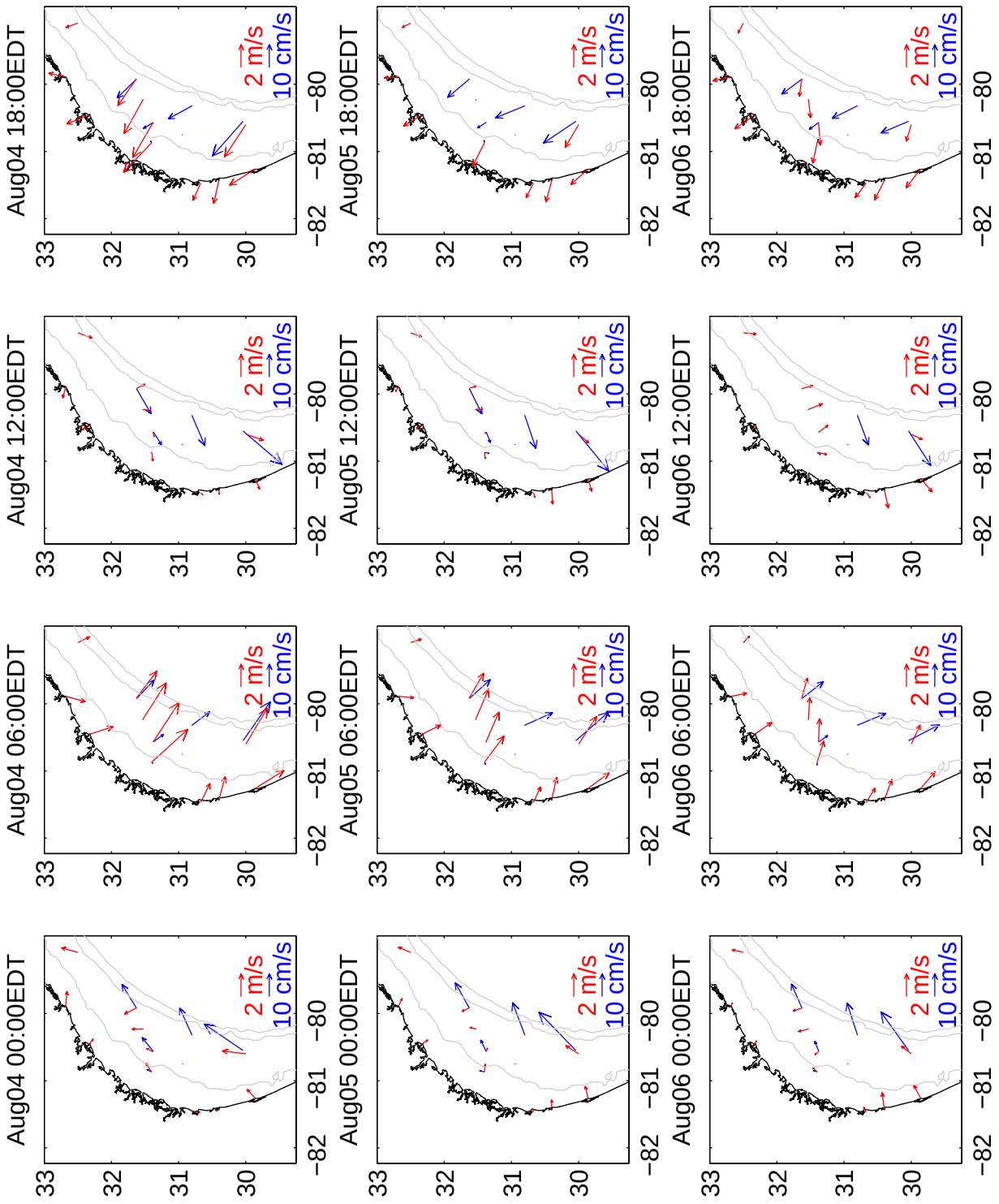

Figure 28: Time series of snapshots of SBLB (red) and D1 surface currents (blue) over a 3-day time period in August 2006 shows the directional coherence and cross-shore variability of the surface response over the shelf.

efficiency of the wind forcing assesses this difference between phase of the clockwise (CW) component of the D1 wind field and the phase of the D1 near-surface currents (*Jarosz et al.*, 2007). Neither the D1 wind field nor the near-surface currents is purely diurnal in character, but the D1 near-surface currents are nearly purely CW-rotating. The difference between θ, the phase of the CW-rotating component of the purely diurnal portion of the wind field, and ϕ, the phase of the D1 (20-28 hr) surface currents is shown in Figure 29b. SBLB propagation explains some of the trend in phase difference with distance offshore, as the phase of the wind forcing, θ, at offshore locations will lag inshore locations by approximately 30°per 100 km offshore (*Edwards and Seim*, 2008b). However, relative phase as a measure of wind efficiency suggests that SBLB grows *less* effective with distance offshore. The mean value of this phase difference increases to 40-50°over the mid- to outer shelf, which despite the variability about this mean, suggests the increasing importance of Ekman dynamics with depth even over inertial time scales.

Despite the increasing difference in phase of winds and currents, the magnitude of the currents does change significantly cross-shelf (Figs. 25b,c, 28), and is most striking when land or sea breeze is maximum, around 8:00/20:00 local time. The increase of D1 energy with distance offshore causes the surface currents to diverge over the mid-shelf on the land breeze phase, and converge on the mid-shelf at maximum sea breeze. This mid-shelf convergence of surface currents at the diurnal frequency would result in down/upwelling displacements on the order of 4-5 m, which is half the estimate compared to that derived from the strength of the winds alone (*Edwards and Seim*, 2008b).

4.5 Discussion

The near-surface current response appears to be inertial rather than diurnal, suggesting that the energy transfer between SBLB and the surface ocean acts as a filter. The phase difference between CW wind and the D1 near-surface currents is one estimate of the timing efficiency of the wind energy input, but the phase difference increases with distance offshore. The phase formulation of wind efficiency does not consider the strength of the response in the ocean, which appears to be strongly controlled by friction, relative to the SBLB wind strength. To consider the effects of friction and stratification, the ratio of D1 response to the D1 wind stress may be a more practical measure of wind efficiency. Figure 29c shows the ratio of D1 near-surface magnitude and D1 wind variance, which increases with distance offshore as the current response increases. The outlier at R2 is May 2003, and the line with the greatest magnitude and the outlier at R4 correspond to June 2005, but the underlying trend is increased wind efficiency with cross-shore distance.

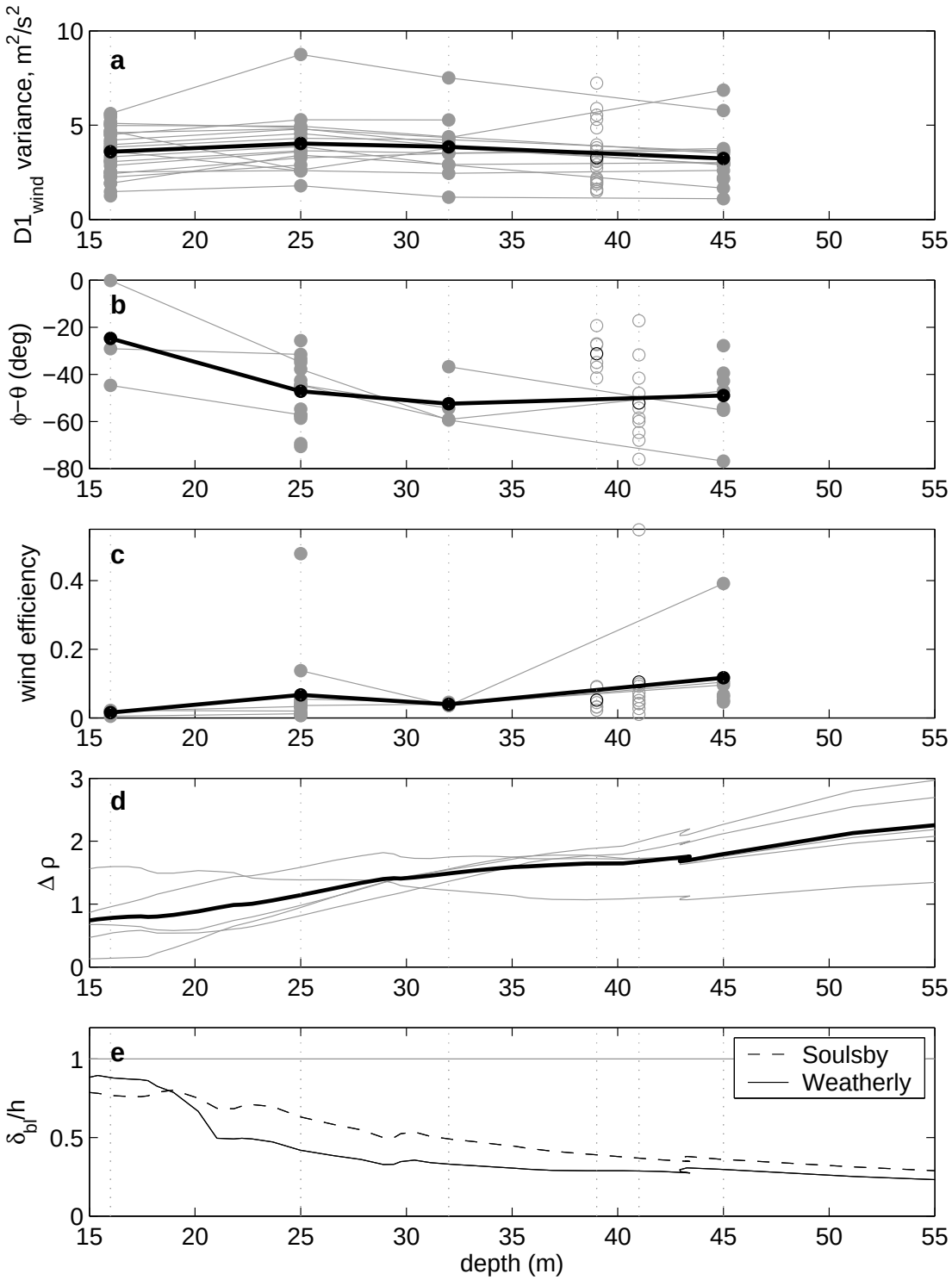

Figure 29: Cross-shore profiles of a) D1 wind variance, b) relative phase of the currents and CW-rotating diurnal wind (ϕ-θ), and c) wind efficiency as a D1 near-surface current magnitude over the D1 wind variance (proportional to wind stress) calculated along the transect made by GR-R2-R6-R8 for all summer (May-Sept.) months when co-located winds and currents are available. Gray lines and dots show the estimate by month, and the black lines and dots indicate the mean of the monthly ensembles at a given location. Empty circles represent values computed for ST and R4, and nearest neighbor winds at R6 are used at R4. The lower panels show d) a cross-shore transect of bulk stratification ($\Delta\rho$ bottom to surface) and e) the ratio of boundary-layer thickness of the barotropic tide relative to water depth from the climatology and tidal databases given by *Blanton et al.* (2003, 2004).

The influence of stratification and bottom friction on the magnitude of the D1 ocean currents is assessed on the cross-shore transect made by GR-R2-R6-R8, using the tidal database of the SAB described by *Blanton et al.* (2004). Bottom-to-surface change in density $\Delta\rho$ is calculated for the monthly climatology of *Blanton et al.* (2003) along the cross-shore transect shown by the light gray line in Figure 21. Summer (May-Sept.) bulk stratification $\Delta\rho$ remains constant on the shelf in May, but increases with distance offshore from June through September, as well as in the mean (black, Fig. 29d).

To assess the degree to which bottom friction dissipates energy within the water column, the height of the bottom boundary layer is assumed to be set by the M_2 barotropic tide, which contributes up to 80% of the total kinetic energy on the shelf (*Pietrafesa et al.*, 1985). Bottom boundary layer thickness is estimated using formulations with (*Weatherly et al.*, 1980) and without (*Soulsby*, 1983) considering the effects of stratification:

$$\delta_{Weatherly} = \frac{1.3u_*}{\sigma(1+N^2/\sigma^2)^{1/4}} \tag{4.5.1}$$

$$\delta_{Soulsby} = 0.0038\left(\frac{\omega\bar{U}_{maj} - f\bar{U}_{min}}{\omega^2 - f^2}\right) \tag{4.5.2}$$

Frequency ω is the M_2 frequency, $\bar{U}_{maj}, \bar{U}_{min}$ are the depth-averaged semi-major and semi-minor tidal ellipse axes, N is the Brunt Vaïsälä frequency, and σ is the absolute value of the frequency difference $|f-\omega|$. Estimates of u_* are derived from the M_2 tidal semi-axes and a quadratic drag coefficient : $u_* = \{C_D\ (|U_{maj}|^2 + |U_{min}|^2)\}^{1/2}$, where C_D=2.5$\times 10^{-3}$. The cross-shore profile shows that the effects of bottom friction are felt through the majority of the water column to the outer shelf (Fig. 29e). The water column is almost completely occupied by the bottom boundary layer at depths below about 15-20 m, where stratification is weakest during summer.

Though simultaneous observations of density and measured currents on the shelf are limited over the 7-year period considered, the efficiency of the wind may then serve as a proxy for stratification. The difference in variability of the R2 wind efficiency at R2 and R6 is striking, and together with the plateau of D1 energy mid-shelf at R6, suggests a minimum of stratification mid-shelf at R6. With less frequent and less strong sources of stratification, and dynamics dominated by wind and tides (*Atkinson et al.*, 1983), the mid-shelf region may support intermittent tidal front formation, and closer analysis may determine the degree to which mixing may overcome stratification mid-shelf.

The strength of near-surface response to SBLB does not track the magnitude of forcing, but rather increases with distance offshore, in agreement with the modeling predictions of *Chen and Xie* (1997);

Lewis (2001); *Davies and Xing* (2004). The observations in the Georgia Bight do not resolve the maximum of near-inertial energy. The spatial patterns of diurnal/inertial variance in the DeSoto Canyon region are clearly topographically controlled on the slope, where mesoscale circulation features which may trap near-inertial energy (*Hamilton et al.*, 2000; *Jarosz et al.*, 2007), but the observations do not extend onto the shelf, where bottom friction becomes a major control on the strength of near-inertial motions. Although the distance from shore of the observations in this study is similar to the DeSoto Canyon Experiment, the 1500 m isobath is 125 km offshore in the Gulf of Mexico but more than 350 km offshore in the Georgia Bight.

SBLB extends to at least 250 km offshore (near the 800 m isobath), and its magnitude is enhanced in the Georgia Bight, but very strong SBLB winds that extend over the entire shelf (e.g., May 2006 or July 2007) do not necessarily elicit a strong response in the surface currents. Conversely, the relatively weak SBLB of June 2005 co-occurs with the strongest diurnal/inertial currents observed in over nearly 7 years of data. The slab-like response of the surface currents to spatially varying wind suggests a "filtered" transfer of energy into the surface ocean. It is clear that SBLB is not the sole control of the surface-enhanced diurnal currents in the Georgia Bight, and that friction and stratification mediate the distribution and fate of SBLB energy on the shelf near the critical latitude.

The Gulf Stream serves as the far cross-shore boundary of the Georgia Bight, though its role as a sink or source of diurnal/inertial energy remains unclear. The WERA data become gappier with distance offshore, and filtering becomes less reliable. However, tidal analysis at diurnal tidal frequencies is more robust through missing data, and shows that the sum of K_1 and O_1 energy increases from the outer shelf into the Gulf Stream (D. Savidge, pers. comm., 2008). The Gulf Stream could trap near-inertial energy at its shoreward density front, where the effective Coriolis parameter, f_{eff}, is larger than the local inertial frequency. NIIW generated on the shelf will either be absorbed or reflected by the Gulf Stream. The Gulf Stream may also serve as a source of near-inertial energy, or may Doppler-shift NIIWs (*Zhai et al.*, 2005), allowing them to travel north of the turning latitude given by the intrinsic inertial frequency.

The vertical structure of the diurnal/inertial currents changes with distance offshore, as well. The subsurface maximum detaches from the bottom, and lies at about mid-depth at the offshore locations. Cross-shore structure of the energy in modes 1 and 2 mirror the trend in total D1 energy, as the subsurface maximum becomes more pronounced on the mid- to outer shelf (Fig. 23). However, the relative magnitude of mode 1 and mode 2 do not change in time, unlike the relationship found by *MacKinnon and Gregg* (2005), wherein mode 2 energy increased at the expense of mode 1. This difference in the interaction of energy in different modes is likely due to the difference in the wind that forces the near-

inertial response. The near-surface energy is continuously reinforced by SBLB in the Georgia Bight, whereas the response to a wind impulse will require a trade-off of modal energy to compensate for the growth of energy in higher modes.

The influence of stratification and the vertical structure of shear are examined further through case studies by *Edwards and Seim* (2008c), a companion paper to this study. The interaction of shear and stratification is considered over shorter time scales, and the vertical structure of the diurnal/inertial motions and the propagation of NIIWs are considered to explore how these baroclinic motions may mediate the transfer and redistribution of diurnal/inertial energy on the shelf near the critical latitude.

4.6 Summary

Wind-induced currents on the shallow shelf of the Georgia Bight are on the order of 10-30 cm/s in a shelf-wide response to SBLB forcing. The vertical structure is surface-enhanced, with a 180°phase change in the upper half of the water column. These currents increase with distance offshore, up to 35 cm/s, and approach the magnitude of the currents of the barotropic M_2 tide on the mid- to outer shelf. The vertical structure of the diurnal/inertial currents becomes more pronounced on the mid- to outer shelf, but the continued forcing at the surface allows the energy in higher modes to increase without compensation in the mode 1 magnitude.

The SBLB wind forcing decreases with distance offshore, and the relative phase of the winds and the currents indicates the decreased quality of the SBLB resonator at larger distances from the shoreline. Rather, the magnitude of the diurnal/inertial response corresponds with the relative influence of stratification and friction on the shelf. These spatial patterns suggest the importance of the ability of wind stress to penetrate the surface ocean, enhanced by stratification, in setting the maximum in the cross-shore direction in the Georgia Bight.

CHAPTER 5. Coastal ocean response to SBLB in the Georgia Bight: Stratification and shear

5.1 Introduction

Edwards and Seim (2008d) found that the magnitude of SBLB-forced currents near the critical latitude of 30°N is set by the relative influence of SBLB wind forcing, friction, and stratification. SBLB winds decrease with distance offshore, but become more efficient in generating near-inertial motions as the relative influence of bottom friction decreases. Stratification appears to be the link that determines how input wind energy is distributed in space and time – greater stratification leads to increased kinetic energy of the near-surface currents, enabling decoupling in the vertical to inhibit dissipation of the surface-forced diurnal/inertial currents via bottom friction, and permitting the radiation of near-inertial energy via near-inertial internal waves (NIIWs).

Under spatially uniform periodic wind stress at the inertial frequency, NIIW are generated at a coastal boundary (*Davies and Xing*, 2003) or where fronts intersect topography (*Davies and Xing*, 2002; *Xing and Davies*, 2004; *Davies and Xing*, 2005) in a narrow swath 10-20 km wide termed the coastal boundary layer (CBL) by *Davies and Xing* (2003). In the more general case where topography, stratification, and wind stress vary in space, local divergence or convergence of near-surface currents due to coastline curvature, frontal boundaries, or spatial variability of the forcing wind field or the coastal response will elevate or depress the pycnocline in response.

In the Georgia Bight, phase propagation of SBLB offshore results in persistent spatial gradients in the wind field that force the coastal ocean at the near-resonant diurnal frequency (*Edwards and Seim*, 2008b). The cross-shore structure of the coastal ocean response to SBLB forcing may also result in significant divergence and convergence of diurnal/inertial surface currents on the inner to mid-shelf. The pycnocline is moved vertically at the diurnal/inertial frequency, and NIIW may propagate in the

directions permitted by stratification and vorticity dynamics.

Dynamically, these internal waves may be important in redistributing wind energy input into the ocean on the shelf. In the cross-shore direction, NIIWs propagating offshore will encounter less friction and likely more stratification as the water depth increases. However, in the South Atlantic Bight, these waves will reflect shoreward off of the Gulf Stream, which lies close to the shelfbreak; the Gulf Stream front represents a turning point for NIIWs because the horizontal shear on the anticyclonic side of the stream increases the effective Coriolis parameter $f_{eff} = f + \zeta/2$ (*Mooers*, 1975). Here, ζ is dominated by $\partial v/\partial x$ in the E-N positive x-y coordinate frame. The angle of incidence of the incoming NIIW and degree of reflection by the front determines the nature of the reflected wave (*Lee and Eriksen*, 1997). Westward propagation is unfavorable due to the increase of frictional effects in shallower water. Even if stratification is sufficient to allow propagation into shallow water, the wave will be reflected offshore by the coastal front on the inner shelf. Along a cross-shore transect, f_{eff}has local maxima at the nearshore and shelfbreak boundaries. Only NIIWs generated at the local maximum at the north wall of the Gulf Stream can exit the shelf in the cross-shore direction.

Alongshelf propagation of NIIWs is necessarily equatorward except under limited circumstances; northward propagating waves quickly reach their turning latitude beyond which the waves may no longer freely propagate, and their energy is reflected southward (e.g., *Gill*, 1984; *Garrett*, 2001). Doppler shifting by the Gulf Stream may allow near-inertial wave propagation northward of the critical latitude (*Zhai et al.*, 2005), but poleward-traveling waves on the shelf are more likely to be reflected southward. However, the width of the shelf decreases to less than 25 km at the southernmost tip of the Georgia Bight, the Gulf Stream hugs the narrow shelf, and southward propagation beyond Cape Canaveral is unlikely.

Thus, it appears that the shelf of the Georgia Bight may trap near-inertial energy. SBLB winds force near-surface currents that grow in magnitude under continued forcing, and some portion of this energy is dissipated by friction (internal or external). Where a divergence or convergence of the surface currents occurs – at the coastal boundary, fronts, horizontal gradients of wind forcing, or resulting from changes in relative importance of water column stratification and bottom friction – NIIW can be radiated away in directions supported by stratification and vorticity dynamics. If the NIIW cannot exit the shelf, their energy must be redistributed through nonlinear interactions (resulting in higher frequency waves that may freely propagate offshore) or be dissipated locally through reflection, partial absorption or trapping at the fronts, wave-wave interaction, or friction (bottom and/or internal).

This trapping of near-inertial energy may result in increased mixing forced by SBLB winds shelf-

wide. Wind-generated near-inertial internal waves have been shown to be very effective at removing surface energy (*Tintoré et al.*, 1995), and *van Haren* (2000) shows that inertial shear may be more efficient at vertical mixing than tidal shear, as the energy propagation is nearly purely vertical, though less predictable. Trapping of near-inertial energy on the shelf has important implications for diapycnal mixing particularly because the Georgia Bight contains the critical latitude of 30°N, where the energy in the inertial band is enhanced in both the atmosphere (*Stockwell et al.*, 2004; *Edwards and Seim*, 2008b) and the ocean (*Skyllingstad et al.*, 2000; *van Haren*, 2005).

The density field on the shelf will impose a strong control on propagation of near-inertial energy. Propagation over significant distances is possible only if the shelf dynamics are weakly frictional. The Ekman depth is infinite for oscillations rotating near the inertial frequency (*Soulsby*, 1983), and vertical structure of wind-forced inertial oscillations and waves is often observed to extend all the way to the bottom of the coastal ocean (*Davies*, 1985a,b; *Maas and van Haren*, 1987; *Davies and Xing*, 2004; *MacKinnon and Gregg*, 2005), even as deep as 150-175 m near the critical latitude (*Chen et al.*, 1996; *Simpson et al.*, 2002). Though at least two modeled dimensions are required to successfully capture the generation of NIIW (*Davies and Xing*, 2003), the vertical structure of the near-inertial motions in these observational studies is generally well-approximated by a two-layer single-point model, which reproduces the strong near-inertial currents in the upper layer and weaker currents in the lower layer, 180°out of phase with the surface motions. In these point models (e.g., *Millot and Crépon*, 1981; *Kundu et al.*, 1983; *Orlic*, 1987), the wind stress is balanced by the pressure gradient set up by the wind against the coastline in the upper layer. In the lower layer, the pressure gradient, directed opposite the surface forcing, accelerates a return flow, and its flux is equal and opposite that of the surface layer.

On the shallow shelf of the Georgia Bight, the diurnal/inertial currents do not typically extend through the entire water column. The vertical structure of diurnal/inertial variance appears to be more removed from the bottom, with seasonal variability in the vertical position of the subsurface maximum of diurnal/inertial energy (*Edwards and Seim*, 2008d). The barotropic M_2 tide is typically thought to compose 80% of the kinetic energy on the shelf of the Georgia Bight (*Pietrafesa et al.*, 1985, though this estimate neglects the diurnal/inertial contributions described here), and the strength of the tide may result in diurnal/inertial motions with different dynamics than observed in the Gulf of Mexico (*Jarosz et al.*, 2007), the Namibian shelf (*Simpson et al.*, 2002), or the New England shelf (*MacKinnon and Gregg*, 2005), where the tides are weaker.

The bottom boundary layer of the energetic semidiurnal barotropic tide can occupy most of the water column on the shelf of the Georgia Bight (*Edwards and Seim*, 2008a), and the surface and bottom

boundary layers may interact. *MacKinnon and Gregg* (2005) describe the interaction of mixing of near-inertial energy with stratification on the New England shelf, and finds that the growing influence of bottom friction altered the vertical structure of IOs and NIIWs. Inertial motions excited by storms are found to be affected by tidal shear in the bottom boundary layer of the North Sea (*van Haren*, 2000), but the interaction may differ when the inertial motions are forced directly rather than being free oscillations following a wind impulse.

In the case of a wind impulse, the pycnocline is pushed down under wind stress and is expected to stop deepening within one inertial period after the wind stress is released (*Pollard et al.*, 1973). In the Georgia Bight, the level at which the currents change phase is observed to deepen only through the first few days of SBLB wind forcing. Tidal friction through the bottom boundary layer of the energetic barotropic tide will mix the water column from the bottom up, and thus the level of the pycnocline may be set by the competition between tidal and wind-generated shear. This competition between sources of mixing at the surface and the bottom can sharpen the pycnocline significantly on the continental shelf (*Turner*, 1973), and may allow the decoupling of the surface and bottom layers at the pycnocline, as seen by *van Haren* (2000).

The previous observational studies near the critical latitude for diurnal/inertial resonance (*Chen et al.*, 1996; *Simpson et al.*, 2002; *Jarosz et al.*, 2007) have not examined the vertical structure of the diurnal/inertial currents generated by SBLB. The Louisiana-Texas (LATEX) data in the western Gulf of Mexico were measured with single-point current meters (*Chen et al.*, 1996; *DiMarco et al.*, 2000), so the vertical structure of the currents in not well-resolved. The *Simpson et al.* (2002) and *Jarosz et al.* (2007) studies focus on ADCP deployments on the continental slope rather than on the shelf, and their observations suggest vertical representation of the currents in two layers.

The dynamical setting of the Georgia Bight and the simultaneous observations of winds, currents, and density stratification available make it a unique laboratory for investigating the processes that control the fate of wind energy input near the resonant frequency. In the following, the role of stratification in mediating the effects of bottom friction, propagating NIIWs, and changing the vertical structure of the diurnal/inertial response is considered. Section 2 recounts the observations of currents and density on the shelf of the Georgia Bight, and describes the methods used to isolate non-tidal diurnal/inertial variance. Three month-long periods are chosen to highlight the role of stratification in determining the magnitude and vertical structure of the response to SBLB forcing. The interaction of shear and stratification on diurnal and tidal time scales is explored. Finally, the results are considered in the frameworks of 1-D wind-forced inertial oscillations, internal waves, and Ekman dynamics.

Table 4: Availability of measurements of currents on the shelf of the Georgia Bight. Water depth, temporal and spatial resolution, and availability of co-located winds are listed for ADCP data available through SABSOON, NC-COOS, and NDBC.

	Station name	Water depth (m)	Δt	$\Delta z/\Delta x$ (m)	Winds coverage	Density information
SABSOON	R2	25	6 min	0.5-1	$\surd$	2000-2008: surf/bot TS
	R6	32	6 min	0.5-1	$\surd$	2000-2003: surf/bot TS
	R8	45	6 min	1	$\surd$	2005-2006: surf TS/bot T
NC-COOS	R4	41	10s-1hr	0.5-2	-	Aug. 2006:glider
NDBC	GR	16	1hr	1	$\surd$	–
	ST	39	1hr	2	$\surd$	–

5.2 Observations

Observations of currents measured by Acoustic Doppler Current Profilers (ADCPs) at six locations on the shelf are compiled from three sources: the South Atlantic Bight Synoptic Offshore Observing Network (SABSOON), North Carolina Coastal Offshore Observing System (NCCOOS), and National Data Buoy Center (NDBC). The upper left panel of Figure 30 shows the ADCP at Gray's Reef (GR, $*$) on the inner shelf, R2 and R6 on the mid-shelf ($\bullet$), and R8, R4, and offshore of St. Augustine (ST) on the mid- to outer shelf ($\triangledown$). Table 4 summarizes the availability of measured currents and vertical and temporal resolution; the companion paper, *Edwards and Seim* (2008d), gives more detail on the individual deployments.

The ADCP records are processed to isolate non-tidal diurnal/inertial variability through a combination of complex EOF analysis (CEOF) and filtering methods as described by *Edwards and Seim* (2008d). CEOF methods are applied to ADCP currents ($\psi(z,t) = u(z,t) + iv(z,t)$, where u and v are the zonal and meridional components of velocity) by season, which isolates the barotropic vertical structure in the gravest mode, $\psi_0(z,t)$; the baroclinic portion, $\psi_{bc}(z,t)$ is the sum of the higher modes $\psi_j(z,t)$ (*Edwards and Seim*, 2008a). For the data under consideration, the three lowest modes, $j = 0-2$, contain at least 99% of the variance in the total velocity record for all locations and seasons. The baroclinic velocities at each location are then filtered to pass the diurnal band, defined to be 20-28 hrs, resulting in the non-tidal diurnally varying portion of the baroclinic currents, $\psi_{bc}[\mathrm{D1}](z,t)$.

The energy in each vertical mode is quantified using the combination of CEOF and cross wavelet methods. The CEOF is recast to normalize each vertical mode, and cross-wavelet analysis is applied to the complex time series of the modal coefficients that describe the contraction/dilation and rotation of the vertical structure in the each mode (see *Edwards and Seim*, 2008d, for details). Scale-averaging the

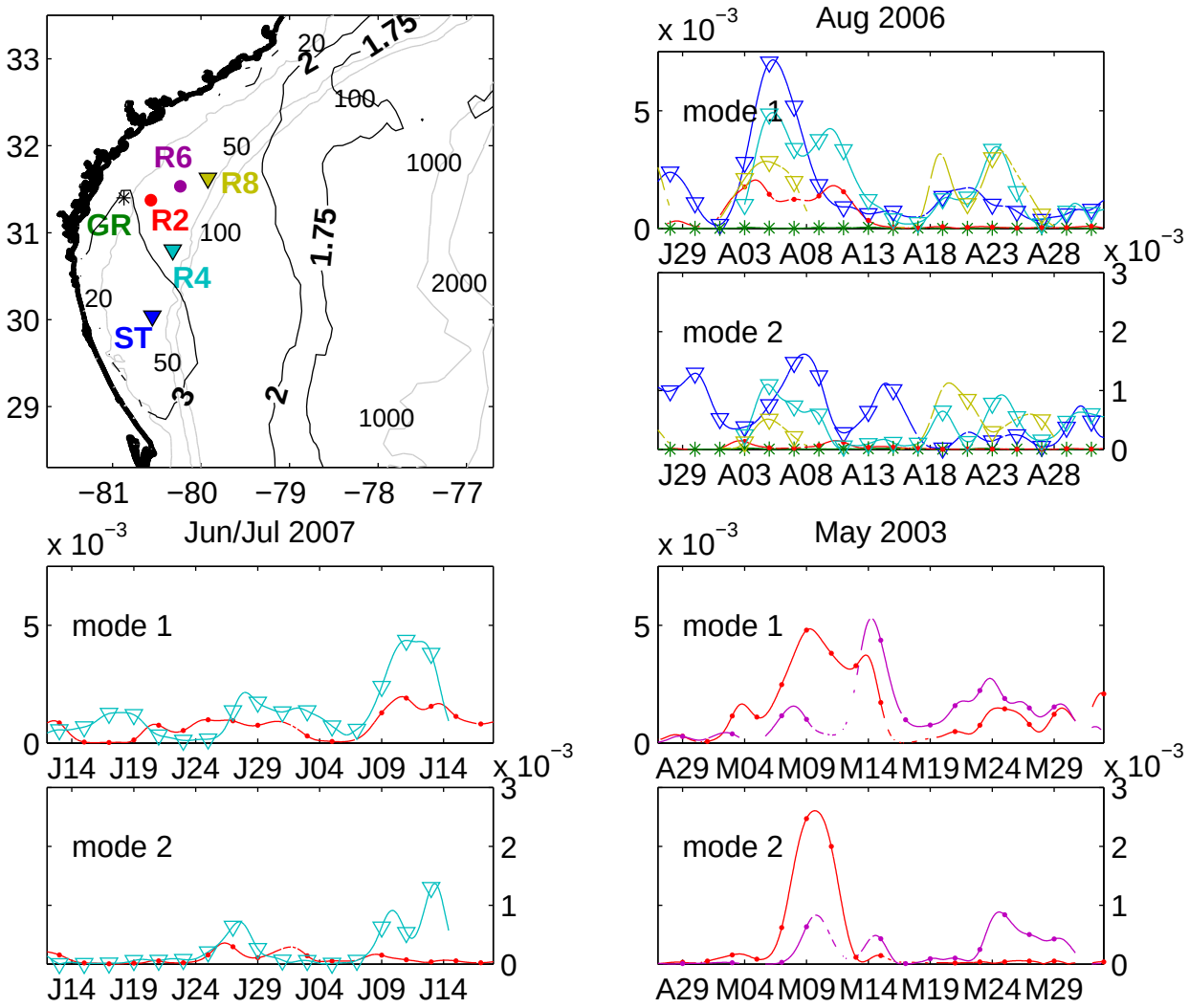

Figure 30: Upper left: map of the Georgia Bight, with the six locations of ADCP deployments from 2000-2008. The symbol marks the location as either on the inner shelf ($*$), the mid-shelf ($\bullet$), or the mid- to outer shelf ($\triangledown$). The remaining panels show time series of $\mathcal{E}_j[\mathrm{D1}](t)$ ($\mathrm{m^2 s^{-2}}$) for the lowest two modes, $j = 1, 2$, for each case study for all available data. The color and symbol denote the ADCP location as given by the map in the upper left.

resulting cross wavelet energy, $\mathcal{E}(t,s)$, over scale $s = s_{D1}$ results in $\mathcal{E}_j[\text{D1}](t)$, a variance-preserving estimate of D1-band energy in mode j as a function of time. Calculations of shear in the raw or baroclinic D1 currents are made after time-averaging the high temporal resolution records at R2 and R8 to a half-hour interval.

Observations of the density field are limited on the shelf over the full 7-years of observations, but stratification can be described over shorter time scales at some locations using near-surface and near-bottom CTD data. Biofouling of the CTDs has been a persistent problem, as planktonic organisms are often "inhaled" by the CTD pump, resulting in spurious jumps in the conductivity record that are irregular in magnitude and timing. The offsets are difficult to identify, and the measured data are unrecoverable due to the random magnitude of the offset. When available and not affected by biofouling, the surface and bottom records are used to estimate a bulk measure of stratification in the water column through the density difference $\Delta\rho$.

A month-long glider deployment at R4 in August 2006 (Aug 2-31) is used to compare the density and velocity fields when information about the mass field is available. The Slocum glider, outfitted with a free-stream SeaBird CTD set to measure only on the downcast, profiled near the R4 tower while trying to maintain its position. The glider generally remained within 2-4 km of R4, but low #93L, an unnamed tropical low pressure system, developed on the edge of the Georgia Bight with sustained winds of 25 knots on August 18-20. The resulting 25-35 cm/s mean southwestward alongshore flow on the shelf pushed the glider 23 km south of R4, but the glider was able to recover its position within two days. Density (ρ) is calculated from measured temperature and conductivity, and N^2 ($\equiv \frac{-g}{\rho_o}\frac{\partial \rho}{\partial z}$, where ρ_o is the mean density and g is the gravitational acceleration) is calculated over each density profile to identify the location and strength of the pycnocline at R4.

Though the temperature and conductivity sensors are co-located on the glider, the measured data are sensitive to the vehicle speed and differences in the response times of the temperature and conductivity sensors. Because of this mismatch, computed salinity is artificially enhanced as the instrument passes through the pycnocline. No attempt is made to correct for this salinity spiking (on the order of 0.2-0.8 psu for this deployment), which is concentrated at the main pycnocline and does not appear through the weakly stratified portion of the water column. The calculated density ρ will be a slight overestimate of the true density near the pycnocline, and yields a value of N^2 which overestimates the stratification at the pycnocline by 10-15%. Away from the pycnocline, the estimates of ρ and N^2 are not changed. For the purposes of identifying the position of the main pycnocline and estimating its strength, the salinity spiking in the observed data will not significantly affect the outcome.

5.3 Effect of stratification on magnitude of diurnal/inertial response

The following periods were chosen as case studies to better understand how stratification affects the strength and vertical structure of the diurnal/inertial response to SBLB: August 2006, June/July 2007, and May 2003. Month-long estimates of mean winds, currents, SBLB wind variance, and near-surface D1 variability are given by *Edwards and Seim* (2008d) (Figs. 26, 27). August 2006 and June/July 2007 were used as case studies of SBLB structure and variability by *Edwards and Seim* (2008b); the coastal ocean response is considered here. ADCP observations are available at five locations on the shelf in August 2006, and are used in concert with glider-measured CTD data. The coastal response to SBLB is markedly diminished in June and July 2007, despite the very strong SBLB wind forcing over that period. May 2003 is also examined in greater detail to consider the roles of larger scale circulation patterns and stratification on the coastal response and internal wave propagation.

Time series of energy in modes 1 and 2 for each of the case studies are shown in Figure 30, and provide context for the description of the vertical structure and variability over the periods considered. In general, mode 1 does not decrease in magnitude as mode 2 grows, unlike the observations on the New England shelf that suggest growth of mode 2 at the expense of mode 1 (*MacKinnon and Gregg*, 2005). Mode 2 may indeed correlate with changes in stratification and the location of the pycnocline, but because the energy is continually renewed near-surface when forced by SBLB, the modal energy need not be strictly conserved among the modes.

5.3.1 August 2006

The most complete spatial coverage of wind and current measurements over the 7-year ADCP data set was achieved in August 2006. Details of the SBLB structure and variance for the month are given by *Edwards and Seim* (2008b). Compared to all summer months 2000-2007, August 2006 represents average summertime conditions on the shelf: the Bermuda high dominates the mean wind field and SBLB winds are relatively strong, but the coastal ocean response is generally weak on the inner to mid-shelf and sharply enhanced at the outer shelf locations (*Edwards and Seim*, 2008d, Figs. 26, 27). Large-scale winds on the shelf are dominated by the Bermuda High, but show a departure from summertime Bermuda high-dominated winds due to the influence of the low pressure system 93L (Aug. 18-20) and Hurricane Ernesto (Aug. 31-Sept. 1).

Time series of diurnal wind energy and contours of $\psi_{bc}[\mathrm{D1}]$ are given in Figure 31, and are consistent with the pattern of increasing diurnal/inertial currents with distance offshore at synoptic scales, as

was observed over seasonal time scales (*Edwards and Seim*, 2008d). The diurnal/inertial currents develop quickly in response to periods of strong SBLB wind forcing. Consistent with the trend found by *Edwards and Seim* (2008d), there is no significant signal at GR (16 m water depth); despite this location receiving the strongest SBLB forcing, diurnal/inertial currents remain below 3 cm/s. At R2, the currents increase to about 10 cm/s magnitude under SBLB forcing. The level of maximum shear deepens to about 7-8 m below the sea surface and then shoals as SBLB relaxes and reforms. The slope of the lines of constant phase differentiates propagating near-inertial internal waves from purely inertial motions. Tilting lines of constant phase indicate phase propagation perpendicular to the isophase lines; energy propagation is parallel to lines of constant phase and of opposite sign. The sharp 180°change of phase at R2 suggests that D1 currents at R2 are purely inertial motions over this time period. The currents at R2 spin down within several inertial periods after the wind forcing diminishes, which suggests that enhanced currents were truly forced oscillations rather than a free inertial response. After the dissipation of 93L, however, diurnal/inertial currents remain less than 1-2 cm/s despite the two SBLB cycles forcing the sea surface, presumably because, at this location on the shelf, 93L produced well-mixed conditions that cannot support strong surface-trapped near-inertial motions.

The response at the outer shelf locations is much stronger, and the surface currents at a given location appear to be enhanced by increasing or continued SBLB wind energy. The water column is at least weakly stratified for the entire month, with bottom to surface density differences on the order or 1.5-3 kg/m^3 measured by the glider at R4, and is only weakly stratified ($\Delta\rho \approx 0.6$ kgm^{-3}) during the influence of 93L. The strongest response occurs while the water column at R4 is most strongly stratified (August 3-13), and diminishes at R4 when SBLB energy is near-zero and stratification weakens slightly. The spatial and temporal current patterns along the outer shelf transect differ greatly, with at least four "events" that do not necessarily co-occur among locations. These patterns are identifiable in the time series of modal energy (Fig. 30); R4 at times co-varies with ST or R8, but no clear or consistent pattern emerges in or among modes. As seen in Figure 31, the inshore locations contain significantly less energy than ST, R4, or R8, and the modal structure at R2 is essentially mode-1, with very little energy in mode 2 (Fig. 30).

Upward-tilting lines of constant phase indicate downward energy propagation of NIIWs, and phase speed can be inferred from their slopes. NIIWs are observed propagating downward through the water column at ST and R4 from August 3-10, after which ST currents weaken and appear to be cast into higher modal structure. After August 16, R8 currents strengthen and diurnal/inertial currents at R4 briefly propagate energy upward from a near-bottom maximum before downward propagation of energy

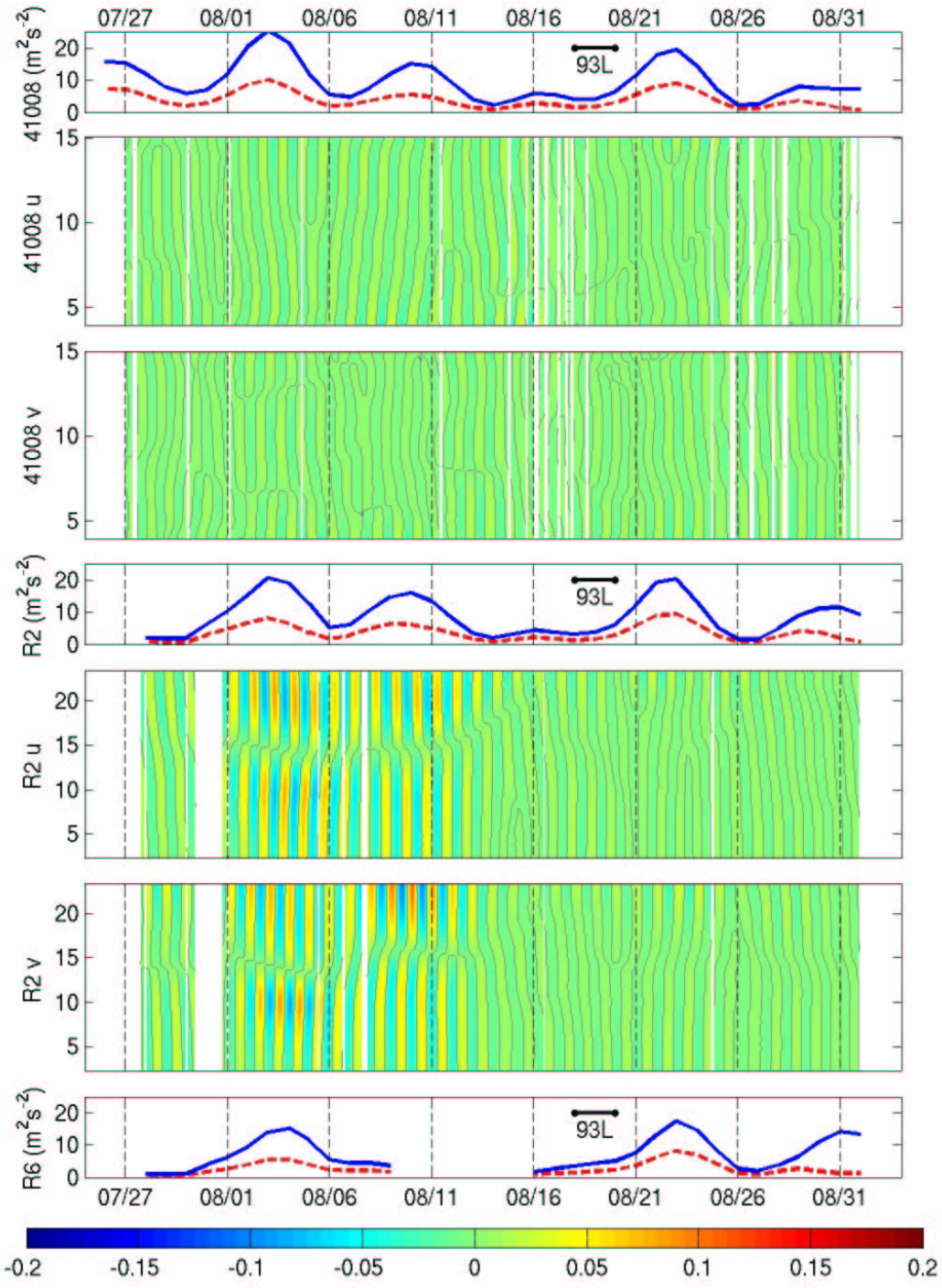

Figure 31: Case study: Aug 2006. Diurnal wind variance of the total (blue) and clockwise-rotating (CW) components of D1 wind, and the u- and v-components of ψ_{bc}[D1](z,t) where data are available over August 2006 (winds: 41008, R2, R6, 41012; currents: R2, R6, R8, ST). The data are broken into cross-shore (41008-R2-R6) and alongshore sections (ST-R4-R8). The vertical axis indicates meters below sea surface for buoy-mounted ADCP records (41008, ST) and meters above bottom for locations where the instruments were bottom-moored (R2, R6, R8, R4).

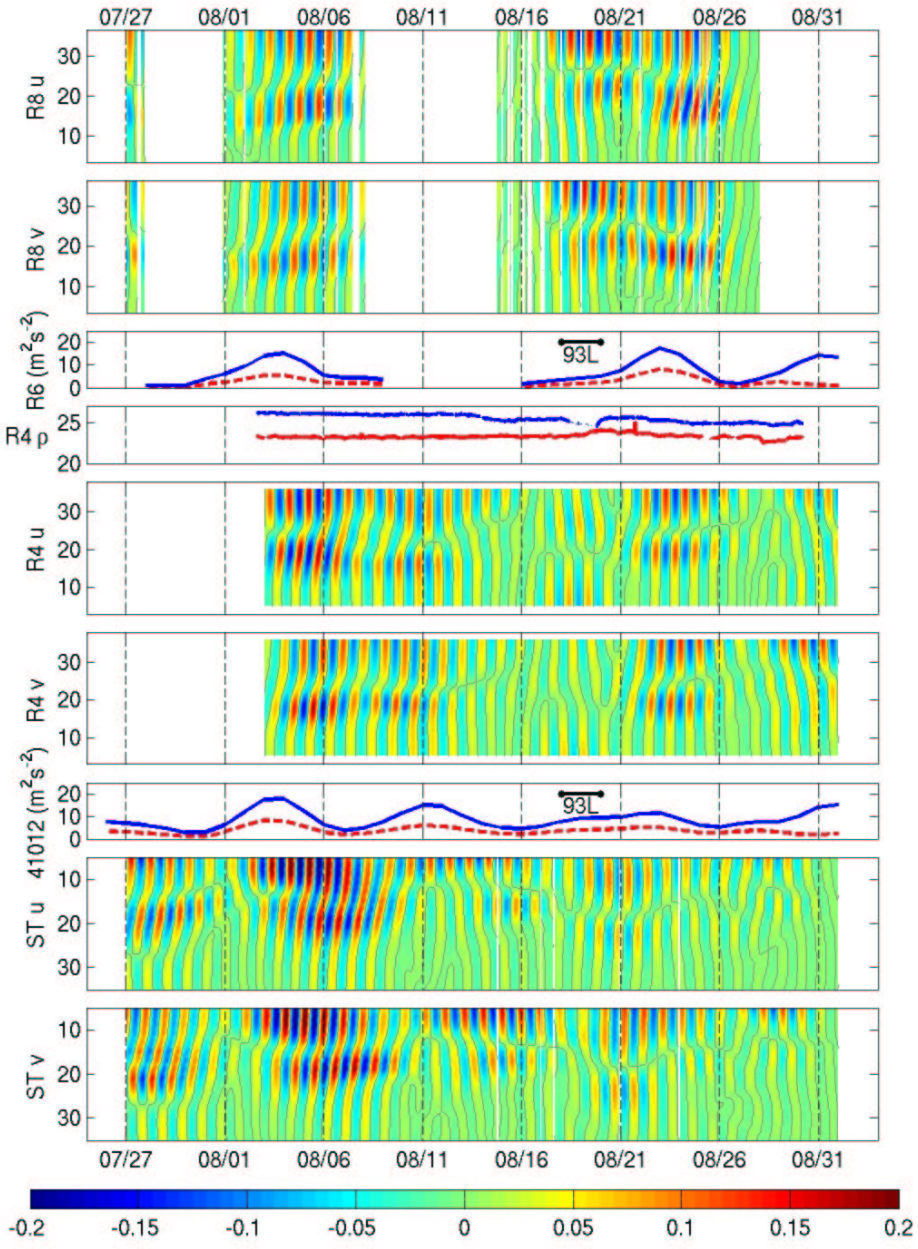

Fig. 31: panel 2

resumes. Propagation of the NIIWs does not appear to be unidirectional; progression of wave packets in time is not obvious. Spatial patterns of either upward or downward propagating energy and higher modal structure do not emerge as consistent in either the cross- or alongshore direction, but rather appear to be consistent with reflection and interference of NIIWs on the mid- to outer shelf. Potential NIIW generation locations are not immediately obvious from the time series of modal energy at the diurnal frequency, but are suggested by the analysis to lie offshore of R2 and inshore of the 40 m isobath. Mode 2 energy at ST lags R4 by several days, but this lag may signal differences in local forcing or propagation of NIIWs generated elsewhere. The direction and group speed of propagation is difficult to estimate because the internal wave velocities cannot easily be separated from those of the forced inertial oscillations.

The relative magnitudes and the vertical structure at each location are generally consistent with the seasonal variance profiles shown in Figure 23, but the position of the subsurface maximum at ST is more variable compared to R8 and R4. Energy in modes 1 and 2 is greater at ST than for the other outer shelf locations (Fig. 30). A comparison of the time series of $\mathcal{E}_j[D1](t)$ for modes 1 and 2 with the occurrence of sloping phase contours in Figure 31 suggests that mode 2 energy may correlate with NIIW propagation.

While the maximum of both mode 1 and mode 2 energy lies at ST, the energy at R4 is more broadly distributed in time compared to the peaks of energy elsewhere, and suggests that NIIWs from different sources may interfere on this portion of the shelf. The vertical structure at R4 over August 7-9 and 17-22 has patterns in common with the structure to both its north and south, particularly during the latter period, and may be a combination of downward propagating energy from ST and upward propagating energy from R8. R4 lies along the mid-line of the Georgia Bight, and if the inner or mid-shelf develop NIIW, coastline curvature may focus offshore-propagating near-inertial energy onto this section of the mid- to outer shelf.

5.3.2 June/July 2007

This 36-day window of observations is chosen to mirror that of *Edwards and Seim* (2008b), for which there is an improved spatial description of the wind forcing. SBLB winds are strong in the Georgia Bight and increase into July, with the strongest forcing of the coastal ocean on the inner to mid-shelf near the ADCP array (Fig. 27 *Edwards and Seim*, 2008d). The diurnal/inertial response on the shelf is small in magnitude relative to other years, with less pronounced subsurface maximum (Fig. 23 in the same). The ST/41012 buoy winds are not available for this period; currents at ST are compared to the

NOS-maintained station SAUF1 at the coastline instead.

Despite the coherence of a 2-3 m/s SBLB over the shelf, the coastal ocean response to wind forcing is weak compared to that of August 2006 (Figs. 26, 30). The strength of the diurnal/inertial currents at R2 appears to be tightly controlled by stratification. Near-surface D1 variability develops once the water column is nominally stratified by 0.5 kg/m^3 bottom-to-surface difference in density. This density difference is weak relative to the climatology of *Blanton et al.* (2003), and likely reflects the influence of the 2007 drought. Precipitation was classified as severely to extremely dry from March through May, and resulted in a record dry spring season (National Climatic Data Center, NCDC). The influence of the drought on river outflow into the Georgia Bight likely explains the surface salinity at R2, which remains above 35 from mid-April through July. From June 14-20, the SBLB energy is relatively strong, but because the water column is well-mixed, no diurnal/inertial response is observed in the ocean at R2.

The near-surface D1 currents at R2 are slightly stronger than those that develop at R4 in late June, opposite of the trend of increasing variance with distance offshore seen in general. The depth of penetration of the wind energy, as measured by the depth of the zero-crossing, is shallow at both locations, and weak NIIWs propagate downwards at R4 as the SBLB slackens June 25-July 1. A stronger SBLB event occurs July 7-14, and the typical cross-shore distribution of energy is restored, with currents at R4 in excess of 25 cm/s, more than twice the magnitude observed at R2.

Compared to the August 2006 case study, NIIWs at R4 appear over a greater range of depths. The depth of D1 shear moves away from the surface June 24th-July 5th as SBLB winds decrease, suggesting a deepening of the wind influence and perhaps the downward propagation of this beam-like NIIW energy. The features of the disturbance appear to be lagged at R4 relative to R2, which may reflect propagation of energy from the inner to mid-shelf offshore, but a cross-shore lag is not mirrored in the time series of modal coefficients. As found for August 2006, the amplitude of mode 2 grows with propagating NIIW, but mode 1 and mode 2 are not anticorrelated.

The interannual variability of the diurnal/inertial response is striking, and this example confirms the necessity of stratification for diurnal/inertial response to SBLB on the inner to mid-shelf, but also suggests that stratification is highly variable on the mid-to outer shelf on interannual time scales. The variability of the diurnal/inertial currents may serve as a proxy for variability in stratification at a given location.

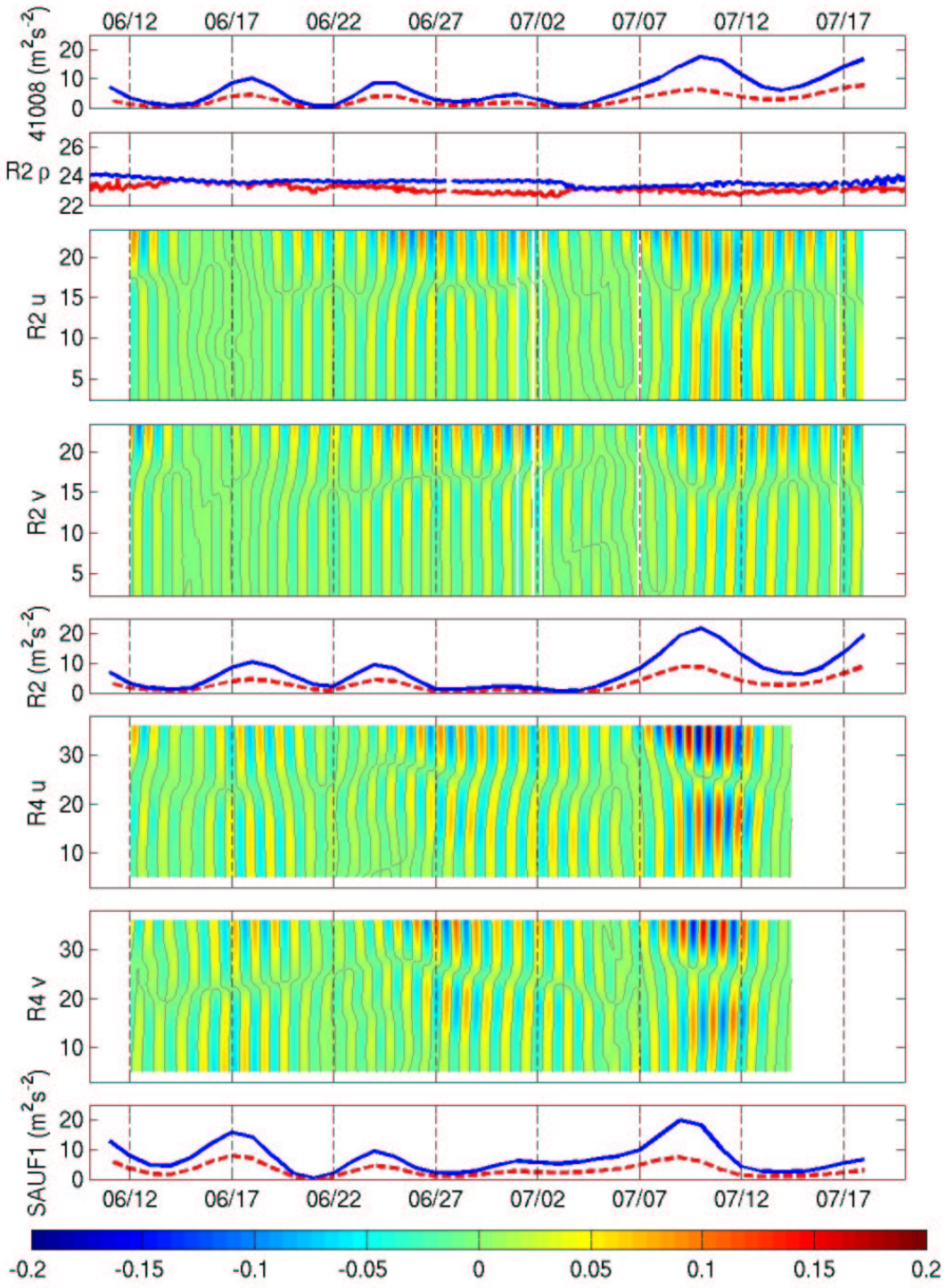

Figure 32: Case study: Jun/Jul. Diurnal wind variance of the total (blue) and clockwise-rotating (CW) components of D1 wind, surface (red) and bottom (blue) density ρ calculated from CTD measurements, and the u- and v-components of ψ_{bc}[D1](z,t) where data are available, Jun. 15 - Jul. 15 2007 (winds: 41008, R2, SAUF1; currents: R2, R4, CTD: R2).

5.3.3 May 2003

In May 2003, D1 currents on the inner to mid-shelf exceed 35 cm/s, a 7-year maximum over all measurement locations (*Edwards and Seim*, 2008d) at a time of anomalously strong stratification shelf-wide. Though the ADCP data are sparse in space compared to other case studies, the density field is well-described and the influence of anomalously strong stratification on the inner to mid-shelf can be examined.

Arextabaleta et al. (2006) describe the upwelling event of summer 2003, during which sustained, anomalously strong upwelling winds drew 18°water over much of the Atlantic coast of the United States. Bottom water in the Georgia Bight shares T/S characteristics with deep Gulf Stream water (*Arextabaleta et al.*, 2006), and enhanced the already significant stratification of early spring caused by the release of a massive spring freshet. A cross-shelf temperature section aligned with the R6 tower on May 7th shows strong thermal stratification extending offshore from about the 15 m isobath (see *Arextabaleta et al.*, 2006, Figs. 2, 9 for density sections and locations). The temperature and salinity signature of the Gulf Stream water is notable at both mid-shelf locations (Fig. 33), but appears more starkly at R6 relative to R2. However, it is the freshet water near-surface that controls the stratification at both locations. At R2, the surface and bottom layers differ by as much as 5.5 σ units from top to bottom in just 25 m water depth (Fig. 33).

SBLB increases May 1-12 (Fig. 34), as surface freshet water moves north- and eastward alongshore from R2 to R6. The diurnal/inertial current response to SBLB develops, deepens, and increases considerably in the stratified waters of R2 as SBLB and stratification strengthen simultaneously. No appreciable motion is observed in the weakly stratified waters mid-shelf at R6 as SBLB ramps up, but the confluence of the two anomalous water masses (fresh surface water and warm, salty bottom water) stratifies the water column at R6 after May 7th, and the diurnal/inertial signal increases rapidly. Diurnal/inertial shear deepens at both locations as SBLB continues to strengthen, and 35 cm/s maximum currents develop at R6 in response by May 14th.

After May 17th, when the Gulf Stream water begins to retreat offshore from the shelf, the response at R2 is significantly weaker than at R6, despite similar levels of stratification surface to bottom. This pattern may reflect the difference between background upwelling circulation that delivers Gulf Stream water to nearly the inner shelf, predicted to move the cross-shore maximum of the diurnal/inertial currents onshore, and downwelling circulation, predicted to move the cross-shore maximum of diurnal/inertial currents offshore (*Davies and Xing*, 2004).

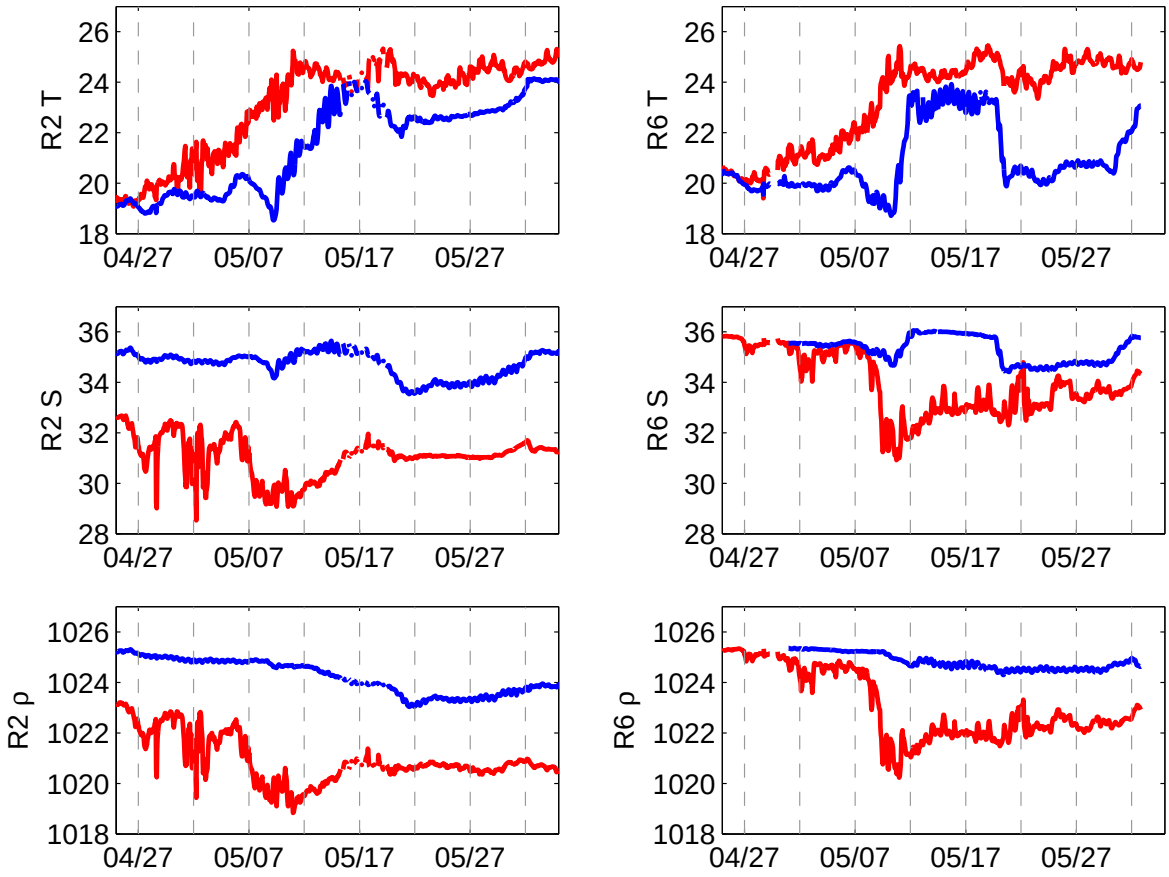

Figure 33: Time series of near-surface (r) and near-bottom (b) temperature, salinity, and density at R2 (left panels) and R6 (right panels) in late spring 2003. The confluence of warm, salty Gulf Stream water near-bottom and fresh, warm freshet water near-surface result in density differences of 3-5.5 kg/m^3 surface-to-bottom over most of the month.

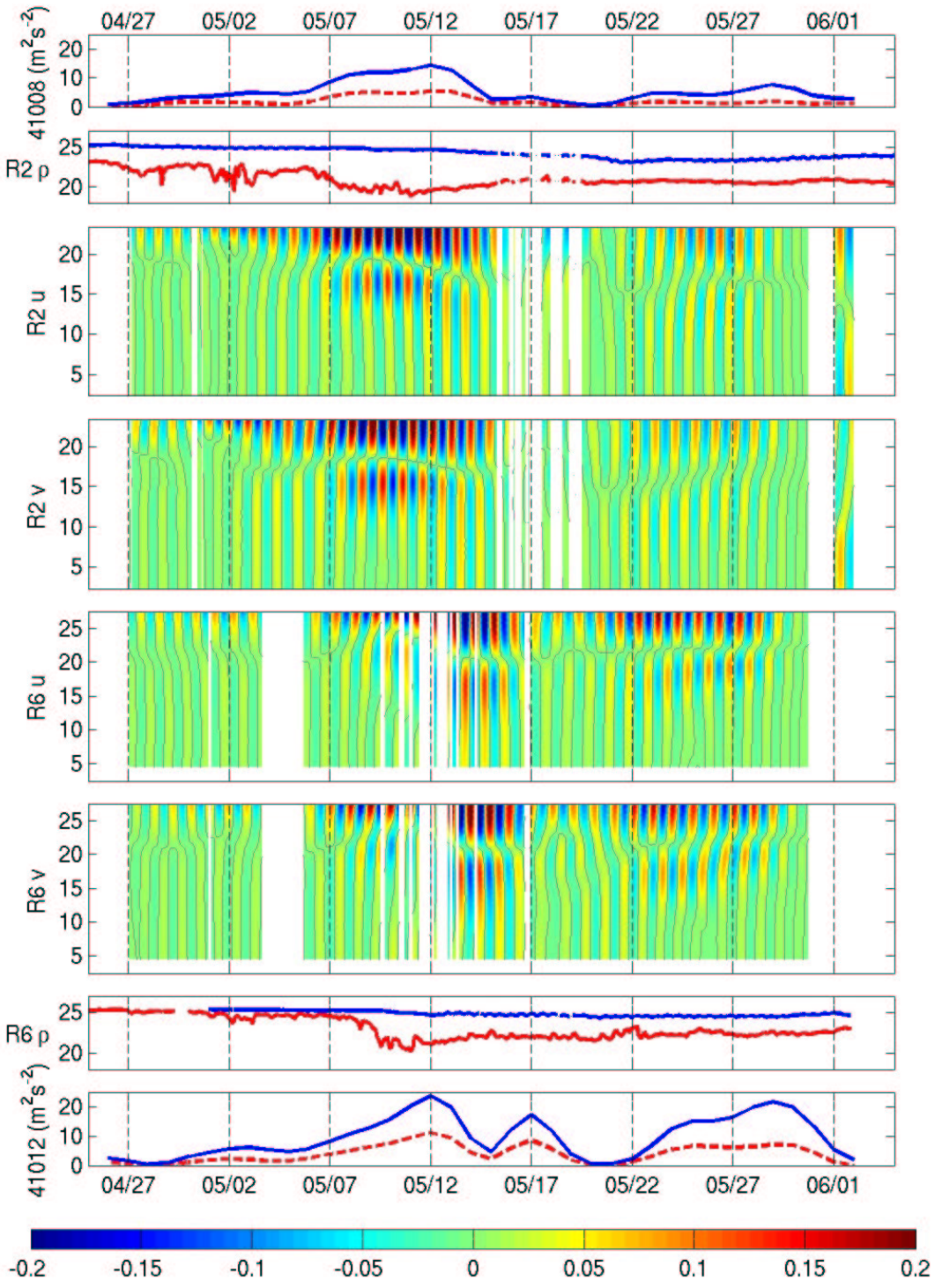

Figure 34: Case study: May 2003. Diurnal wind variance of the total (blue) and clockwise-rotating (CW) components of D1 wind, surface (red) and bottom (blue) density ρ calculated from CTD measurements, and the u- and v-components of ψ_{bc}[D1](z,t) where data are available, Jun. 15 - Jul. 15 2007 (winds: 41008, 41012; currents: R2, R6, CTD: R2, R6). Note the change of scale of the density panel.

The currents at R2 appear to be purely inertial, with only weak propagation after May 20th. Inertial wave propagation is directed downwards at R6 mid-month, after which it is cast into higher modes and reverses as SBLB calms and the Gulf Stream water mass moves offshore. After May 22nd, diurnal/inertial energy increases again; the absence of near-bottom currents suggests more beam-like propagation compared to periods over which the diurnal/inertial energy feels the bottom (e.g., August 1-7, 2006). The relative energy in the vertical modes (Fig. 30) reflects the surface-trapped energy at R2 from May 8th through 12th. The mode 2 energy in the diurnal band approaches the level of energy in mode 1, coincident with the zero-crossing moving upward. Mode 2 energy exceeds mode 1 energy at R6 toward the end of the month, when the zero-crossing is closest to the surface.

5.3.4 Case study comments

As concluded by *Edwards and Seim* (2008d), stratification is a major control on the ability of SBLB winds to excite diurnal/inertial motions in the coastal ocean. Both stratification and wind forcing appear to be necessary conditions for the development of near-inertial currents near surface; neither is sufficient by itself to induce surface motion. The magnitude of near-inertial currents at inshore locations appear to be largely controlled by stratification rather than SBLB winds. Generally, the weather disturbances that destroy stratification also disrupt the SBLB system, but in each of the case studies examined at R2, there is at least one 5-8 day period over which SBLB winds are strong, but stratification is weak or non-existent, and a diurnal/inertial response in the ocean to SBLB is not observed (e.g., Aug. 20-26, 2006; Jun. 15-19, 2007; Apr 27-May 1, 2003; May 19-21, 2003).

The outer shelf is generally more stratified and less dependent on direct forcing – the water depth allows more of the water column to be free of frictional effects, and stratification inhibits mixing from the bottom boundary layer. The water column can be stratified on the outer shelf, and higher modal structure develops in the absence of SBLB forcing (e.g., Aug. 15-19), but it remains unclear whether the vertical structure is induced by lack of direct wind forcing or the interference of NIIWs.

At a given location, the magnitude of the diurnal/inertial signal appears to be a reasonable proxy for stratification. For example, the response to SBLB in June 2007 appears to be muted shelf-wide compared to the relatively strong wind forcing. Surface and bottom CTD records in June 2007 confirm that the water column is more weakly stratified at R2 compared to the other case studies examined, but there is at least circumstantial evidence that stratification is weak over most of the shelf. Freshwater input to the shelf in 2007 was lower than in previous years due to drought conditions (NCDC), and stratification from this smaller than average freshet may have been mixed by earlier than average (sub)tropical

activity in the Georgia Bight – early May (Subtropical Storm Andrea) and early June (Tropical Storm Barry).

5.4 Shear and stratification

The case studies presented indicate that the position of the sub-surface maximum of D1 currents varies in time, as does the extent of D1 currents near-bottom. At times, the diurnal/inertial currents extend all the way to the bottom, consistent with the vertical structure of currents observed in other locations. Frequently, however, the D1 subsurface maximum is bounded by strong shear and has detached from the bottom, with D1 currents near zero below this level. To examine when and how this variability of near-bottom structure occurs, the shear structure is examined over August 2006, when glider data are also available for high resolution estimates of stratification.

The diurnal/inertial currents measured on the mid- to outer shelf (25-35 cm/s) are comparable to the magnitude of the semidiurnal barotropic tide, but the shear associated with these two major currents operate at different depths and frequencies. The combined effect is temporal variability of the current magnitude and shear depending on the relative phase of the M_2 tide and the diurnal/inertial currents. Figure 35 overlays isopycnals of glider-measured density on the magnitude of raw velocity $|\psi(z,t)|$, and suggests that the surface and bottom layers are at least partially decoupled by stratification. Near surface, the current magnitude is dominated by variance at the diurnal frequency; this diurnal variability near-surface is greatest in the beginning of the record, Aug. 3-6, when SBLB wind forcing is strongest (Fig. 31). Below the pycnocline, the variability of the semidiurnal tide is dominant.

This decoupling of the tidal shear and mixing below the pycnocline and diurnal/inertial shear/mixing above the pycnocline suggests that wind energy into the surface ocean doesn't mix down to the bottom, and must do one of three things: move the pycnocline down, dissipate internally, or be radiated away by NIIWs. NIIW wave characteristics are difficult to infer from time series of density near R4 (contoured in Fig. 36), which shows the level of the pycnocline to be lifted and depressed at semidiurnal and synoptic time scales. The semidiurnal internal tide appears to have an amplitude on the order of 5-8 m, and M_2 variability of the pycnocline position dominates over the potentially small displacement of the pycnocline at the near-inertial frequencies. However, the shear associated with the raw currents does indicate variability near the diurnal frequency.

Figure 36 superimposes isopycnals of measured glider data on the absolute value of shear ($|S| = |\partial\psi(z,t)/\partial z|$, where $\psi(z,t)$ and S are complex) from the raw measured velocities. Elevated shear is

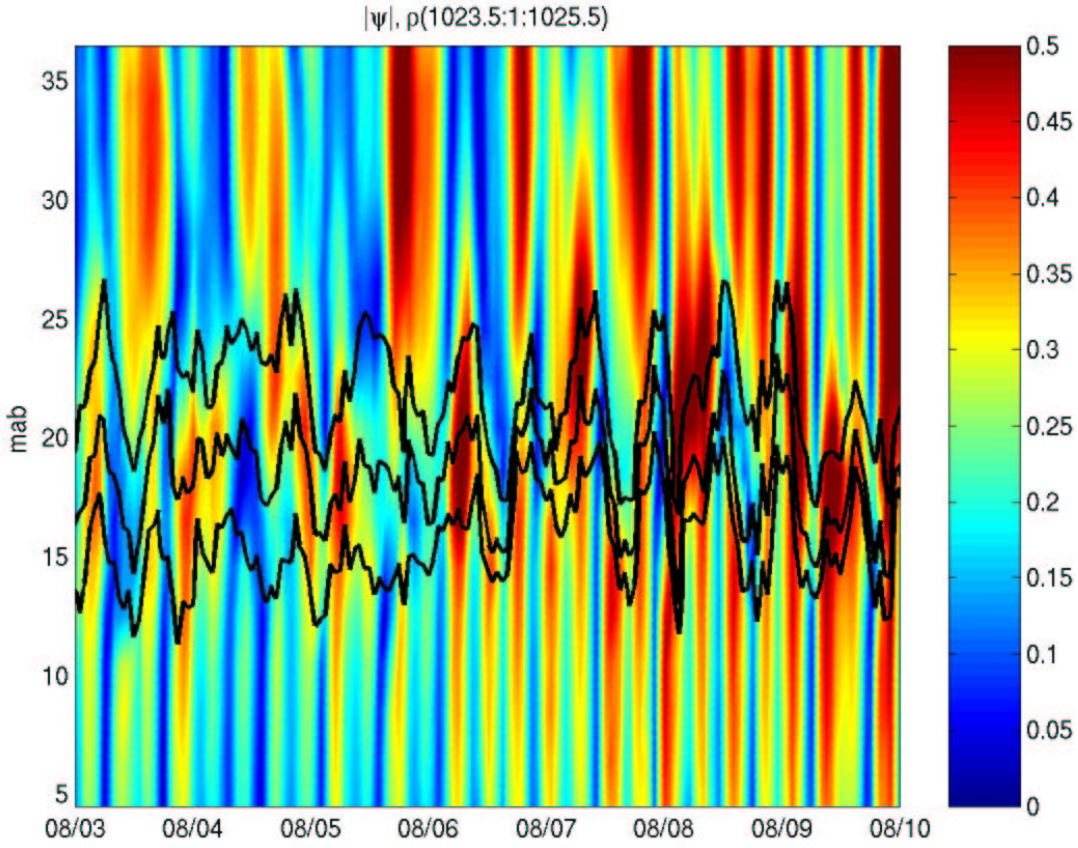

Figure 35: Magnitude of the raw velocity, $|\psi(z,t)| = |u(z,t) + iv(z,t)|$, shows current minima that are not stationary in time or space. Density contours at $\rho =$ 1023.5, 1024.5, and 1025.5 kg m^{-3} show the level of the pycnocline, which is displaced 5-8 m at the semidiurnal frequency, presumably due to the presence of the M_2 internal tide.

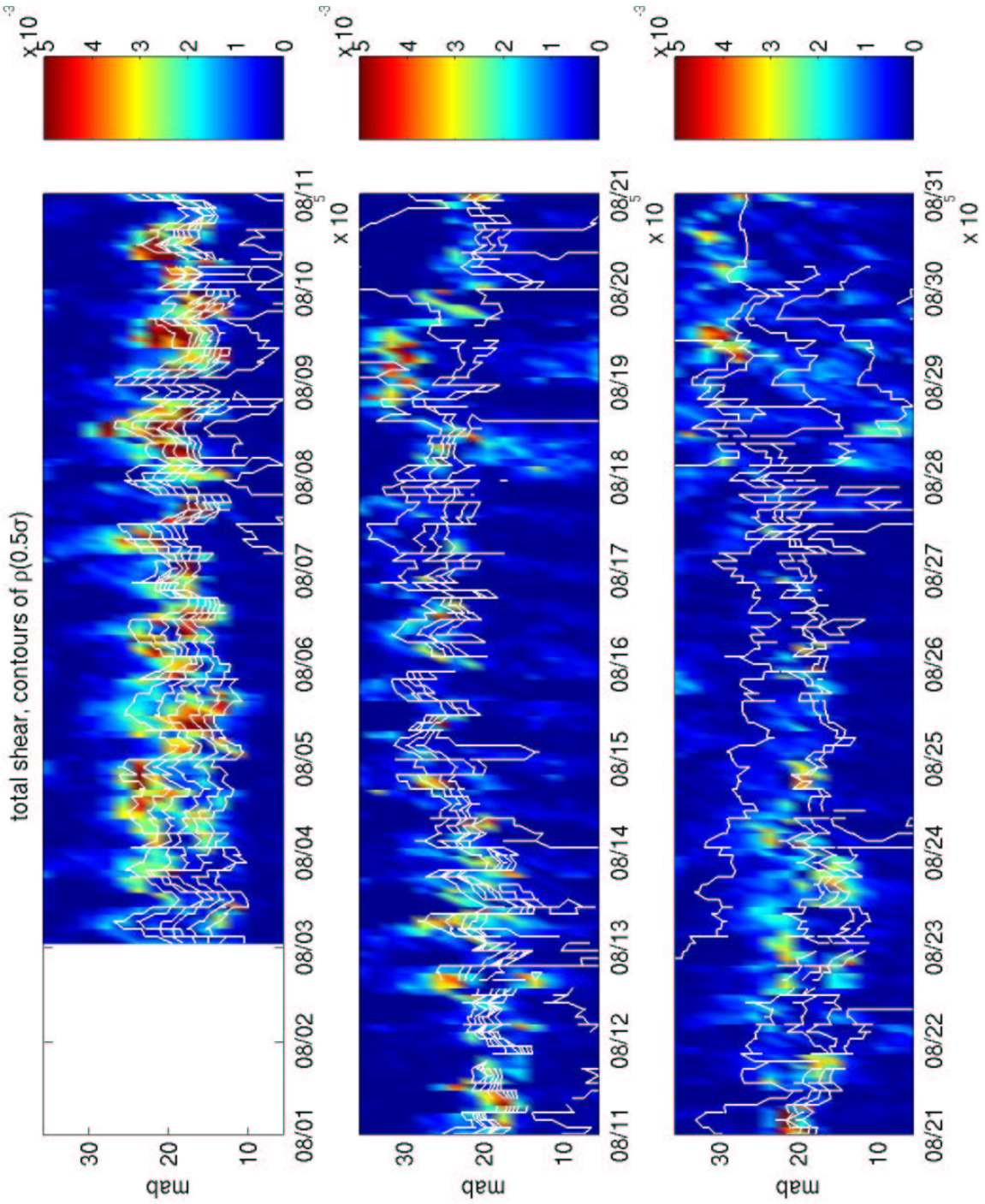

Figure 36: Case study: Aug 2006. Absolute value of shear, $|S|$, calculated for raw ADCP data at R4. Contours of ρ at 0.5 kg m^{-3} intervals from 1023.5 to 1025.5 show the level of the pycnocline in the glider data.

generally contained within the isopycnals from 1023.5 to 1025.5 kg m^{-3}, but the level of maximum shear bounces between the top and the base of the pycnocline, switching positions on a time scale of 12-48 hrs. The maximum shear is easily identified at the top of the pycnocline at about 12:00GMT from August 8-11, alternating with shear near the base of the pynocline at the diurnal frequency. Later in the month, the diurnal variability returns, but the time of day changes; the maximum shear is found at the base of the pycnocline at 12:00GMT August 21-24. Generally, these periods when the level of maximum shear moves between alternating sides of the pycnocline at the diurnal frequency correspond to times when the D1 surface currents are strong. In contrast, when the D1 currents are weak (e.g., August 12-14), the variability appears to be semidiurnal in character.

Thus, shear is not aligned with the pycnocline at R4, but rather, bounds it. At this location, the correlation between density and shear structure is explicit. The ability to correlate the strength of the coastal response to SBLB at this location with the presence of stratification may be powerful in interpreting the shear at other locations on the shelf, where vertically resolved density measurements are not available. The absolute value of shear of the raw currents and the associated change of the vertical structure of shear with increasing water depth illustrates the interaction of stratification and bottom friction in setting the cross-shore structure of the diurnal/inertial response (Fig. 37). Diurnal/inertial currents are appreciable at R2 until Aug. 15, and the shear is concentrated mid-water column. With D1 shear as a proxy for the strength of stratification, the changes in the vertical structure at R2 in August 2006 may be attributed to the destratification of the water column mid-month. Despite two SBLB cycles in the latter half of the month, D1 currents do not develop in response, and the total shear remains small, suggesting that the water column is well-mixed for the latter half of the month after the influence of low pressure system 93L. In contrast, shear at Gray's Reef is distributed over much of the water column, and though diurnal pulses of enhanced shear extend from surface to bottom in early August, when SBLB is strong over the entire shelf, the water column appears to be well-mixed, and neither D1 currents nor mid-water column shear develops.

The shear structures at R8 and ST indicate a mid-water maximum with vertical variability on similar time scales as seen of the pycnocline at R4. The qualitative similarity of the vertical patterns of shear at the outer shelf locations (and to a lesser degree, R2) suggests that the bounding of the pycnocline by shear might extend shelf-wide. The vertical structure of shear at R4 and ST suggest two maxima, which lie typically just above and below the pycnocline. Below the pycnocline, shear varies at the semidiurnal frequency; above the pycnocline, shear varies at the diurnal frequency. The shear structure appears to change in the alongshore direction, which may signal some dynamical differences along the 40 m

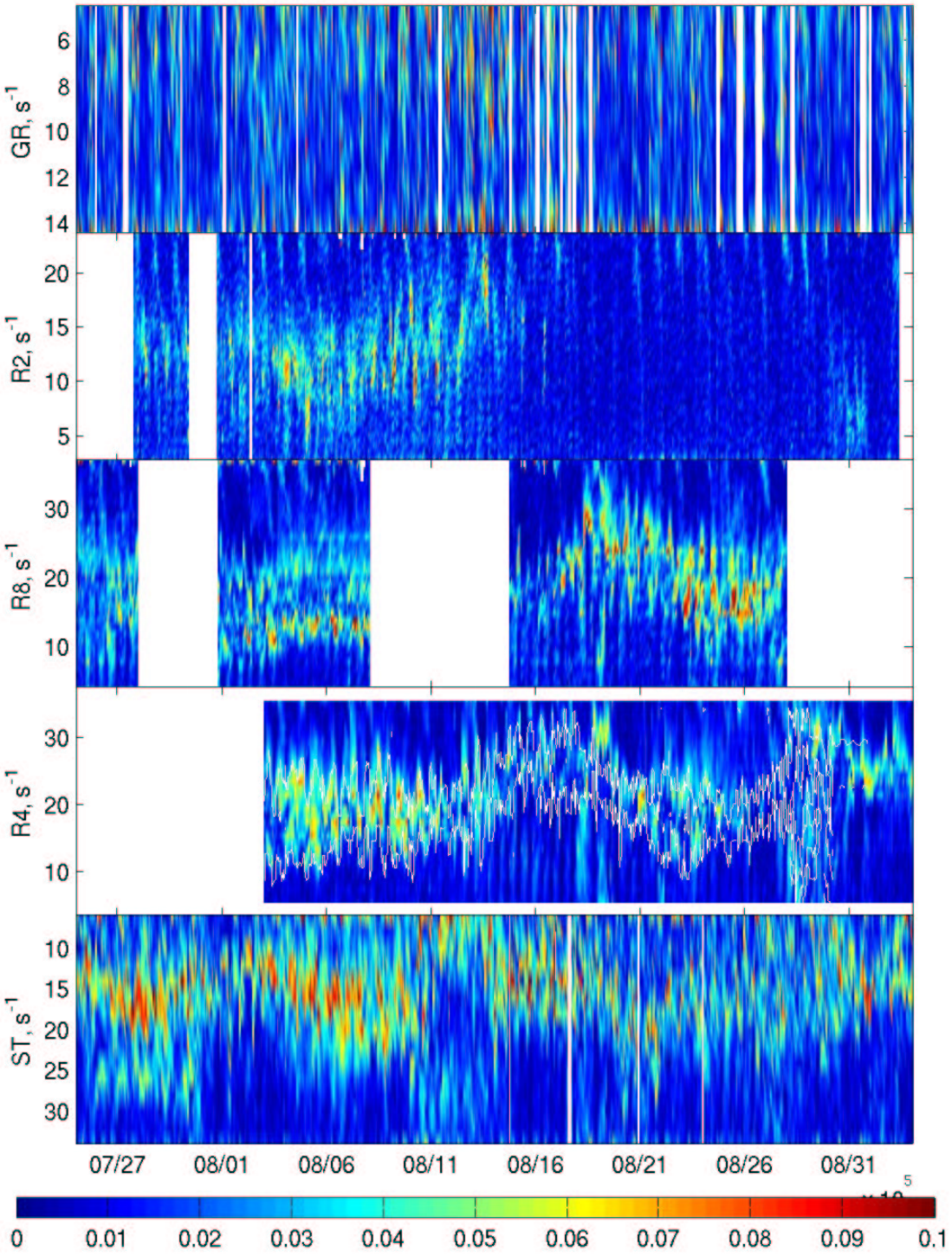

Figure 37: Case study: Aug 2006. Absolute value of shear $|S|$, calculated for raw ADCP data at GR, R2, R8, R4, and ST. Contours of N^2=5$\times 10^{-4}$ s^{-2} from glider data show the level of the pycnocline at R4.

isobath. The level of maximum shear tilts downward from ST to R8, where it is closer to the bed than the surface, and more diffuse than observed at either R4 or ST.

The diurnal currents shown in Figures 31-34 show only smooth, low frequency variation in the level of the zero-crossing, which corresponds to the level of maximum D1 shear, $|S_{D1}|$. The diurnal shear fraction, $|S^2_{D1}|/|S^2|$, indicates the degree to which the shear is diurnal, and is shown for all five ADCP records in Figure 38. At all locations on the mid- to outer shelf, the shear is almost purely diurnal in the upper half of the water column. The D1 shear in the lower portion of the water column corresponds to the base of the sub-surface maximum, and its strength represents the degree to which the sub-surface maximum is detached from the bottom. However, the shear at mid-depth is not diurnal and must arise from processes at other frequencies. At R4, this minimum of diurnal shear fraction coincides with the center of the pycnocline, and both move up and down in the water column in tandem at subtidal frequencies. The spatio-temporal trends in this level of minimum diurnal shear at R8 and ST are generally coherent with those of R4, and it is assumed that the minimum of diurnal shear is also coincident with the pycnocline at R8 and ST.

The location of the diurnal shear minimum within the pycnocline results from the subsurface maximum of non-tidal D1 currents being aligned with the pycnocline. Time series of the u- and v- components of ψ_{bc} measured near-surface and interpolated to the level of the pycnocline (taken here to be the 1024.5 kg m^{-3} isopycnal) are given in Figure 39. The motion at the surface and within the pycnocline are clearly anti-correlated, and variability in both levels is strongly diurnal/inertial. Though the pycnocline appears to decouple the tidally-dominated bottom layer from the layers above it, the pycnocline itself is strongly affected by motion at both tidal and inertial frequencies; its vertical position is moved at the semidiurnal frequency (presumably due to the M_2 internal tide), but its horizontal motion is largely at the diurnal frequency, and is coupled to the surface currents.

The diurnal shear fraction highlights the difference in frequency content of shear above and below the pycnocline, with diurnal variance above and semidiurnal below. These patterns, together with the variability of the shear maximum at the base and top of the pycnocline, suggest a sort of competition between diurnal shear and semidiurnal shear. When the shear maximum lies at the base of the pycnocline, bottom friction at semidiurnal tidal frequency dominates the shear in the water column, and when diurnal currents are strong, diurnal shear dominates bottom boundary shear, and the maximum shear lies at the base of the wind-forced region in the pycnocline. In either case, the level of maximum shear is closer to the boundary from which the dominant shear originates.

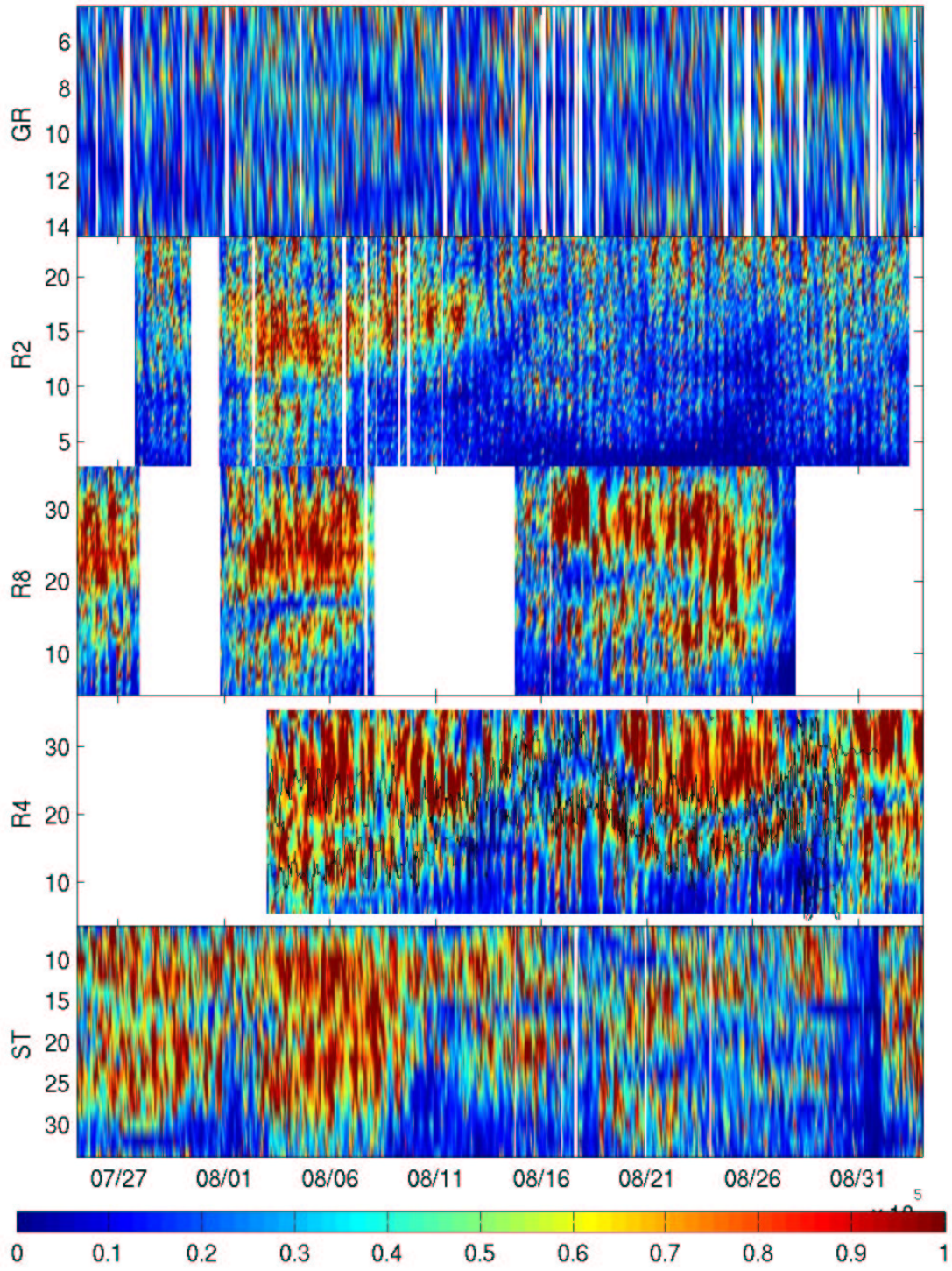

Figure 38: Diurnal shear fraction, $|S^2_{D1}|/|S^2|$, with contours of N^2=5$\times$10^{-4} s^{-2} to reference the location of the pycnocline.

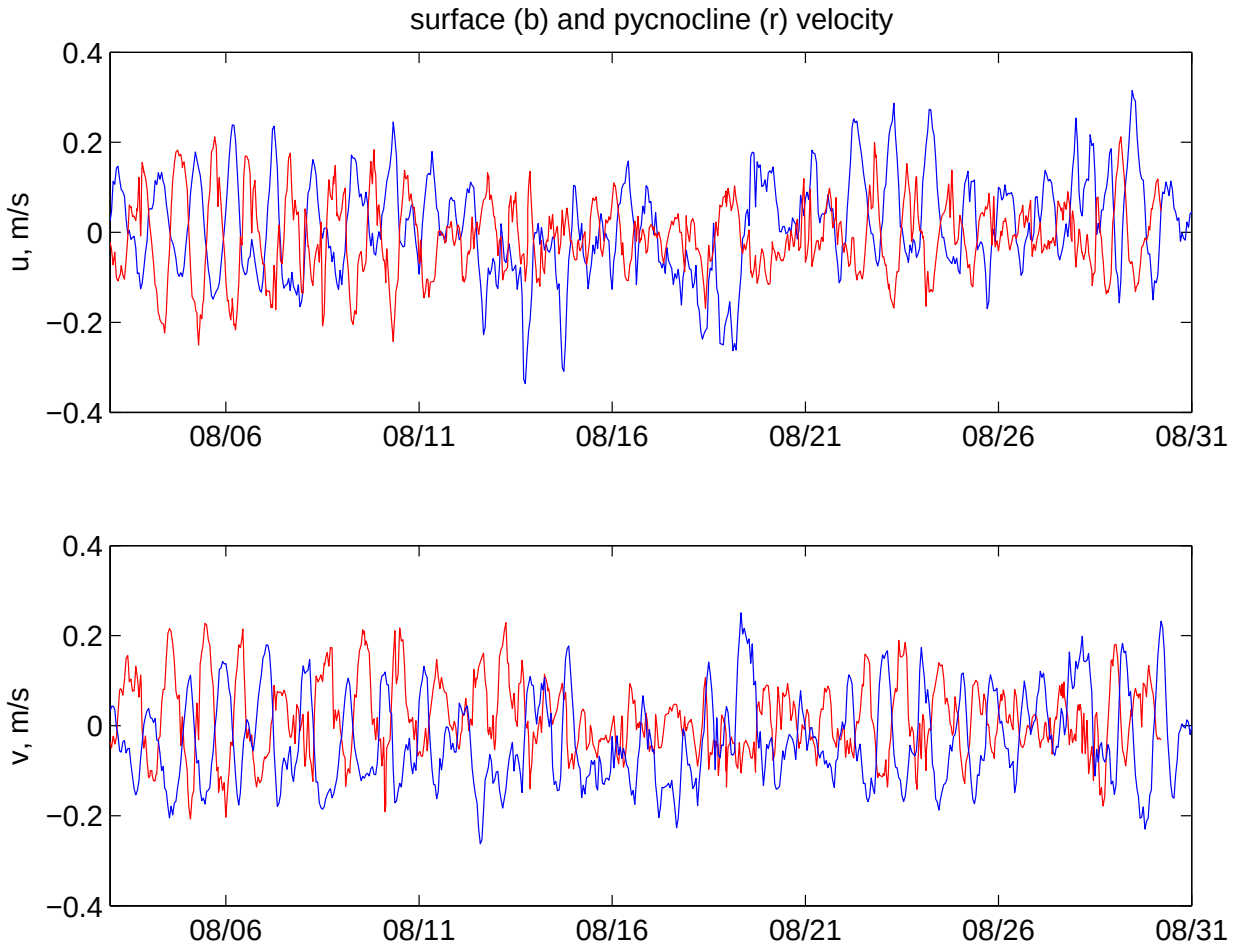

Figure 39: Time series of the u- and v-components of $\psi_{bc}(z,t)$, evaluated at the surface (b) and within the pycnocline (r). The ρ=1024.5 kg m^{-3} isopycnal is taken to be the center of the pycnocline. The baroclinic velocity in the pycnocline is 180°out of phase with the surface currents.

5.5 Discussion and speculation

Examination of the vertical structure of shear and stratification on the shelf of the Georgia Bight reveals that their maxima do not necessarily coincide; stratification is bounded by shear rather than aligned with the shear maximum. The second surprising result extends from the first: the flow which compensates for the surface layer motions is often separated from the bottom by a vertical region of near-zero D1 currents, and the subsurface maximum lies within rather than below the pycnocline. This vertical structure is not observed in other locations where inertial motions are forced by transient storms (*Tintoré et al.*, 1995; *Chant*, 2001; *Knight et al.*, 2002; *MacKinnon and Gregg*, 2005) or by SBLB near the resonant frequency (*Simpson et al.*, 2002; *Jarosz et al.*, 2007). In those locations, the vertical structure of the near-inertial motions are well-represented by two-layer point models (e.g., *Millot and Crépon*, 1981; *Kundu et al.*, 1983; *Orlic*, 1987), which assign the vertical shear of the currents to the level of the pycnocline.

In a two-layer formulation, there is no instantaneous vertically-averaged net transport, but measured currents at R4 vertically integrate to a non-zero depth-averaged current of 5-7 cm/s rotating at the diurnal/inertial frequency opposite the surface motion. If the maximum D1 currents measured by the ADCP are extrapolated through the near-surface portion of the water column not measured by the instrument due to wave contamination, the net depth-averaged motion is reduced to 2-4 cm/s.

The Georgia Bight differs from other locations where the vertical structure of inertial currents is well-described by two layer inertial oscillations and/or low mode NIIW. The diurnal/inertial currents are continuously forced at the surface rather than forced by storm activity, occur on the shelf rather than in deeper water, and unlike the Gulf of Mexico or New England shelf, the barotropic tide on the Georgia Bight has a strong bottom boundary layer (BBL) structure that extends well into the water column and can even interact with surface boundary layers. Some net motion (or a portion of it) could be explained by Ekman dynamics rather than interaction with the coastal wall, but the vertical structure of inertial shear is not well-explained by frictional dynamics alone. The observed vertical structure is not consistent with the normal mode formulation based on inviscid dynamics, but the vertical structure of the currents would not be altered by the addition of linear friction, as the vertical structure of the normal mode formulation is independent of f (and then, of $f + r$). On the other hand, Ekman dynamics predict a functional dependence of the vertical structure of oscillatory boundary layers on the frequency of the motions relative to f, and some change in the vertical structure with latitude might be expected. No latitudinal patterns in the vertical structure of diurnal/inertial currents in observed in the alongshore

transect from 30.04 to 31.6°N.

The observed vertical structure is quite unlike that seen by *Maas and van Haren* (1987), who describe a circularly polarized shear vector which remained constant in magnitude under rotation. Though inertial motions in the Georgia Bight arise from continued forcing near the resonant frequency rather than response to storms, the vertical structure and interaction with an energetic barotropic tide most resembles that observed in the North Sea by *van Haren et al.* (1999), where the water column is decoupled by two pycnoclines. With a beat period between the barotropic M_2 tide and the inertial motions, the upper pycnocline induces the compensating flow, and the lower pycnocline is associated with Ekman veering of the inertial signal (*van Haren*, 2000).

While observations in the North Sea show that stratification and shear coincide, unlike observed in the Georgia Bight, the combination of modal and frictional dynamics and the three-layer description suits the observations in the Georgia Bight. The D1 vertical structure appears to consist of three major layers: the surface layer which is directly forced by wind stress, a stratified layer in which the motion is 180°out of phase with surface currents, and a well-mixed layer near-bottom with no motion at the D1 frequency. The top of the pycnocline is sufficient to decouple the surface layer, below which interaction with the coastal wall induces a return flow. The bottom of the pycnocline separates the BBL from stratified waters of the pycnocline, which are moving opposite the surface to counteract the surface motion. Within the BBL, D1 motion is suppressed – perhaps by the "rubbing" of the pycnocline on the BBL. Stratification at outer shelf locations seems to be strong enough to decouple the surface layer from the effects of bottom friction, but the circulation spins down within 4-5 days without forcing. The dynamical normal modes seem not to be applicable due to frictional effects.

The potential for mixing across the edges of the stratified layer is examined through the gradient Richardson number (Fig. 40). Contours of diurnal baroclinic currents (ψ_{bc}[D1]) overlaid on the log of Richardson number shows the diurnal/inertial currents exist only in the portion of the water column not occupied by the (tidally-induced) BBL. When the wind-forced currents are strong (e.g., Aug. 3-10), the BBL is small, but as the diurnal/inertial currents diminish (e.g., Aug 10-15), the vertical extent of the bottom boundary layer expands. This contraction and expansion of the BBL is correlated with the magnitude of the diurnal/inertial winds rather than the spring/neap cycle, and suggests the competition of wind-induced mixing from the surface and tidally-induced mixing up from the bottom in setting the level of the pycnocline.

This conceptual framework explains the separation of the sub-surface maximum from the bottom at the level where the base of the pycnocline, where momentum transfer into the bottom boundary

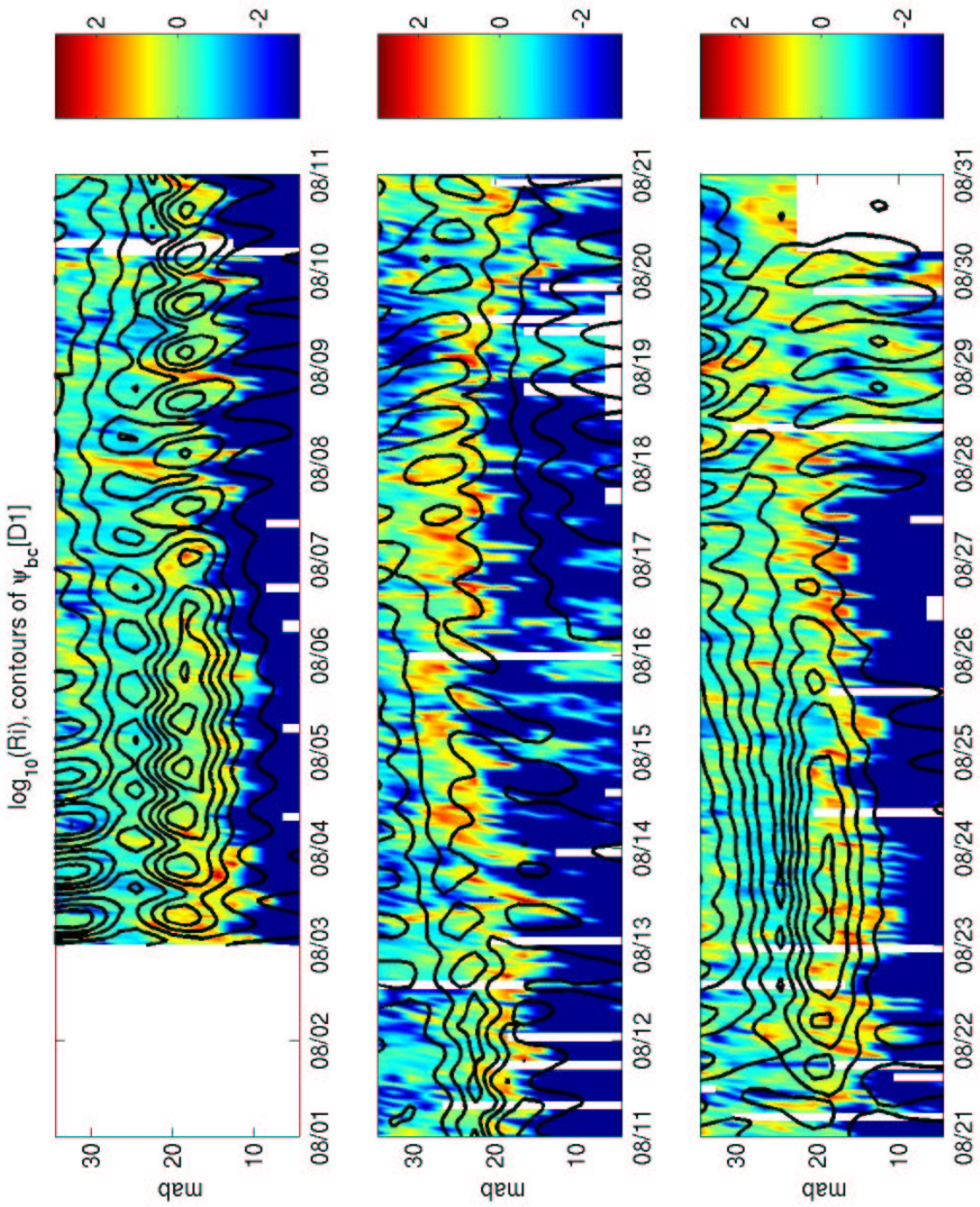

Figure 40: Log_{10}, of Richardson number (Ri), with contours of $|\psi_{bc}[D1](z,t)|$ overlaid for comparison. Shades of cyan and blue indicate Ri$<$0.25. The diurnal shear is contained within the portion of the water column that is not dominated by bottom friction.

layer is suppressed, and the wind-forced motion within the pycnocline, which is not observed in other locations. However, the observations of diurnal/inertial shear are more difficult to explain dynamically than conceptually, as some force must balance the external pressure gradient that acts upon the quiescent lower layer (directed opposite the surface). It is not clear whether internal pressure gradients create this balance and are masked by the semidiurnal variability in pycnocline position, or if internal friction acting on the pycnocline's inertial jet nearly balance the pressure gradient, and perhaps even less clear is how these terms vertically average to yield a net flow opposite the surface-forced currents.

The observed vertical density and current structure is similar to that seen in the marine inversion layer off the coast of California (*Ralph et al.*, 2000; *Samelson*, 1999). The surface boundary layer is capped by a stably stratified thermal inversion layer, upon which a well-mixed third layer sits. The upper and lower layers have constant velocity with height, but the inversion layer between them develops a jet that resembles the pycnocline jet observed in the Georgia Bight. The dynamics of the inversion layer can best be described as an internal bore traveling in the wave guide on the leading edge of a coastally trapped wind reversal (*Samelson*, 1999). While clearly the jet within the pycnocline rotates at the inertial frequency and can hardly be described as an internal bore, the roles of the internal pressure gradient and BBL of the two cases may be analogous.

The observations suggest that NIIW may be generated over multiple "coastal boundary layers" on the shelf, and that the waves reflect and interfere, resulting in significant changes in the phase propagation and vertical structure of diurnal/inertial currents. The shelf of the Georgia Bight may indeed trap near-inertial energy that cannot exit the shelf due to interaction with density fronts, associated jets, turning latitudes, or bottom friction. As a result, the wind input energy redirected into the NIIW wave field may not escape the shelf and ends up redistributed, dissipating due to friction (internal and bottom) and maybe partial reflections (*Lee and Eriksen*, 1997). In addition, energy in the near-inertial band may easily be converted to energy at smaller scales as fM_2 internal waves. The pycnocline couples the diurnal/inertial surface layer to the tidally-dominated bottom layer; its vertical motion is semidiurnal, but its horizontal motion is diurnal/inertial and on the order of 20 cm/s. The combination suggests the presence of fM_2 internal waves generated via nonlinear interactions similar to that found by (e.g., *Xing and Davies*, 2002). Unlike the NIIWs which remain trapped on the shelf of the Georgia Bight, these shorter period waves may be able to freely propagate off the shelf.

Figure 40 suggests that both surface and bottom friction actively mix across the pycnocline. The base of the pycnocline rubs against the BBL, but the Richardson number is also sub-critical at the top of the pycnocline, where both shear and stratification are significant. Interpretation of shear and stratifi-

cation measured at R4 in August 2006 suggests that mixing generally takes the form of internal mixing whereby the shear at the pycnocline thickens its boundary over time (*Turner*, 1973), signaling mixing in the interface (*Thorpe*, 1971). When shear is strong (e.g., August 3-8), the pynocline occupies a visibly larger portion of the water column, signifying active mixing (*Linden*, 1979), and thins when the diurnal/inertial currents decrease in magnitude and shear (August 10-15). The pycnocline appears to be eroded by boundary layer processes from both above and below, but the wind-forced mixing at the top of the pycnocline may be the greater control of its thickness. A full description of the mixing characteristics is not possible with the available observations, but the addition of dissipation measurements could confirm this speculation on the form of mixing.

5.6 Summary

Case studies highlight the influence of stratification on the coastal response of diurnal/inertial currents to SBLB wind forcing. Both stratification and wind forcing appear to be necessary conditions for the development of near-inertial currents near surface; neither is sufficient by itself to induce surface motion. The magnitude of near-inertial currents at inshore locations appear to be largely controlled by stratification rather than SBLB winds. Variation of the magnitude of diurnal/inertial currents may be used as a proxy for stratification at a given location. Phase propagation and vertical structure of diurnal/inertial currents on the outer shelf suggests multiple sources of NIIW which often interfere, consistent with the notion that Georgia Bight may trap near-inertial energy due to constraints on propagation.

A closer examination of shear and stratification on the mid- to outer shelf reveals at least a partial decoupling of the water column dynamics by the pycnocline. Further, the level of maximum shear bounds rather than coincides with the pycnocline, which contains a sub-surface jet that rotates anticyclonically but is 180°out of phase with the directly forced surface currents. The vertical structure of the diurnal/inertial current response to SBLB is not-well represented by the two layer single-point models which describe the vertical structure observed in other locations, and more closely resembles a three layer structure in which diurnal/inertial motions in the bottom boundary layer is near-quiescent, and internal pressure gradients nearly balance the external pressure gradient produced by wind set-up. Mixing across the base of the pycnocline occurs through interaction with the tidal bottom boundary layer, and SBLB-forced currents induce mixing across the top of the pycnocline. The competition of wind- and tidally-generated mixing sets the level of the pycnocline. Though the pycnocline effectively decouples the tidally-dominated bottom layer from the diurnal/inertial motion that dominates the surface layer,

its motion is set by tidal and diurnal/inertial processes, with vertical displacement at the semidiurnal frequency and horizontal motion as an inertial jet rotating 180°out of phase with SBLB-forced surface currents.

CHAPTER 6. Conclusions and future work

Observational wind and current data from 1999-2007 are analyzed from a moored array in the Georgia Bight, where linear theory predicts a maximum of SBLB magnitude and offshore extent. The structure of diurnal variability in observed and modeled wind fields compares well with the predictions of linear SBLB theory, with the greatest SBLB winds near 30°N. SBLB is a source of shelf-wide wind forcing near the resonant frequency; SBLB winds are found to exceed 1-2 m/s at least 250 km offshore, a distance almost an order of magnitude greater than that found at other latitudes.

Though the SBLB winds decrease with distance offshore, the coastal ocean response increases as the presence of stratification increases the efficiency of the wind forcing – preliminary analysis of surface currents from HF radar suggests continued increase past the shelf break into the Gulf Stream. The observed near-inertial energy on the shelf approaches the magnitude of the M_2 barotropic tide, previously thought to contribute 80% of the kinetic energy on the shelf (*Pietrafesa et al.*, 1985). The kinetic energy budget on the shelf should include the seasonal effect of wind-forced diurnal/inertial motions, particularly on the mid- to outer shelf, where the energy of SBLB-forced currents is appreciable in comparison to that of the barotropic tide.

A month-long glider deployment in August 2006 allows for a closer examination of the role of stratification in determining the magnitude and vertical structure of the SBLB-forced currents, and reveals that the pycnocline contains the return flow, rotating 180°out of phase with surface currents. This unusual vertical structure is consistent with neither purely modal nor frictional dynamics. The interaction of the coastal response to SBLB with the bottom boundary layer generated by tidal processes and wind-induced mixing across the top of the pycnocline contraindicates the description of the dynamics on the Georgia Bight with linear modes. The vertical structure and its potential interaction with tidal processes have significant implications for mixing, as the shelf of the Georgia Bight appears to trap near-inertial energy input from the wind, enhanced near the critical latitude for diurnal/inertial resonance.

Though the near-resonant interaction of SBLB and currents is unique to the critical latitude, strong

near-inertial motions are ubiquitous on continental shelves and in the deep ocean. The similarity of the observed vertical structure, in which an inertial jet is sandwiched in the pycnocline by two relatively well-mixed surface and bottom boundary layers, to observations in wildly different dynamical settings suggests broader significance of the work. Clearly, the inertial motions in the pycnocline cannot be described as internal bores, as seen on the leading edge of coastally trapped wind reversals (*Ralph et al.*, 2000; *Samelson*, 1999). The observed vertical structure on the Georgia Bight is different from that observed in other locations near the critical latitude, and shares some features with the vertical structure of near-inertial motions in the North Sea (*van Haren et al.*, 1999; *van Haren*, 2000), most notably, the partial decoupling of the water column by stratification. Observations of near-inertial motions in other locations where tidal energy is significant but not sufficient to completely suppress stratification would make for an interesting comparison, and perhaps allow for a better dynamical description of motions on the shelf of the Georgia Bight.

Due to the shape of the shelf and the position of the Gulf Stream along its boundary, NIIW generated on the shelf cannot escape, and their energy must be dissipated locally. The implications for mixing from this trapping of inertial energy in the Georgia Bight become more significant because of its location near the critical latitude. SBLB is enhanced in magnitude and offshore extent over the shelf, the coastal response is near-resonance with wind forcing near the critical latitude, and the transfer of this enhanced wind energy into the coastal ocean appears to be particularly efficient (*Skyllingstad et al.*, 2000).

The observations were not designed to resolve mixing process, and as a result, the discussion of how the input wind energy is redistributed and dissipated is speculative. However, the observations suggest that internal mixing on the shelf could be significant. The level of the pycnocline appears to be set by the competition between downward energy from wind forcing near the surface and tidal mixing in the bottom boundary layer, but both surface- and bottom-generated mixing appear to erode the pycnocline from above and below. As the wind mixing increases, the pycnocline deepens and thickens over time, and its occupation of a visibly larger portion of the water column signals internal mixing within the pycnocline.

The observed diurnal wind variability offshore may not be attributed solely to sea breeze; the position of the Gulf Stream may also contribute to heterogeneity in the wind field. Time series of D1 wind variance on the outer shelf show a striking seasonal maximum evident in spring and fall, when the thermal gradient between shelf and Gulf Stream water is expected to be greatest, and observed D1 winds increase with distance offshore. The response in the coastal ocean at the outer shelf locations is observed to be smaller in magnitude (10-20 cm/s at R4, compared to 25-30), generally shorter in dura-

tion, and with a vertical structure that suggests interference of NIIW on the outer shelf. The NNM-WRF model reanalysis product predicts the greatest diurnal winds to be located above the north wall of the Gulf Stream, which may be a result of multiple processes enhanced over sharp SST gradients. Extra-tropical cyclone (XTC) passage produces 360°wind shifts over time scales of about a day, mimicking true diurnal variability. Since XTCs can be enhanced in strength over the Gulf Stream, their interaction may contribute to a diurnal Gulf Stream signal. Similarly, atmospheric adjustment after the passage of an XTC may be result in inertial ringing.

Alternately, just as the surface temperature gradient between land and the coastal ocean generates the SBLB system, gradients in sea surface temperature (SST) can induce atmospheric circulation cells over the coastal ocean. Gulf Stream circulation cells have been described by *Sweet et al.* (1981); *Hsu* (1984); *Segal and Arritt* (1992); *Alliss and Raman* (1995), among others, and in the Georgia Bight, the Gulf Stream's proximity may exert a considerable influence on the SBLB system by increasing the sensible heat-flux gradients offshore. *Doyle and Warner* (1990); *Warner et al.* (1990) show that the wind speed of circulation cells over SST gradients is primarily due to the gradients in latent heat flux rather than temperature. Simple estimates of the diurnal variability of latent heat flux gradients calculated with the air-sea toolbox for representative values of the temperature change across the north wall of the Gulf Stream suggest that their diurnal variability can be significant. This potential forcing mechanism would explain the diurnal variability in spring and fall over the Gulf Stream; the idea can be tested through coupling pf idealized Gulf Stream dynamical model with an air-sea interaction model.

The comparison of wind efficiency in summer to the pattern in spring and fall, when the wind forcing increases with distance offshore, would be interesting, and might yield clues about the role of stratification. Is the smaller magnitude of diurnal/inertial winds simply correlated to decreased stratification, or is there an effect of the duration of wind forcing? How does the vertical structure of currents change when the forcing is strongest at the shelfbreak? Is the unusual vertical structure of currents with respect to the mass field reproduced when the coastal boundary is located further away from the wind forcing?

There may be significant implications for larval transport on the shelf of the South Atlantic Bight. Previous modeling work estimating larval transport in the region found that larval behavior did not appear to be a significant control on larval settlement location (*Edwards et al.,* 2008); alongshore currents were the greatest factor in larval transport on the shelf. The phase locking of the surface-intensified inertial oscillations and NIIWs on the Georgia Shelf to the diel cycle is unique to the critical latitude, and is a potential mechanism for cross-shore larval transport not considered by previous studies. The 180°vertical phase difference induced by coastal wall effects not only provides new pathways of

transport in the cross-shore direction, but cross-shore transport requires larval behavior to achieve net movement on- or offshore. At mid-shelf, the onshore surface currents are in phase with the short wave radiation, and species that vertically migrate to the surface during the day are transported onshore. At night, their position in the lower water column likely results in little to no further movement onshore, particularly in deeper water, where the bottom layer is near-quiescent (*Edwards and Seim*, 2008c). An average 15 cm/s current near-surface would advect larvae over 6 km per 12-hour half-diel cycle. This form of cross-shore transport and the requirement for behavior would significantly change the larval settlement locations predicted by models if wind-forced inertial oscillations are included in the dynamics.

BIBLIOGRAPHY

Alliss, R., and S. Raman, Diurnal variations in cloud frequency over the Gulf Stream Locale, *J. Appl. Meteor., 34*, 1578–1594, 1995.

Apel, J., M. Badiey, C.-S. Chiu, S. Finette, R. Headrick, J. Kemp, J. Lynch, A. Newhall, M. Orr, B. Pasewark, D. Tielbuerger, A. Turgut, K. von der Heydt, and S. Wolf, An overview of the 1995 SWARM shallow-water internal wave acoustic scattering experiment, *IEEE J. Ocean. Eng.*, *22*, 465–500, 1997.

Arextabaleta, A., J. Nelson, J. Blanton, H. Seim, F. Werner, J. Bane, and R. Weisberg, Cold event in the South Atlantic Bight during summer of 2003: Anomalous hydrographic and atmospheric conditions, *J. Geophys. Res.*, *111*, C06,007, doi:10.1029/2005JC003,105, 2006.

Arritt, R., Numerical modelling of the offshore extent of sea breezes, *Q.J.R. Meteorol. Soc.*, *115*, 547–570, 1989.

Atkinson, L., T. Lee, J. Blanton, and W. Chandler, Climatology of the southeastern United States continental shelf waters, *J. Geophys. Res.*, *88*, 4705–4718, 1983.

Barnett, T., Variations in near-global sea level pressure, *J. Atmos. Sci.*, *42*, 478–501, 1985.

Blanton, B., A. Aretxabaleta, F. Werner, and H. Seim, Monthly climatology of the continental shelf waters of the South Atlantic Bight, *J. Geophys. Res.*, *108*, C8, doi:10.1029/2002JC001,609, 2003.

Blanton, B., F. Werner, H. Seim, R. Luettich, D. Lynch, K. Smith, G. Vougaris, F. Bingham, and F. Way, Barotropic tides in the South Atlantic Bight, *J. Geophys. Res.*, *109*, C12,024, doi:10.1029/2004JC002,455, 2004.

Blanton, J., Ocean currents along a nearshore frontal zone on the continental shelf of the southeast United States, *J. Phys. Oceanogr.*, *11*, 1627–1637, 1981.

Buckley, R., and R. Kurzeja, An observational and numerical study of the nocturnal sea breeze. Part II: Chemical transport, *J. Appl. Meteor.*, *36*, 1599–1619, 1997a.

Buckley, R., and R. Kurzeja, An observational and numerical study of the nocturnal sea breeze. Part I: Structure and circulation, *J. Appl. Meteor.*, *36*, 1577–1598, 1997b.

Byers, H., and H. Rodebush, Causes of thunderstorms of the Florida peninsula, *J. Meteor.*, *5*, 275–280, 1948.

Chant, R., Evolution of near-inertial waves during an upwelling event on the New Jersey inner shelf, *J. Phys. Oceanogr.*, *29*, 746–764, 2001.

Chen, C., and L. Xie, A numerical study of wind-induced, near-inertial oscillations over the Texas-Louisiana shelf, *J. Geophys. Res.*, *102*, 15,583–15,593, 1997.

Chen, C., R. Reid, and W. Nowlin, Near-inertial oscillations over the Texas-Louisiana shelf, *J. Geophys. Res.*, *101*, 3509–3524, 1996.

Clarke, R., Some observations and comments on the sea breeze, *Austr. Meteor. Mag.*, *11*, 93–106, 1955.

Craig, P., Constant eddy-viscosity models of vertical structure forced by periodic winds, *Cont. Shelf Res.*, *9*, 343–358, 1989.

Crouch, A., A climatology of the sea breeze front in the coastal Carolinas and Georgia, Master's thesis, North Carolina State University, Raleigh, NC, 2006.

Daddio, E., W. Wiseman, and S. Murray, Inertial currents over the inner shelf near 30°N, *J. Phys. Oceanogr.*, *8*, 728–733, 1978.

Dalu, G., and R. Pielke, An analytical study of the sea breeze, *J. Atmos. Sci.*, *46*, 1815–1825, 1989.

Davies, A., A three-dimensional modal model of wind induced flow in a sea region, *Prog. Oceanogr.*, *15*, 71–128, 1985a.

Davies, A., Application of a sigma coordinate sea model to the calculation of wind-induced currents, *Cont. Shelf Res.*, *4*, 389–423, 1985b.

Davies, A., and J. Xing, Influence of coastal fronts on near-inertial internal waves, *Geophys. Res. Lett.*, *29*, 1–4, 2002.

Davies, A., and J. Xing, Processes influencing wind-induced current profiles in near coastal stratified regions, *Cont. Shelf Res.*, *23*, 1379–1400, 2003.

Davies, A., and J. Xing, Modelling processes influencing wind-induced internal wave generation and propagation, *Cont. Shelf Res.*, *24*, 2245–2271, 2004.

Davies, A., and J. Xing, The effect of a bottom shelf front upon the generation and propagation of near-inertial internal waves in the coastal ocean, *J. Phys. Oceanogr.*, *35*, 976–990, 2005.

Davis, R., Predictability of sea surface temperature and sea level pressure anomalies over the North Pacific Ocean, *J. Phys. Oceanogr.*, *8*, 249–266, 1976.

DiMarco, S., M. Howard, and R. Reid, Seasonal variation of wind-driven diurnal current cycling on the Texas-Louisiana continental shelf, *Geophys. Res. Lett.*, *27*, 1017–1020, 2000.

Doyle, J., and T. Warner, Mesoscale coastal processes during GALE IOP 2, *Mon. Wea. Rev.*, *118*, 283–308, 1990.

Edwards, C., and H. Seim, Complex EOF analysis as a method to separate barotropic and baroclinic velocity structure in shallow water, *J. Atmos. Oceanic Tech.*, *25*, 808–821, 2008a.

Edwards, C., and H. Seim, Sea breeze/land breeze near the resonant critical latitude in the Georgia Bight, *J. Geophys. Res.*, 2008b, in prep.

Edwards, C., and H. Seim, Coastal ocean response to SBLB in the Georgia Bight: Stratification and shear, *J. Geophys. Res.*, 2008c, in prep.

Edwards, C., and H. Seim, Coastal ocean response to SBLB in the Georgia Bight: Structure and variability, *J. Geophys. Res.*, 2008d, in prep.

Edwards, K., J. Hare, and F. Werner, Dispersal of black sea bass (Centropristis striata) larvae on the southeast U.S. continental shelf: results of a coupled vertical larval behavior - 3D circulation model, *Fish. Oceanogr.*, *17*, 299–315, 2008.

Estoque, M., The sea breeze as a function of the prevailing synoptic situation, *J. Atmos. Sci.*, *19*, 244–250, 1962.

Foreman, M., R. Walters, R. Henry, C. Keller, and A. Dolling, A tidal model for eastern Juan de Fuca Strait and the southern Strait of Georgia, *J. Geophys. Res.*, *100(C1)*, 721–740, 1995.

Frysinger, J., and B. Lindner, A statistical sea-breeze prediction algorithm for Charleston, South Carolina, *Wea. and Forecasting*, *18*, 614–625, 2003.

Garrett, C., What is the "near-inertial" band and why is it different from the rest of the internal wave spectrum?, *J. Phys. Oceanogr.*, *31*, 962,971, 2001.

Gill, A., On the behavior of internal waves in the wake of storms, *J. Phys. Oceanogr.*, *14*, 1129–1151, 1984.

Gille, S., S. L. Smith, and N. Statom, Global observations of the land breeze, *Geophys. Res. Lett.*, *32*, L05,605, doi:10.1029/2004GR022,139, 2005.

Grinsted, A., J. Moore, and S. Jevrejeva, Application of the cross wavelet transform to geophysical time series, *Nonlinear Proc. Geophysics*, *11*, 561–566, 2004.

Hall, P., and A. Davies, Analysis of time-varying wind-induced currents in the North Channel of the Irish Sea, using empirical orthogonal functions and harmonic decomposition, *Cont. Shelf Res.*, *22*, 1269–1300, 2002.

Hamilton, P., T. Berger, J. Singer, E. Waddell, J. Churchill, R. Leben, T. Lee, and W. Sturges, DeSoto Canyon eddy intrusion study, final report, Volume II: Technical Report, *Tech. rep.*, US Department of the Interior, Minerals Management Service, Gulf of Mexico Region, New Orleans, LA, 2000.

Haurwitz, B., Comments on the sea-breeze circulation, *J. Meteor.*, *4*, 1–8, 1947.

Holloway, P., A regional model of the semidiurnal internal tide on the Australian North West Shelf, *J. Geophys. Res.*, *106(C9)*, 19,625–19,638, 2001.

Holloway, P., P. Chatwin, and P. Craig, Internal tide observations from the Australian North West Shelf in summer 1995, *J. Phys. Oceanogr.*, *31*, 1182–1199, 2001.

Horel, J., Complex principal component analysis: theory and examples, *J. Climate App. Meteor.*, *23*, 1660–1673, 1984.

Hsu, S., Sea breeze-like winds across the north wall of the Gulf Stream: An analytical model, *J. Geophys. Res.*, *89*, 2025–2028, 1984.

Huthnance, J., Internal tides and waves near the continental shelf edge, *Geophys. Astrophys. Fluid Dyn.*, *48*, 81–106, 1989.

Jacobs, G., J. Book, H. Perkins, and W. Teague, Inertial oscillations in the Korea Strait, *J. Geophys. Res.*, *106*, 26,843–26,957, 2001.

Jarosz, E., Z. Hallock, and W. Teague, Near-inertial currents in the DeSoto Canyon region, *Cont. Shelf Res.*, *27*, 2407–2426, 2007.

Kaihatu, J., R. Hadler, G. Marmorino, and L. Shay, Empirical orthogonal function analysis of ocean surface currents using complex and real-vector methods, *J. Atmos. Oceanic Tech.*, *15*, 397–414, 1998.

Knight, P., M. Howarth, and T. Rippeth, Inertial currents in the northern North Sea, *J. Sea Res.*, *47*, 269–284, 2002.

Kumar, P., and E. Foufoula-Georgiou, Wavelet analysis for geophysical applications, *Rev. Geophys.*, *35*, 385–412, 1997.

Kundu, P., S. Chao, and J. McCreary, Transient coastal currents and inertio-gravity waves, *Deep-Sea Res.*, *30(10A)*, 1059–1082, 1983.

Kurzeja, R., S. Berman, and A. Weber, A climatological study of the nocturnal planetary boundary layer, *Bound.-Layer Meteor.*, *54*, 105–128, 1991.

Lee, C., and C. Eriksen, Near-inertial wave interactions with mesoscale fronts: observations and models, *J. Geophys. Res.*, *102*, 3237–3253, 1997.

Lee, T., and D. Brooks, Initial observations of current, temperature, and coastal sea level response to atmospheric and Gulf Stream forcing, *Geophys. Res. Lett.*, *6*, 321–324, 1979.

Lee, T., J. Yoder, and L., Gulf Stream frontal eddy influence on productivity of the Southeast U.S. continental shelf, *J. Geophys. Res.*, *96*, 22,191–22,205, 1991.

Lentz, S., Current dynamics over the northern California inner shelf, *J. Phys. Oceanogr.*, *24*, 2461–2478, 1994.

Lerczak, J., C. Winant, and M. Hendershott, Observations of the semidiurnal internal tide on the southern California slope and shelf, *J. Geophys. Res.*, *108*, 3068, doi:10.1029/2001/JC001,128, 2003.

Lewis, J., Cross-shelf variations of near-inertial current oscillations, *Cont. Shelf Res.*, *21*, 531–543, 2001.

Linden, P., Mixing in stratified fluids, *Geophys. and Astrophys. Fluid Dyn.*, *13*, 3–23, 1979.

Maas, L., and J. van Haren, Observations on the vertical structure of tidal and inertial currents in the central North Sea, *J. Mar. Res.*, *45*, 293–318, 1987.

MacKinnon, J., and M. Gregg, Mixing on the late-summer New England shelf, *J. Phys. Oceanogr.*, *33*, 1476–1492, 2003a.

MacKinnon, J., and M. Gregg, Shear and baroclinic energy flux on the summer New England shelf, *J. Phys. Oceanogr.*, *33*, 1462–1475, 2003b.

MacKinnon, J., and M. Gregg, Near-inertial waves on the New England shelf: the role of evolving stratification, turbulent dissipation, and bottom drag, *J. Phys. Oceanogr.*, *35*, 2408–2424, 2005.

Malone, F., An analysis of current measurements in Lake Michigan, *J. Geophys. Res.*, *73*, 7065–7081, 1968.

Millot, C., and M. Crépon, Inertial oscillations on the continental shelf of the Gulf of Lions – observations and theory, *J. Phys. Oceanogr.*, *11*, 639–657, 1981.

Mooers, C., Several effects of a baroclinic current on the cross-stream propagation of inertial-internal waves, *Geophys. Fluid Dyn.*, *6*, 245–275, 1975.

Muglia, M., H. Seim, and B. Blanton, Mike's unpublished paper with harvey, brian?, 2003, unpublished.

Münchow, A., and R. Chant, Kinematics of inner shelf motions during the summer stratified season off New Jersey, *J. Phys. Oceanogr.*, *30*, 247–268, 2000.

Mwale, D., T. Gan, S. Shen, T. Shu, and K.-M. Kim, Wavelet empirical orthogonal functions of space-time-frequency regimes and predictability of Southern Africa summer rainfall, *J. Hydrologic Eng.*, *12*, 513–523, 2007.

Neumann, J., Land breeze and nocturnal thunderstorms, *J. Meteor.*, *8*, 60–67, 1951.

Nielsen Gammon, J., The subtropical sea breeze, in *Ninth Conf. on Mesoscale Processes*, AMS, Fort Lauderdale, FL, 2001.

Niino, H., The linear theory of land and sea breeze circulation, *J. Meteorol. Soc. Jap.*, *65*, 901–921, 1987.

Orlic, M., Oscillations at the inertial period on the Adriatic Sea Shelf, *Cont. Shelf Res.*, *7*, 577–598, 1987.

Pairaud, I., and F. Auclair, Combined wavelet and principal component analysis (weof) of a scale-oriented model of coastal ocean gravity waves, *Dyn. Atmos. Oceans*, *40*, 254–282, 2005.

Pawlowicz, R., B. Beardsley, and S. Lentz, Classical tidal harmonic analysis including error estimates in matlab using t_tide, *Comp. Geosci.*, *28*, 929–937, 2002.

Pietrafesa, L., J. Blanton, J. Wang, V. Kourafalou, T. Lee, and K. Bush, The tidal regime in the South Atlantic Bight, in *Oceanography of the southeastern U.S. continental shelf*, vol. 2, pp. 63–76, Amer. Geophys. Union, 1985.

Pollard, R., and R. Millard, Comparison between observed and simulated wind-generated inertial oscillations, *Deep-Sea Res.*, *17*, 813–821, 1970.

Pollard, R., P. Rhines, and R. Thompson, The deepening of the wind-mixed layer, *Geophys. Fluid Dyn.*, *3*, 381–404, 1973.

Preisendorfer, R., Principal component analysis in meteorology and oceanography, Developments in atmospheric science, 1988.

Ralph, F., P. Neiman, P. Persson, J. Bane, M. Cancillo, J. Wilczak, and W. Nuss, Kelvin waves and internal bores in the marine boundary layer inversion and their relationship to coastally trapped wind reversals, *Mon. Wea. Rev.*, *128*, 283–300, 2000.

Ray, R., and G. Mitchum, Surface manifestation of internal tides generated near Hawaii, *Progr. Oceanogr.*, *40*, 135–162, 1997.

Redfield, A., The influence of the continental shelf on the tides of the Atlantic coast of the united states, *J. Mar. Res.*, *1492*, 432–448, 1958.

Rippeth, T., and M. Inall, Observations of the internal tide and associated mixing across the Malin Shelf, *J. Geophys. Res.*, *107*, C43,028, doi:10.29/2000/JC000,761, 2002.

Rippeth, T., J. Simpson, R. Player, and M. Garcia, Current oscillations in the diurnal-inertial band on the Catalonian shelf in spring, *Cont. Shelf Res.*, *22*, 247–265, 2002.

Rotunno, R., On the linear theory of the land and sea breeze, *J. Atmos. Sci.*, *40*, 1999–2009, 1983.

Samelson, R., The vertical structure of linear coastal-trapped disturbances, *Mon. Wea. Rev.*, *127*, 201–213, 1999.

Segal, M., and R. Arritt, Nonclassical mesoscale circulations caused by surface sensible heat-flux gradients, *Bull. Amer. Meteor. Soc.*, *73*, 1593–1604, 1992.

Seim, H., Implementation of the South Atlantic Bight Synoptic Offshore Observational Network, *Oceanogr.*, *13*, 18–23, 2000.

Seim, H., and C. Edwards, Comparison of buoy-mounted and bottom-moored ADCP performance at Gray's Reef, *J. Atmos. Oceanic Tech.*, *24*, 270–284, 2007.

Shay, L., H. Seim, D. Savidge, R. Styles, and R. Weisberg, High frequency radar observing systems in SEACOOS, *MTS Journal*, 2008, in review.

Simionato, C., V. Meccia, W. Dragani, and M. N. nez, Barotropic tide and baroclinic waves observations in the Rio de la Plata Estuary, *J. Geophys. Res.*, *110*, C06,008, doi:10.1029/2004/JC002,842, 2005.

Simpson, J., *Sea Breeze and Local Winds*, Cambridge University Press, Cambridge, UK, 1994.

Simpson, J., P. Hyder, T. Rippeth, and I. Lucas, Forced oscillations near the critical latitude for diurnal-inertial resonance, *J. Phys. Oceanogr.*, *32*, 177–187, 2002.

Skamarock, W. C., J. B. Klemp, J. Dudhia, D. O. Gill, D. M. Barker, W. Wang, and J. G. Powers, A description of the advanced research wrf version 2, *Tech. Rep. NCAR/TN-468+STR*, National Center for Atmospheric Research (NCAR), 2005.

Skyllingstad, E., W. Smyth, and G. Crawford, Resonant wind-driven mixing in the ocean boundary layer, *J. Phys. Oceanogr.*, *30*, 1866–1890, 2000.

Soulsby, R., The bottom boundary layer of shelf seas, in *Physical Oceanography of Coastal and Shelf Seas*, edited by B. Johns, vol. 30, pp. 189–266, Elsevier, Amsterdam, 1983.

Soulsby, R., Tidal-current boundary layers, in *The Sea: Ocean engineering science*, edited by B. Mehaute and D. Hanes, vol. 9, pp. 523–566, Wiley-Interscience, 1990.

Steyn, D., Scaling the vertical structure of sea breezes revisited, *Boundary-Layer Meteorol.*, *107*, 177–188, 2003.

Stockwell, R., W. Large, and R. Milliff, Resonant inertial oscillations in moored buoy ocean surface winds, *Tellus, 56A*, 536–547, 2004.

Sweet, W., R. Fett, J. Kerling, and P. LaViolette, Air-sea interaction effects in the lower troposphere across the north wall of the Gulf Stream, *Mon. Wea. Rev.*, *109*, 1042–1052, 1981.

Tebeau, P., and T. Lee, Wind induced circulation on the Georgia shelf, *Tech. Rep. 79003*, Univ. of Miami, Miami, FL, 1979.

Thorpe, S., Experiments on the instability of stratified shear flows, *J. Fluid Mech.*, *46*, 299–319, 1971.

Tintoré, J., D.-P. Wang, E. García, and A. Viúdez, Near-inertial motions in the coastal ocean, *J. Mar. Systems*, *6*, 301–312, 1995.

Torrence, C., and G. Compo, A practical guide to wavelet analysis, *Bull. Amer. Meteor. Soc.*, *79*, 61–78, 1998.

Tunney, D., Numerical studies of the Georgia coast sea breeze, Master's thesis, Florida State University, Tallahassee, FL 32303-3034, 1996.

Turner, J., *Buoyancy effects in fluids*, Cambridge University Press, Cambridge, MA, 1973.

Ueda, H., Effects of external parameters on the flow field in the coastal region – a linear model, *J. Appl. Meteor.*, *22*, 312–321, 1983.

van Haren, H., Properties of vertical current shear across stratification in the North Sea, *J. Mar. Res.*, *58*, 465–491, 2000.

van Haren, H., Tidal and near-inertial peak variations around the diurnal critical latitude, *Geophys. Res. Lett.*, *32*, L23,611, doi:10.1029/2005GL024,160/L23,611, 2005.

van Haren, H., L. Maas, J. Zimmerman, H. Ridderinkhof, and H. Malschaert, Strong inertial currents and marginal internal wave stability in the central North Sea, *Geophys. Res. Lett.*, *26*, 2993–2996, 1999.

Walsh, J., Sea breeze theory and applications, *J. Atmos. Sci.*, *31*, 2012–2026, 1974.

Wang, J., C.-S. Chern, and A. Liu, The wavelet empirical orthogonal function and its application to the analysis of internal tides, *J. Atmos. Oceanic Tech.*, *17*, 1403–1420, 2000.

Warner, T., M. Lakhtakia, and J. Doyle, Marine atmospheric boundary layer currents forced by Gulf Stream sea surface temperature gradients, *Mon. Wea. Rev.*, *118*, 309–323, 1990.

Waseda, T., L. Jameson, H. Mitsudera, and M. Yaremchuk, Optimal basis from empirical orthogonal functions and wavelet analysis for data assimilation: optimal basis WADAi, *J. Oceanogr.*, *59*, 187–200, 2003.

Weatherly, G., S. Blumsack, and A. Bird, On the effect of diurnal tidal currents in determining the thickeness of the turbulent Ekman bottom boundary layer, *J. Phys. Oceanogr.*, *10*, 297–300, 1980.

Weber, A., Wind climate analyses for National Weather Service stations in the southeast (U), *Tech. Rep. WSRC-TR-2002-00515*, Westinghouse Savannah River Company, Savannah River Site, Aiken, SC, 2003.

Weber, A., and J. Blanton, Monthly mean wind fields for the South Atlantic Bight, *J. Phys. Oceanogr.*, *10*, 1256–1263, 1980.

Webster, I., The vertical structure of currents on the North West Shelf of Australia at subtidal frequencies, *J. Phys. Oceanogr.*, *16*, 1145–1157, 1986.

Williams, D., A preliminary report on 1968 spring season sea breeze fronts that passed the Project Theo basic surface network, *Tech. rep.*, Unpublished report from the U.S. Forest Service, obtained at the Savannah NWS office, 1969.

Xing, J., and A. Davies, Processes influencing the non-linear interaction between inertial oscillations, near inertial internal waves and internal tides, *Geophys. Res. Lett.*, *29*, 1067, doi:10.1029/2001GR014,199, 2002.

Xing, J., and A. Davies, On the influence of a surface coastal front on near-inertial wind-induced internal wave generation, *J. Geophys. Res.*, *109*, C01,023, doi:10.1029/2003JC001,794, 2004.

Yan, H., and R. Anthes, The effect of latitude on the sea breeze, *Mon. Wea. Rev.*, *115*, 936–956, 1987.

Zhai, X., R. Greatbatch, and J. Sheng, Doppler-shifted inertial oscillations on a β-plane, *J. Phys. Oceanogr.*, *35*, 1480–1489, 2005.